TARGETING HUMAN TELOMERIC DNA WITH AZACYANINES

A THESIS SUBMITTED TO
THE GRADUATE SCHOOL OF NATURAL AND APPLIED SCIENCES
OF
MIDDLE EAST TECHNICAL UNIVERSITY

BY

AYÇA KÜÇÜKAKDAĞ DOĞU

IN PARTIAL FULFILLMENT OF THE REQUIREMENTS
FOR
THE DEGREE OF MASTER OF SCIENCE
IN
CHEMISTRY

MAY 2019

Approval of the thesis:

TARGETING HUMAN TELOMERIC DNA WITH AZACYANINES

submitted by **AYÇA KÜÇÜKAKDAĞ DOĞU** in partial fulfillment of the requirements for the degree of **Master of Science in Chemistry Department, Middle East Technical University** by,

Prof. Dr. Halil Kalıpçılar
Dean, Graduate School of **Natural and Applied Sciences** _____

Prof. Dr. Cihangir Tanyeli
Head of Department, **Chemistry** _____

Assoc. Prof. Dr. Özgül Persil Çetinkol
Supervisor, **Chemistry, METU** _____

Examining Committee Members:

Prof. Dr. Cihangir Tanyeli
Chemistry Department, METU _____

Assoc. Prof. Dr. Özgül Persil Çetinkol
Chemistry, METU _____

Assist. Prof. Dr. Şaziye Betül Sopacı
Chemistry Department, Ahi Evran University _____

Assoc. Prof. Dr. Serhan Türkyılmaz
Chemistry Department, METU _____

Assoc. Prof. Dr. Salih Özçubukçu
Chemistry Department, METU _____

Date: 21.05.2019

I hereby declare that all information in this document has been obtained and presented in accordance with academic rules and ethical conduct. I also declare that, as required by these rules and conduct, I have fully cited and referenced all material and results that are not original to this work.

Name, Surname: Ayça Küçükakdağ Doğu

Signature:

ABSTRACT

TARGETING HUMAN TELOMERIC DNA WITH AZACYANINES

Küçükakdağ Doğu, Ayça
Master of Science, Chemistry
Supervisor: Assoc. Prof. Dr. Özgül Persil Çetinkol

May 2019, 149 pages

Small molecules targeting telomeric DNA or its interactions with telomerase have been an active area of cancer research. Within this thesis, a series of five new benzimidazole compounds differing from each other in alkyl chain length and branching in the benzimidazole ring (ethyl, propyl, isopropyl, butyl, and isobutyl) were synthesized and characterized using Nuclear Magnetic Resonance (NMR) spectroscopy, High Resolution Mass spectroscopy and C/H/N elemental analysis. Their interactions with human telomeric DNA (tel24) along with the previously investigated methyl derivative were investigated using UV-VIS, Circular Dichroism, and Fluorescence spectroscopy. All the compounds were found to be binding to tel24 and inducing a weak CD band between 320 nm and 360 nm in 1:1 complexes. Substantial red-shift and hypochromic effect were observed only in the UV-VIS spectrum of Azamethyl and Azabutyl upon binding to tel24. No red shift or hypochromic effect was observed in the UV-VIS spectrum of Azaisopropyl in the presence of tel24. Among the compounds investigated, the butyl derivative was found to be binding to tel24 tighter than the previously investigated methyl derivative. Association constants were found to be $6.61 \times 10^5 \pm (3.74 \times 10^4)$, $7.84 \times 10^5 \pm (3.44 \times 10^4)$, and $4.55 \times 10^5 \pm (1.23 \times 10^4)$ M^{-1} for Azamethyl, Azabutyl, and Azaisobutyl respectively. Azaisopropyl showed the lowest binding affinity towards tel24. As a result, this study revealed that tel24 was a specific target for Azamethyl, Azabutyl,

and Azaisobutyl and azacyanines might be plausible drug candidate molecules in targeting G-quadruplexes.

Keywords: G-quadruplex, Human Telomeric DNA, Azacyanine, Small Molecule Binding, Intercalation

ÖZ

İNSAN TELOMERİK DNA'SININ AZASİYANİNLER İLE HEDEFLENMESİ

Küçükakdağ Doğu, Ayça
Yüksek Lisans, Kimya
Tez Danışmanı: Doç. Dr. Özgül Persil Çetinkol

Mayıs 2019, 149 sayfa

Telomerik DNA'yı hedefleyen küçük moleküller ve onların telomeraz enzimi ile etkileşimleri yoğun olarak çalışılan kanser araştırmalarındandır. Bu tez çalışması kapsamında, birbirlerinden alkil grubu uzunlukları ve dallanmaları bakımından farklılık gösteren beş yeni benzimidazol türevi molekül (etil, propil, izopropil, bütil, ve izobütil) sentezlenmiş, ve Nükleer Manyetik Rezonans (NMR) spektroskopisi, Yüksek Çözünürlüklü Kütle spektroskopisi, ve C/H/N elemental analiz yöntemleri kullanılarak karakterize edilmiştir. Bu moleküllerin daha önce sentezlenmiş ve karakterize edilmiş Azametil ile birlikte insan telomeric DNA'sı (tel24) ile etkileşimleri UV-VIS, Circular Dichroism, ve Floresans spektroskopisi kullanırak incelenmiştir. Tel24 ile1:1 oranında kompleks oluşturan bütün moleküller 320 nm ve 360 nm arasında zayıf bir CD bantı vermiştir. Tel24'e bağlanan Azametil ve Azabütil'in UV-VIS spektrumunda önemli bir oranda kırmızıya kayma (yüksek dalga boyuna kayma) ve hipokromik etki oluştuğu gözlenmiştir. Azaisopropil'in UV-VIS spektrumunda heredeyse hiç kırmızıya kayma ve hipokromik etki gözlenmemiştir. Bütün moleküller arasında bütil türevinin Tel24'e daha önce incelenmiş metil türevine göre daha kuvvetli bağlandığı gözlemlenmiştir. Tel24'e bağlanma sabitleri Azametil, Azabütil, ve Azaizobütil için sırasıyla $6.61x10^5 \pm (3.74x10^4)$, $7.84x10^5 \pm (3.44x10^4)$, ve $4.55x10^5 \pm (1.23x10^4)$ M^{-1} olarak bulunmuştur. Ayrıca, Azaizopropil'in tel24'e en zayıf bağlanan molekül olduğu belirlenmiştir. Sonuç olarak bu çalışma ile birlikte

tel24'ün Azametil, Azabütil ve Azaizobütil moleküllerine özgü bir hedef olabileceği ve azasiyaninlerin G-quadrupleksleri hedeflemek için kullanılabilecek makul ilaç adayı moleküller oldukları gösterilmiştir.

Anahtar Kelimeler: G-dörtlüsü, İnsan Telomerik DNA'sı, Azasiyanin, Küçük Molekül Bağlanması, İnterkalasyon

To my family…

ACKNOWLEDGEMENTS

I sincerely acknowledge my supervisor Assoc. Prof. Dr. Özgül Persil Çetinkol for giving the opportunity to conduct research in her lab and for her support and guidance. I thank my laboratory associates Serra Tütüncü, Sercan Güloğlu, and Aynur Özel for helping me with my research.

I would also like to thank Prof. Dr. Ali Çırpan and his PhD. Student Res. Assist. Şevki Can Cevher, Prof. Dr. Ahmet M. ÖNAL and his PhD. student Res. Assist. Merve AKBAYRAK and Prof. Dr. Metin ZORA and his PhD. Student Res. Assist. Yılmaz KELGÖKMEN for allowing me to use their laboratory equipment and for their generous supports.

I gratefully acknowledge Middle East Technical University funds BAP-08-11-2016-026 and Scientific and Technological Research Council of Turkey (TUBITAK) for financial support via project number 116Z219. This work was supported also by L'Oréal-UNESCO for Women in Science Turkey Scholarship and METU Chemistry Department.

I am grateful to METU Chemistry Department for giving me the opportunity to get educated by wonderful faculty members and assistants. Through their guidance, I was able acquire the scientific knowledge and the scientific world view. I also would like to thank METU Chemistry Department for giving me the chance to conduct research using department's facilities.

I would like to thank my family, my beloved husband Berk Doğu and my life-changing friend Sercan Erer for their faith in me, and their support and love. I also thank to my dear friends Beril Özdemir, Güzin Turkay, Fatma Çalılı, Sevtap Güven Gökçe and İpek Hazal Önen for their faithful friendship, being an enjoyable lab partners, and filling in our undergraduate years with such unforgettable memories.

TABLE OF CONTENTS

LIST OF TABLES

TABLES

LIST OF FIGURES

FIGURES

LIST OF ABBREVIATIONS

ABBREVIATIONS

BCL-2	B-cell lymphoma 2
c-KIT	CD117, also called KIT/C-kit receptor, Mast/stem cell growth factor
c-MYB	Myeloblastosis viral oncogene transcriptional activator
c-MYC	DNA binding transcription factor
CD	Circular Dichroism
DNA	Deoxyribonucleic acid
dsDNA	Double stranded deoxyribonucleic acid
h-TERT	Human telomerase reverse transcriptase
HIF-1α	Hypoxia inducible factor 1 subunit alpha
HRMS	High Resolution Mass Spectrometry
K-Ras	Proto-oncogene
UV-Vis	Ultraviolet – Visible
recQL	ATP-dependent DNA helicase Q1
RET	Proto-oncogene tyrosine-protein kinase receptor
RNA	Ribonucleic acid
SPR	Surface plasmon resonance
ssDNA	Single stranded deoxyribonucleic acid
Tel24	[d(TTGGG(TTAGGG)$_3$A]
Tel26	[d(AAAGGG(TTAGGG)$_3$AA]

T_m	Thermal denaturation temperature
VEGF	Vascular endothelial growth factor
YY1	Transcriptional Yin Yang 1 repressor protein

CHAPTER 1

INTRODUCTION

1.1. Purpose and Justifications

Within the scope of this project, five new benzimidazole derivative compounds were synthesized, characterized and their interactions with human telomeric DNA sequence, tel24, were investigated. The main purpose of the project is to discover new drug candidate molecules towards cancer treatment that are binding tightly and selectively to human telomeric DNA sequences. The benzimidazole derivatives that were synthesized within this project differ from each other by the length and type of the alkyl groups (ethyl, propyl, isopropyl, butyl, and isobutyl) in the benzimidazole ring system. Additionally, understanding the effect of molecular structure in DNA binding affinity and selectivity allow us to perform rational drug design. Considering the effect of molecular structure in terms of the chain length and molecular surface area on binding strength between these derivatives and DNA, new drug candidate molecules can be designed with the desired features, such as tight binding and high selectivity.

1.2. Current Chemotherapeutic Agents Targeting DNA

Chemotherapy is a widely used treatment for cancer. It is a technique used either to eliminate cancer cells selectively without damaging the normal cells, or reduce tumor growth, or alleviate pain that cancer causes, using chemicals called chemotherapeutic agents. Some of the basic mechanisms of action of the current chemotherapeutic drugs targeting DNA are damaging DNA by generating DNA-crosslinks that destabilize DNA during replication by alkylating agents, replacing the normal building blocks of DNA and RNA by anti-metabolites, interfering with the enzymes involved in DNA replication process by causing DNA intercalation and over-

generation of reactive oxygen species by cytotoxic antibiotics, inhibiting the Topoisomerase I or II enzymes by impeding the correct unwinding of DNA strands by topoisomerase inhibitors, inhibiting mitosis and cell division by micro-tubular poisons, and finally treating cancer cells by corticosteroids [1, 2].

Some of the current chemotherapeutic agents are cis-platin, doxorubicin, 5-fluorouracil, etoposide, and gemcitabine. Cis-platin binds irreversibly to DNA or RNA via covalent bond formation between the two nucleic acid bases, mostly through N7 of two adjacent guanines and causes failure in replication and the cell-cycle arrest. Unfortunately, cancer cells develop resistance to cis-platin very quickly due to the changes in drug transport systems, drug detoxification, DNA repair system, DNA damage tolerance mechanisms, or the apoptotic cell death pathways [1]. On the other hand, Doxorubicin and etoposide, inhibit Topoisomerase II which is an enzyme responsible from controlling the topology of DNA by cleaving the both strands of the double helix, generating relaxation and rotation. Inhibition of Topoisomerase II by etoposide, or generation of DNA strand breaks due to the formation of Topo-DNA adducts by doxorubicin ultimately hinders the replication, translation and transcription [3,4].

Most of the current chemotherapeutic agents are not selective towards cancer cells and they bind to duplex DNA sequences found in every cell. Therefore, they also bound to DNA, RNA or the enzymes in healthy living cells and cause their death along with the cancer cells. In other words, these drugs have serious adverse effects, so there is a continuing need for new selective molecules [5-7]. There are several other reasons that limits the effectiveness of the current agents, such as the development of resistance to them and even developing more resistant to further treatment, which results in the reoccurrence of the cancer. Another reason is the loss of a cell surface receptor or a mutation in the specific drug target that can result in therapeutic failure. The toxicity of the drug to the non-targeted cells/tissues, and the loss of penetration of drug molecule to blood brain barrier can also be counted as other reasons that limit the effectiveness of a drug molecule [3].

1.3. The Importance of Targeting Nucleic Acids in the Cancer Treatment

Nucleic acids (DNA and RNA) have been targeted in cancer treatment for years due to their vital roles in cellular function. The idea behind this strategy was to interfere with uncontrollable cellular replication, translation, or transcription by altering the nucleic acid structure using small molecules (drugs) [8-12]. In the last decade, especially targeting non-canonical nucleic acid structures such as telomeres became one of the extensively exploited research areas in the development of such small molecules [8].

Telomeres are repetitive guanine rich nucleic acid sequences found at the end of the chromosomes. For instance, human telomeres consist of a double helical region of about 10-15 Kb consisting of repeated TTAGGG sequences followed by another guanine rich single stranded chain of about 200 nucleotides (nt) [13, 14]. The main functions of telomeres are to protect the chromosome ends from fraying and, to prevent chromosome fusion and chromosome degradation. Thus, they are providing chromosomal stability and genomic integrity [15-17]. Telomeres get shorten with each cell division at a rate of 50-150 base pairs due to incomplete replication at the 5'end by DNA polymerase. Such shortening creates a 3' overhang at the end of the telomeres [18-20]. And the continual shortening of telomeres beyond a certain length induces apoptosis, the programmed cell death [19, 21-23]. On the other hand, in the cancer cells, it has been observed that the shortening of telomeric DNA is impeded due to an active telomerase. Telomerase is a ribonucleic protein and is responsible for the elongation of the repetitive TTAGGG sequences. Telomerase is able to replicate $(TTAGGG)_n$ sequences which cannot be replicated by DNA polymerases in normal cells [24]. Hence, in cancer cells the apoptosis is hindered and the cancer cells continue to grow and divide. Recent studies have shown that telomerase is repressed in most normal somatic cells, meanwhile is upregulated in 85-90% of the cancer cells, providing them a rapid proliferative activity [17, 22, 25, 26]. In fact, since most somatic cells in our bodies do not show any or show very low levels of telomerase activity, targeting and selectively inactivating telomerase became one of the

commonly accepted strategies in cancer research [16, 25]. A visual of the difference in the cell division processes between a normal somatic cell and a cancer cell is shown in Figure 1.

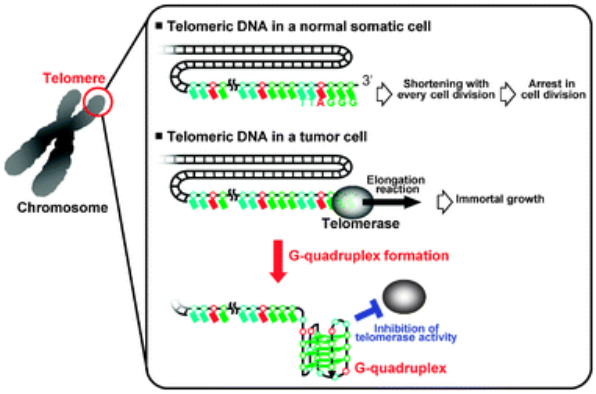

Figure 1: Telomeric DNA. *(Retrieved from Yaku et. al., 2012)*

1.4. G-quadruplex Structures

One of the accepted approaches in inhibiting telomerase-telomeric DNA interactions is either to drive the formation of G-quadruplex structures and/or to increase their stability using small molecules in the guanine rich regions [12, 27-30]. G-quadruplex structures are formed when the guanine-rich DNA sequences spontaneously fold into four stranded DNA structures [21]. Folding results in the planar arrangement of four guanines called G-quartets and the stacking of two or more G-quartets results in the formation of G-quadruplex structures (Figure 2) [31]. A G-quartet is the result of the association of four Guanine bases through Hoogsten hydrogen-bonding, while G-quadruplex is formed by the stacking of G-quartets on top of each other, creating a four-stranded helical chain, with an occurrence of four equivalent phosphate grooves with the three TTA loops on the sides [14, 23]. G-quartet stacking is stabilized by both the coordination of positively charged monovalent cations with electronegative oxygen atoms in the center of the channel,

and the π-π interactions between G-quartets [18, 20, 23, 32-34]. The structures of a G-quartet and G-quadruplex are shown in the Figure 2.

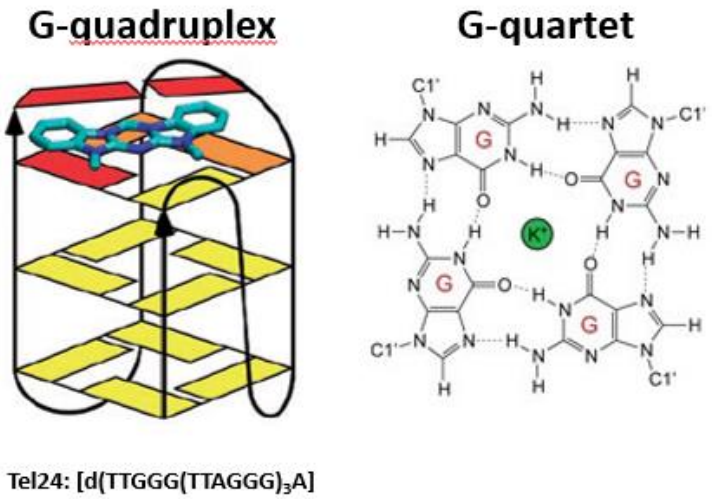

Figure 2: Left: Schematic representation of the G-quadruplex forming tel24 structure based on NMR studies (pdb id code: 2GKU), and the binding of Azamethyl to tel24. Right: The structure of a G-quartet. (Retrieved from Persil Çetinkol et.al., 2008)

Genome-wide analyses have revealed that guanine rich sequences are present in human genome, particularly at the end of the chromosomes, telomeres, and in the promoter regions of c-MYC, c-KIT, VEGF, HIF-1α, RET, PDGF-A, c-MYB, BCL-2, h-TERT, K-Ras, and YY1 genes [10, 33-35]. They appear to be emerging at non-random, very strategic locations in the genome, and it is believed that they play an important role, correlating with their function, in regulating multiple biological processes such as, replication and transcription [14]. Usually, our DNA is packaged into chromatins in the double helical form. However, ds-DNA can be converted into single-stranded DNA during DNA replication, transcription, and repair processes. Compared to double-stranded DNA or RNA hairpin structures, G-quadruplex are more thermodynamically stable, therefore they less likely to unfold with their slow kinetics. Due to their stability, the presence of G-quadruplex structures, might have

serious negative effects on DNA and RNA metabolism, so that their formation must be regulated [14].

Existence of a G-quadruplex structure in the proximity of a promotor region of an oncogene can lead to downregulation of the gene expression [36]. For example, Kota et. al. measured the recQ transcription by stabilizing the G-quadruplex formation region with TmPyP4, and they observed ~5-fold downregulation of recQ transcription than the control group [36]. There is another example that the Nucleolin phosphoprotein has high binding affinity to DNA G-quadruplexes, and when Nucleolin binds to the G-quadruplex structures in aborted RNA transcripts, the RNA processing is perturbed and encountering with the nucleolar stress, resulted in a neurodegenerative disorder [14]. In another study, it is stated that the stabilization of G-quadruplex structure of the preS2/S promoter by BRACO19 leads to the enhancement of the promoter activity, meaning that the presence of G-quadruplex motif in this promoter region has a positive regulatory effect on transcription of preS2/S [37].

1.5. Small Molecules Targeting G-quadruplex Structures

The binding of a small molecule to a G-quadruplex structure occurs mostly in three distinct modes; by ligand intercalation, external stacking, or groove-binding. Intercalation is observed as the result of the insertion of the ligand into the interspace of two consecutive G-tetrads. Due to the G-quartets being coordinated by positively charged cations, it is suggested that ligand intercalation can occur only in-between the two consecutive G-quartets, and only occur by displacing the cation [18]. External stacking is observed due to the stacking of the ligand having π-delocalization systems onto the ends of the G-quadruplex through the π-π stacking interactions. Groove or loop binding is observed as a result of the binding of the ligand to the grooves or loops of the G-quadruplex mostly through the electrostatic interactions and H-bonding [18, 23, 38].

Many small molecules targeting G-quadruplex structures have been discovered in the last two decades. Some of these molecules are quarfloxin, TMPyP4, telomestatin, Quindoline, Braco-19, BIBR1532 and CX-5461 (Figure 3) [11, 26, 39-42].

Quarfloxin is one of the first molecules that have been examined in clinical trials due to its binding ability to G-quadruplex structure, and disruption of G-quadruplex-nucleolin complexes. Unfortunately, it was not able to pass phase 2 of the clinical trials due to the lack of bioavailability [23, 33, 43]. TMPyP4 is one of the most investigated molecules that is binding to G-quadruplexes, mainly due to its high binding affinity. In addition, its molecular size, planar structure, positive charge, and hydrophobicity makes it an ideal drug candidate. The symmetric cyclic fused ring structure of TMPyP4 similar to telomestatin is thought to provide very favorable stacking interactions with the G-quartets. However, it was revealed that the selectivity of TMPyP4 towards G-quadruplex structures is low mainly due to the high positive charge on it. The selectivity of telomestatin to G-quadruplexes compared to duplex DNA is also found to be low [20, 23, 33, 43]. Quindoline is another molecule that is known to be stabilizing the G-quadruplex structure in c-MYC promoter region, and it acts as an inhibitor in the carcinoma cell line linked to the c-MYC gene. C-MYC gene encodes the transcription factors which regulate the cell proliferation, differentiation and apoptosis. In cancer cells, the over-expression of this gene is generally encountered. And so, targeting the G-quadruplex structures formed in the c-MYC sequence can be an effective strategy in cancer treatment [33, 38]. Interestingly, it had been shown that Quindoline binds to the two ends of the G-quadruplex forming c-MYC sequence with different affinities due to different hydrophobic/hydrophilic interactions at the physiological salt conditions. It had been also shown that, the binding of Quindoline increases the stability of G-quadruplex structure [33, 38]. Braco-19 is another promising small molecule, which had been shown to be binding to the G-quadruplex structures with high affinity. The nitrogen atom in Braco-19's structure can be protonated at physiological conditions, making it an electron deficient

structure that is more likely to interact with G-quadruplex structures. Braco-19 also binds to G-quadruplex mainly through π-π interactions and it acts as a telomerase inhibitor. Although, Braco-19 has higher affinity towards G-quadruplex DNA than duplex DNA in addition to its high solubility in aqueous solutions, it is not pharmacologically applicable due to its low permeability across biological barriers [20, 23, 33, 43, 44]. Another telomerase targeting drug molecule, BIBR1532, specifically binds to the hydrophobic pocket of catalytic subunit on the outer surface of telomerase, disrupts the DNA binding pocket, and hinders telomerase binding to telomeric DNA. BIBR1532 is proved to have antiproliferative effect on leukemia cells with no effect on normal cells. The treatment of leukemia cells with BIBR1532 resulted in a telomere shortening, loss of telomerase activity, and cell-cycle arrest within several weeks. It is known that it also functions as an adjunctive agent, which refers to a substance used in addition to the primary therapy. There are several studies that BIBR1532 was used in combination with chemotherapeutic drugs, such as paclitaxel, carboplatin and doxorubicin, in order to decrease drug resistance, enhance clinical activity and provide a synergistic effect for the elimination of cancer cells. It was also reported that the combination may lead to reduced toxicity [22, 45-47]. As a selective G- quadruplex stabilizer, CX-5461 blocks the replication forks, damages DNA by induction of ssDNA gaps and breaks, creates genomic instability, and leads to lethality. The binding of CX-5461 interferes with the interactions of rDNA G-quadruplex structures and nucleolin protein. As a result, the transcription process is inhibited, followed by the induction of the apoptosis in the cancer cells, including the drug-resistant myeloma cells. Currently, it is in phase I trials for hematologic malignancies [48-50].

In brief, there is a worldwide interest to design and develop more selective and effective small molecules with minimum side-effects and cytotoxicity. It is believed that, using small molecule inhibitors is still a convenient and an effective option for cancer treatment [14, 16, 51]. Some of the criteria in design of a small molecule as an ideal drug candidate molecule are based on its structural features, such as its molecular

size, shape, charge, hydrophobicity, planarity, and surface area. Small molecules targeting nucleic acids are mostly planar molecules bearing at least one positive charge with a large surface area. Having a large surface area with an aromatic core increases the π-π interactions between the small molecule and nucleic acid bases. The molecules having a V-shaped structure are also more likely to show better binding ability. The positive charge on the molecule increases the solubility in water, enhances the electrostatic interactions between the molecule and the negatively charged phosphate groups of the backbone of the nucleic acid structure. The binding affinity of these molecules to the G-quadruplexes is also usually high, while their selectivity towards different nucleic acid structures is deprived. The positive charge on these molecules promotes the binding to not only to G-quadruplex structure but also to all other DNA sequences. The narrow grooves of DNA sequences have strong affinity towards the positive charges of the cations. Thus, the high positive charge increases the non-specific binding of the small molecule to all negatively charged nucleic acid structures in the cells [10, 16, 20, 23, 27-30, 42, 44]. Due to these non-specific interactions between the small molecules and the duplex DNA, which is found in every cell whether it is cancer cell or not, the cytotoxicity emerges for these molecules [23]. The purpose of the telomerase targeting with therapeutic drugs is to achieve an induction of apoptosis and cell death only in tumor cells, where the telomerase is active [22]. And today, there is still a need for the design of new molecules that are selective G-quadruplex binders which are less toxic.

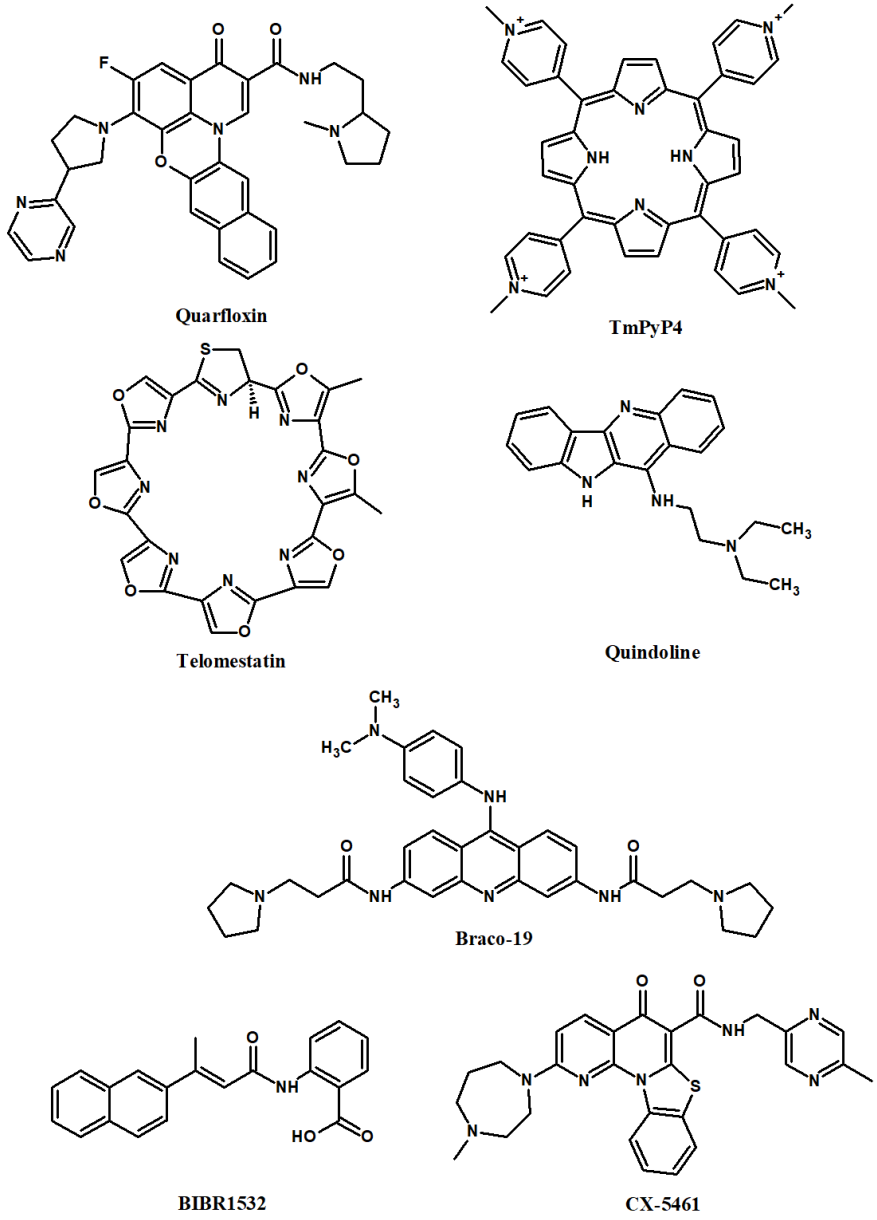

Figure 3: The structures of drugs and drug candidate molecules that bind to G-quadruplex.

1.6. Benzimidazoles and Azamethyl (Aza3)

Benzimidazole is an important scaffold in medicinal chemistry. It is one of the mostly used aromatic ring structures in the design and synthesis of active pharmaceutical ingredients [52-58]. Active pharmaceutical ingredients containing the

benzimidazole ring are used to treat various diseases as anthelmintic, antifungal, antiallergic, antimicrobial and antiviral [59-62]. In addition, benzimidazoles are also commonly used as biological chemical sensors due to their fluorescent light emitting capability [63-65]. It is evident that the ligands with the appropriate modifications in the benzimidazole ring are sufficient and effective binders of G-quadruplex DNA [23]. Targeting G-quadruplexes with benzimidazoles provides also an opportunity for the treatment of cancer, due to the possible stabilization of a G-quadruplex structure and inhibition of the telomerase activity in cancer cells [12, 29, 59-62].

Azamethyl (also known as Aza3) is a benzimidazole derivative, is known to bind to G-quadruplex structures selectively and with high affinity [66]. It was first synthesized by Kurth and his group to regulate the ion channels [67-68]. It had been discovered that Azamethyl molecule binds to tel24 [d(TTGGG(TTAGGG)$_3$A)] and tel26 [d(AAAGGG(TTAGGG)$_3$AA) which are human telomeric sequences forming G-quadruplex structures with high selectivity compared to dsDNA [66]. The benzimidazole rings in its structure are thought to provide π-π interactions with the guanine bases, and therefore help to increase the stability of the quadruplex structure. NMR analysis confirmed that Azamethyl molecule binds between the top of the G-quadruplex and A:T base pair which is found in the loop of the G-quadruplex via intercalation as shown in Figure 4. In intercalation, the planar aromatic small molecule stacks in between the base pairs. The π-π stacking interactions between the aromatic ring of the small molecule and the adjacent bases are the major driving force in intercalation of small molecules [69]. In Persil Çetinkol et. al., Azamethyl molecule, named 7H-1,13-Dimethyldibenzimidazolo [1,2-a:2',1'-d] [1,3,5]-triazin-6-ium, had been found to be binding to tel24 [d(TTGGG(TTAGGG)$_3$A)] with $K_a = 1.28x10^6$ M^{-1}, and to duplex DNA, dd1, [d(GCGCATATATGCGC)] with $K_a = 6.13x10^3$ M^{-1}.This result indicates that the selectivity of Azamethyl against G-quadruplex structure was ~200 times higher than its selectivity against the duplex DNA structure. Such selectivity is great for being considered as a potential drug candidate for selective targeting of quadruplexes [66]. However, its binding affinity needs to be improved.

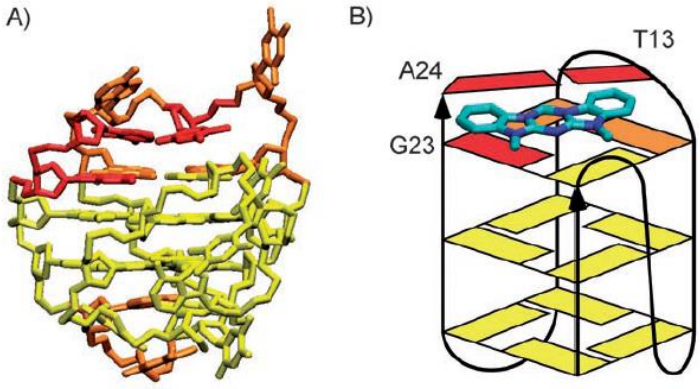

Figure 4: Tel24 structure (A) The structure of tel24 nucleic acid sequence analyzed by NMR in the solution (PDB code: 2GKU) (B) Schematic representation obtained by NOE experiments of Azamethyl molecule which is bound to tel24 (Persil Çetinkol et. al., 2008).

Azamethyl can also be considered as a potential drug candidate molecule due to solely to its structure. According to Lipinski's rule, an ideal drug molecule should have a molecular weight less than 500 Daltons, heteroatoms capable of acting as H-donors/acceptors, in specific there should be no more than 5 H-bond donors and no more than 10 H-bond acceptors, and high solubility in water, in particular the lipophilicity parameter, logP, should be not greater than 5 [23, 70]. Drug candidate molecules are more likely to fail if they have high molecular weights (>500 daltons) and excessive lipophilicity [71]. The small size of a molecule provides freedom of movement to the molecule through the extracellular plasma membrane, and ability to interact with cell-surface ligand-binding receptors, and intracellular signaling proteins, including anti-apoptotic proteins [44, 72]. Azamethyl is moderately soluble in water with a molecular weight of around 300 Daltons [66].

1.7. Scope of the Thesis

Within the scope of this thesis, five new benzimidazole derivative compounds were synthesized, characterized and their interactions with human telomeric DNA

sequence - tel24 were investigated. The main purpose of this thesis is to discover new anti-cancer candidate molecules that are binding tightly and selectively to a G-quadruplex forming human telomeric DNA sequence, tel24. We hypothesized derivatives of Azamethyl, bearing a longer or a bulkier chain in the benzimidazole ring might have a higher affinity towards tel24. We anticipated that as the chain length or branching increases, the noncovalent interactions between the small molecule and the quadruplex would increase and result in higher association constants. Therefore, in order to understand the effect of the chain length and branching on the benzimidazole ring on the binding affinity of azacyanines to tel24, here, we synthesized Azaethyl, Azapropyl, Azaisopropyl, Azabutyl and Azaisobutyl in addition to the Azamethyl and investigate their interactions with tel24 using UV-VIS, CD and Fluorescence Spectroscopy [53, 55-58, 73-78].

CHAPTER 2

MATERIALS AND METHODS

2.1. Materials

The starting materials; 1-methyl-1H-benzimidazole-2-ylamine ($C_8H_9N_3$), 1-ethyl-1H-benzimidazole-2-ylamine ($C_9H_{11}N_3$), 1-isopropyl-1H-benzimidazole-2-ylamine ($C_{10}H_{13}N_3$), 1-butyl-1H-benzimidazole-2-ylamine ($C_{11}H_{15}N_3$), 1-isobutyl-1H-benzimidazole-2-ylamine ($C_{11}H_{15}N_3$) were purchased from Sigma Aldrich (Europe) and ABCR (Germany), and 1-propyl-1H-benzimidazole-2-ylamine ($C_{10}H_{13}N_3$), was purchased from Ark Pharm (USA). Tel24 ([d(TTGGG(TTAGGG)$_3$A)]) oligonucleotide was purchased from Integrated DNA technologies, IDT (Europe). The other reagents used during the synthesis; Acetonitrile (CH_3CN), diiodomethane (CH_2I_2), dichloromethane (CH_2Cl_2), acetone (C_3H_6O), dimethyl sulfoxide (C_2H_6OS), deuterated dimethyl sulfoxide (C_2D_6OS), methanol (CH_3OH), ethyl acetate ($C_4H_8O_2$), and liquid vaseline were purchased from Sigma Aldrich (Europe).

2.2. Methods

2.2.1. Synthesis and Characterization of Azacyanines

The synthesis of the azacyanine compound bearing the methyl chain in the benzimidazole ring, named as Aza3 or Azamethyl, had been reported previously by Huang et. al. and Persil Cetinkol et. al. [66, 68]. Here, the previously reported synthesis method was adopted. Briefly, diiodomethane was added to 1-R-1H-benzimidazole-2-ylamine dissolved in acetonitrile in 5/5.6 molar ratio under reflux conditions, in an oil bath, at a temperature of 80 – 85˚C under N_2 gas. The mixture

was refluxed for 5 to 24 hours, depending on the starting material. After reflux, the solution was cooled down and filtered. The precipitate was washed with dichloromethane (CH_2Cl_2) and acetone (C_3H_6O). The characterization of all the compounds investigated here, were recently published in Tutuncu et. al. [79]. The 1-R-1H-benzimidazole-2-ylamine starting materials used in this study are given in Figure 6.

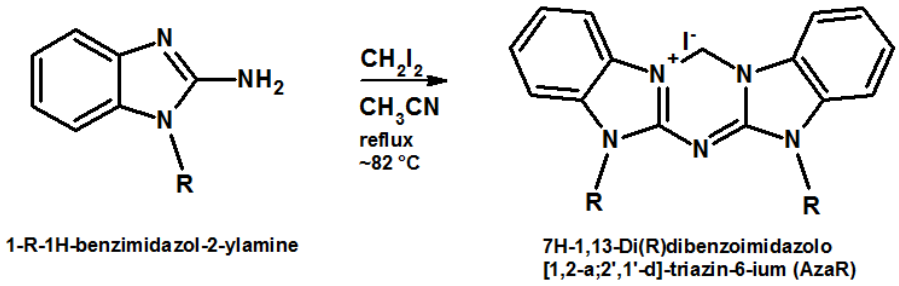

Figure 5: Synthesis of azacyanines.

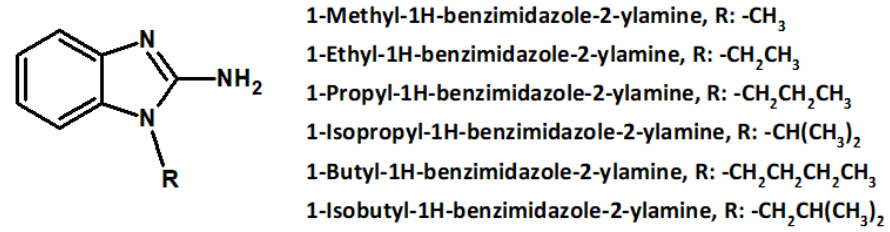

Figure 6: Structures of the starting materials used in azacyanine synthesis.

2.2.1.1. Azamethyl (Aza3)

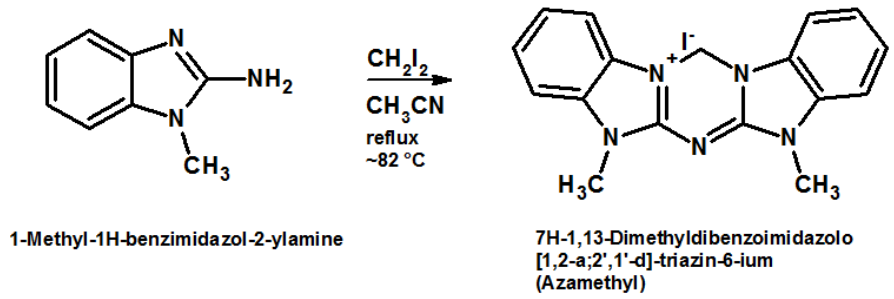

Figure 7: Synthesis of Azamethyl.

0.8 g of 1-methyl-1H-benzimidazole-2-ylamine was dissolved in 20 ml of acetonitrile and 3.0 g (902.0 µl) diiodomethane was added into it. The reaction mixture was refluxed at about ~82˚C for 5 hours. Once the solution was cooled down, the precipitate was filtered and washed with 15 ml of dichloromethane followed by 15 ml of acetone. The white product obtained as the precipitate was dried in oven at 50˚C. The yield of the reaction was 34%.

The ^{1}H NMR spectra given in Figure 16 are clean for both the starting material and the product. The peaks are as follows; for Azamethyl starting material (1-methyl-1H-benzimidazole-2-ylamine); 1H NMR (400 MHz, DMSO-d6) δ 3.51 (3H), 6.58 (2H), 6.90 (1H), 6.96 (1H), 7.11 (1H), 7.16 (1H) ppm; ^{13}C-NMR δ 28.3, 107.0, 114.7, 117.9, 120.2, 134.8, 142.7, 155.5 ppm; and for Azamethyl product (7H-1,13-dimethyldibenzimidazolo [1,2-a:2',1'-d][1,3,5]-triazin-6ium); ^{1}H NMR (400 MHz, DMSO-d_6) δ 3.82 (6H), 6.54 (2H), 7.50 (4H), 7.61 (2H), 7.74 (2H) ppm; ^{13}C-NMR δ 34.0, 44.8, 62.0, 115.2, 116.2, 129.4, 129.7, 129.7, 132.6, 136.1, 154.0 ppm.

2.2.1.2. Azaethyl

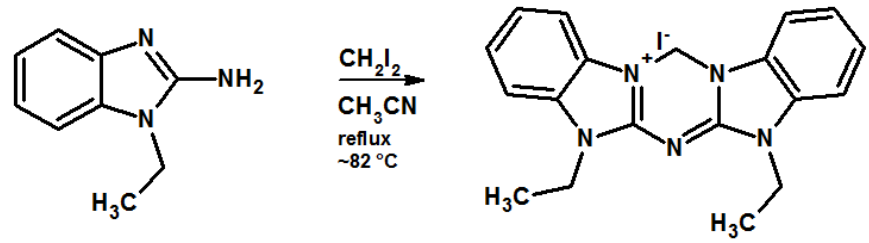

1-Ethyl-1H-benzimidazol-2-ylamine

7H-1,13-Diethyldibenzoimidazolo [1,2-a;2',1'-d]-triazin-6-ium (Azaethyl)

Figure 8: Synthesis of Azaethyl.

1.8 g of 1-ethyl-1H-benzimidazole-2-ylamine was dissolved in 25 ml of acetonitrile. 1010 µl of diiodomethane was added to the reaction mixture. The mixture was refluxed at ~82˚C for 7 hours. A brownish waxy liquid was obtained at the end of the reaction. The waxy product was confirmed as the desired product by quick ^{1}H NMR analysis. The waxy product was precipitated by dropwise addition of it into the ice-cold ethyl acetate. The product obtained as the precipitate was filtered and dried in oven. The amount of the product obtained was 687 mg, indicating 28% yield for the reaction. The ethyl acetate of the filtrate was evaporated using a Rotary Evaporator (Heidolph Laborota 4002), and the ^{1}H NMR analysis of the remnant solid revealed the presence of the product in the filtrate solution. The remnant solid was redissolved in ethyl acetate and the solution was let sit at -20˚C overnight. The precipitate was filtered, washed with acetone to get rid of the impurities, and dried in oven at 50˚C. The amount of the pure product obtained after precipitation was 340 mg.

The ^{1}H NMR spectra given in Appendix A Figure 29 are clean for both the starting material and the product. The peaks are as follows; for Azaethyl starting material (1-ethyl-1H-benzimidazole-2-ylamine); ^{1}H NMR (400 MHz, DMSO-d_6) δ 1.19 (3H), 4.00 (2H), 6.48 (2H), 6.88 (1H), 6.93 (1H), 7.13 (2H) ppm; ^{13}C-NMR δ 14.0, 36.2, 107.4, 114.5, 118.1, 120.2, 133.6, 142.5, 154.4 ppm; for Azaethyl product

(7H-1,13-diethyldibenzimidazolo [1,2-a:2',1'-d][1,3,5]-triazin-6ium); ^{1}H NMR (400 MHz, DMSO-d_6) δ 1.42 (6H), 4.37 (4H), 6.55 (1H), 7.50 (H), 7.65 (2H), 7.82 (2H) ppm; ^{13}C-NMR δ 13.6, 37.4, 56.9, 110.0, 110.2, 111.0, 124.0, 124.4, 127.5, 129.4, 148.2 ppm. UV-Vis (DMSO): λmax (ε) = 343 nm (44700 M^{-1}); HRMS (ESI+): m/z (%): calculated for [$C_{19}H_{20}N_5^+$] 318.3956, found 319.1789; elemental analysis calculated (%) for $C_{19}H_{20}N_5I$: C 51.25, H 4.53, N 15.73; experimental: C 50.57, H 4.43, N 16.16. Yield 28%.

2.2.1.3. Azapropyl

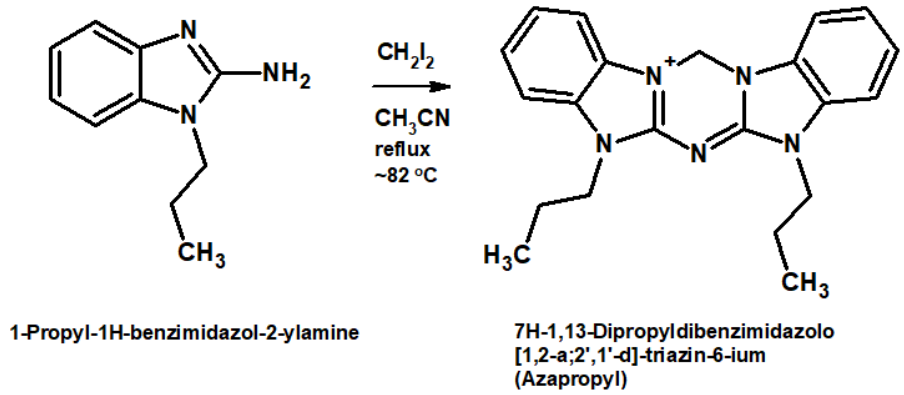

Figure 9: Synthesis of Azapropyl.

0.981 g of 1-propyl-1H-benzimidazole-2-ylamine was dissolved in 20 ml of acetonitrile. 505 µl of diiodomethane was added to the solution. Solution was refluxed at ~82˚C for 5 hours. The reaction mixture was analyzed by UV-Vis and both the starting material and the product were detected in the spectra. The product in the reaction mixture was precipitated by mixing the reaction mixture with ice-cold ethyl acetate and letting it to sit at -20˚C overnight. The precipitate was filtered and dried in oven at 50˚C overnight. 0.614 g Azapropyl was obtained at the end of the process, indicating 46 % yield for the reaction.

The ^{1}H NMR spectra given in Appendix A Figure 32 are clean for both the starting material and the product. The peaks are as follows; for Azapropyl starting material (1-propyl-1H-benzimidazole-2-ylamine); ^{1}H NMR (400 MHz, DMSO-d6) δ 1.47 (6H), 4.58 (1H), 6.29 (2H), 6.83 (1H), 6.91 (1H), 7.12 (1H), 7.30 (1H) ppm; ^{13}C-NMR δ 20.5, 45.4, 109.5, 115.0, 117.7, 119.8, 132.5, 143.2, 154.0 ppm; for Azapropyl product (7H-1,13-dipropyldibenzimidazolo [1,2-a:2',1'-d][1,3,5]-triazin-6ium); ^{1}H NMR (400 MHz, DMSO-d6) δ 0.95 (6H), 1.88 (4H), 4.29 (1H), 6.53 (2H), 7.49 (4H), 7.62 (2H), 7.80 (2H) ppm; ^{13}C-NMR δ 20.0, 21.4, 43.8, 57.1, 110.2, 111.0, 124.0, 124.3, 127.2, 130.2, 148.6 ppm. UV-Vis (DMSO): λmax (ε) = 343 nm (43300 M^{-1}); HRMS (ESI+): m/z (%): calculated for [$C_{21}H_{24}N_5$+] 346.4488, found 346.2040; elemental analysis calculated (%) for $C_{21}H_{24}N_5I$: C 53.28, H 5.11, N 14.80; experimental: C 52.25, H 5.07, N 14.53. Yield 46%.

2.2.1.4. Azaisopropyl

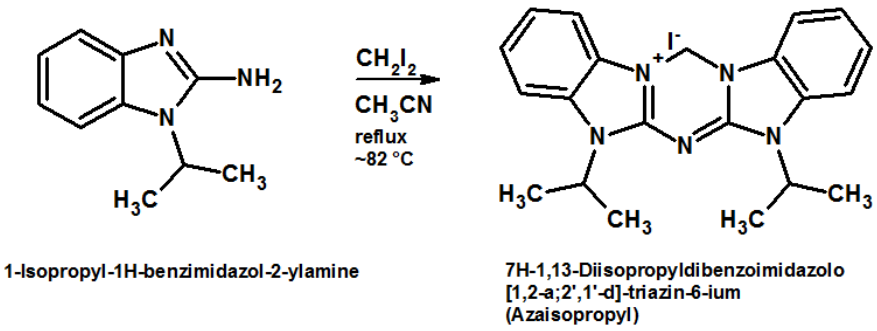

Figure 10: Synthesis of Azaisopropyl.

1.80 g of 1-isopropyl-1H-benzimidazole-2-ylamine was dissolved in 20 ml of acetonitrile. 930 µl of diiodomethane was added to the reaction mixture. The mixture was refluxed at ~82˚C for 5 hours. The liquid product was precipitated in 60 mL ethyl acetate, and let sit at -20˚C overnight. Ethyl acetate was taken out by using a pipette and the product obtained was dried in oven at 50˚C. The product was further washed

with acetone to get rid of impurities and redried. 1286 mg Azaisopropyl product was collected, meaning 53 % yield.

The ^{1}H NMR spectra given in Appendix A Figure 35 are clean for both the starting material and the product. The peaks are as follows; for Azaisopropyl starting material (1-isopropyl-1H-benzimidazole-2-ylamine); ^{1}H NMR (400 MHz, DMSO-d_6) δ 1.47 (6H), 4.58 (1H), 6.29 (2H), 6.83 (1H), 6.91 (1H), 7.12 (1H), 7.30 (1H) ppm; ^{13}C-NMR δ 20.5, 45.4, 109.5, 115.0, 117.7, 119.8, 132.5, 143.2, 154.2 ppm; for Azaisopropyl product (7H-1,13-diisopropyldibenzimidazolo [1,2-a:2',1'-d][1,3,5]-triazin-6ium); ^{1}H NMR (400 MHz, DMSO-d_6) δ 1,66 (6H), 5.13 (1H), 6.51 (1H), 7.49 (2H), 7.62 (1H), 7.90 (2H) ppm; ^{13}C-NMR δ 19.9, 47.3, 56.5, 110.0, 112.0, 123.9, 124.2, 127.5, 129.0, 147.6 ppm. UV-Vis (DMSO): λmax (ε) = 343 nm (45100 M^{-1}); HRMS (ESI+): m/z (%): calculated for [$C_{21}H_{24}N_5^+$] 346.4488, found 347.2105; elemental analysis calculated (%) for $C_{21}H_{24}N_5I$: C 53.28, H 5.11, N 14.80; experimental: C 52.34, H 4.90, N 15.11. Yield 53%.

2.2.1.5. Azabutyl

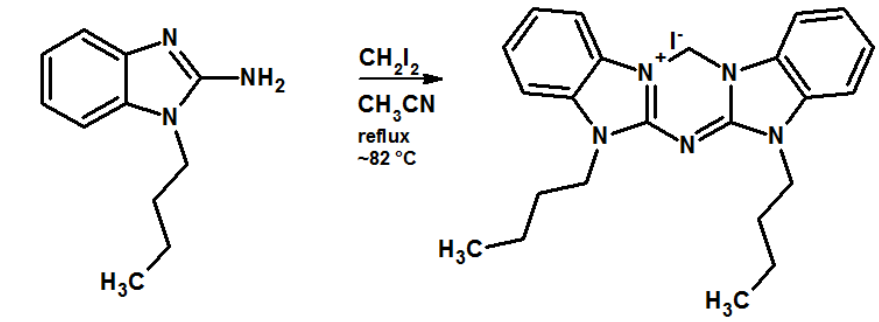

Figure 11: Synthesis of Azabutyl.

947 mg of 1-butyl-1H-benzimidazole-2-ylamine was dissolved in 20 ml of acetonitrile and 500 µl diiodomethane was added into the reaction mixture. The reflux was performed at ~82˚C for 25 hours. No product formation was observed during the reflux. However, the formation of crystals was observed when the mixture was let to cool down. However, when the solution was filtered, and the crystals were washed away with chloroform and passed into the filtrate. UV-VIS absorbance measurements on the filtrate revealed the presence of the desired product in the filtrate. Acetonitrile and chloroform in the filtrate were evaporated using Rotary Evaporator under vacuum. A waxy liquid was obtained as the end product at the end of the evaporation. ^{1}H-NMR analysis of the waxy liquid confirmed the presence of the desired product. The waxy liquid was redissolved in acetonitrile and added by dropwise into chilled ethyl acetate in order to precipitate the product. The solution was let sit at -20˚C overnight. The mixture was filtered the next morning and the precipitate was dried in oven at 50˚C. At the end, 0.79 g of the product was obtained, meaning 63% yield.

The ^{1}H NMR spectra given in Appendix A Figure 38 are clean for both the starting material and the product. The peaks are as follows; for Azabutyl starting material (1-butyl-1H-benzimidazole-2-ylamine); ^{1}H NMR (400 MHz, DMSO-d_6) δ 0.88 (3H), 1.29 (2H), 1.60 (2H), 3.95 (2H), 6.37 (2H), 6.88 (2H), 6.97 (2H) ppm; ^{13}C-NMR δ 13.8, 19.3, 30.6, 41.2, 107.4, 114.7, 117.9, 120.0, 134.2, 142.7, 154.7 ppm; for Azabutyl product (7H-1,13-dibutyldibenzimidazolo [1,2-a:2',1'-d][1,3,5]-triazin-6ium); ^{1}H NMR (400 MHz, DMSO-d_6) δ 0.95 (6H), 1.39 (4H), 1.84 (4H), 4.33 (4H), 6.57 (2H), 4.49 (4H), 7.67 (2H), 7.70 (2H) ppm; ^{13}C-NMR δ 13.4, 19.1, 29.9, 42.0, 57.3, 110.2, 111.0, 124.0, 124.4, 127.3, 130.0, 148.6 ppm. UV-Vis (DMSO): λmax (ε) = 343 nm (44000 M^{-1}); HRMS (ESI+): m/z (%): calculated for [$C_{23}H_{28}N_5$+] 374.5019, found 374.2300; elemental analysis calculated (%) for $C_{23}H_{28}N_5I$: C 55.09, H 5.63, N 13.97; experimental: C 53.84, H 5.88, N 14.77. Yield 63%.

2.2.1.6. Azaisobutyl

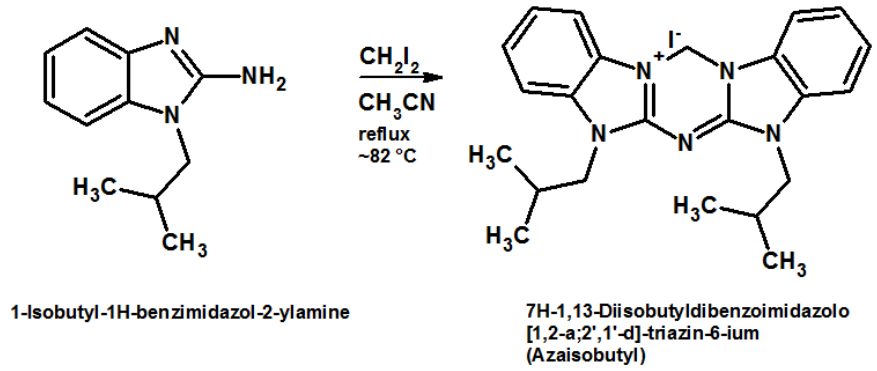

1-Isobutyl-1H-benzimidazol-2-ylamine

7H-1,13-Diisobutyldibenzoimidazolo [1,2-a;2',1'-d]-triazin-6-ium (Azaisobutyl)

Figure 12: Synthesis of Azaisobutyl.

1.61 g of 1-isobutyl-1H-benzimidazole-2-ylamine was dissolved in 25 ml of acetonitrile and 900 µl of diiodomethane was added to the reaction medium. The solution was refluxed at ~82˚C for 24 hours. At the end of reflux, the solution was cooled down and filtered. The precipitate was dried in oven at 50˚C overnight. The product obtained through filtration was not pure based on ^{1}H NMR, and therefore, it was recrystallized in 20.0% methanol solution. 0.75 g of product was collected with 35% yield.

The ^{1}H NMR spectra given in Appendix A Figure 41 are clean for both the starting material and the product. The peaks are as follows; for Azaisobutyl starting material (1-isobutyl-1H-benzimidazole-2-ylamine); ^{1}H NMR (400 MHz, DMSO-d_6) δ 0.86 (6H), 2.10 (1H), 3.35 (1H), 3.77 (2H), 6.36 (2H), 6.85 (1H), 6.90 (1H), 7.11 (2H) ppm; ^{13}C-NMR δ 19.7, 27.8, 48.3, 107.7, 114.7, 117.7, 120.0, 134.6, 142.7, 155.1 ppm; for Azaisobutyl product (7H-1,13-diisobutyldibenzimidazolo [1,2-a:2',1'-d][1,3,5]-triazin-6ium); ^{1}H (400 MHz, DMSO-d_6) δ 1.00 (12H), 2.29 (2H), 4.13 (4H), 6.57 (2H), 7.49 (4H), 7.67 (2H), 7.80 (2H) ppm; ^{13}C-NMR δ 19.9, 27.8, 49.1, 57.1, 110.0, 111.2, 124.0, 124.4, 127.3, 130.4, 148.8 ppm. UV-Vis (DMSO): λmax (ε) = 343 nm (44700 M^{-1}); HRMS (ESI+): m/z (%): calculated for [$C_{23}H_{28}N_5^+$] 374.5019,

found 375.2410; elemental analysis calculated (%) for $C_{23}H_{28}N_5I$: C 55.09, H 5.63, N 13.97; experimental: C 54.18, H 5.80, N 14.04. Yield 35%.

2.2.2. Further characterization of Azacyanines

The five newly synthesized compounds were characterized by using elemental analysis and High-Resolution Mass Spectrometry (Waters SYNAPT G1 MS) methods. The molar absorptivity constants of all of the products in addition to the previously synthesized Azamethyl were determined by using UV-VIS spectroscopy at 343 nm.

Molar extinction coefficient of all the products were determined by using UV-VIS spectrophotometry. Briefly, five different amounts of the product were weighed in using an analytical balance and dissolved in DMSO to obtain sample solutions with five different concentrations. Each of the 5 samples was diluted into 6 different samples in ratios of 1/1.00, 1/1.25, 1/1.50, 1/1.75, 1/2.00, 1/2.25 and the UV-VIS spectra of each set (6 samples) between 190 nm and 1100 nm was collected using. For each solution, Absorption vs. Concentration plot was obtained. Linear regression was applied to this plot and the molar extinction coefficient was obtained using the Beer-Lambert Law at 343 nm. At the end, the molar extinction coefficient for a given compound was determined by averaging out the extinction coefficients obtained for all the five samples [66]. Extinction coefficients reported were used in determining the concentrations of solutions through all of our studies.

2.2.3. Sample Preparation for UV-VIS and CD Experiments

Two sets of tel24-azacyanine samples were prepared. The ratio of tel24 to azacyanines (tel24:azacyanine) was kept constant either as 1:1 or 1:6. The first sample set contained 2.5 μM azacyanine and 2.5 μM DNA in strand, and the second set contained 15.0 μM azacyanine and 2.5 μM DNA in strand for UV-VIS experiments.

Tel24:azacyanine samples in CD experiments were prepared at a tenfold higher concentration than the UV-VIS samples in order to have a higher signal to noise ratio. The concentration of azacyanine stock solutions were calculated using the experimentally determined extinction coefficients. The concentration of tel24 stocks were calculated using the extinction coefficients provided by the supplier. All the samples were prepared in 25 mM potassium phosphate buffer (pH 7.0) and 70 mM KCl, unless otherwise stated. Samples were annealed by heating to 95˚C for 5 minutes in a water bath and then cooling overnight to room temperature prior to each experiment.

2.2.4. Determination Binding Using Circular Dichroism Spectroscopy

CD spectra were acquired on a JASCO J-815 CD spectropolarimeter equipped with a Peltier temperature control unit. The CD spectra were collected from 240 nm to 400 nm at 5.0˚C at 200 nm/min scanning speed with 1.0 nm band width. 25 mM potassium phosphate pH 7.00 buffer and 70 mM potassium chloride were used as blank and all the CD spectra were baseline corrected.

2.2.5. Determination of Binding and Thermal Denaturation Temperatures Using UV-VIS Spectroscopy

Agilent HP 8454 UV-VIS diode array spectrophotometer equipped with an Agilent 89090A peltier was used in UV-VIS and thermal denaturation studies of tel24-azacyanine complexes. Both heating and cooling profiles were acquired as full spectra between 190 nm and 1100 nm from 15.0 to 95.0˚C in 1.0˚C steps with 1-minute hold time. The samples were heated from 15˚C to 95˚C with 1.0˚C/minute heating rate and a UV-VIS spectrum was collected at each 1˚C step between 190 nm and 1100 nm. All UV-VIS spectra were baseline corrected using 25 mM potassium phosphate pH 7.00

buffer solution with 70 mM potassium chloride. The melting curves were obtained from the Normalized Absorbance vs. Temperature plots at 290 nm.

2.2.6. Determination of Association Constants Using Fluorescence Spectroscopy

Binding constants of all azacyanines with tel24 were determined using Cary Eclipse Fluorescence spectrophotometer as previously described [66]. Fluorescence titrations were performed by making incremental additions of 50.0 μM tel24 stock solution containing 1.0 μM azacyanine into the sample containing only 1.0 μM azacyanine. After each titration, the Fluorescence spectrum was collected. Excitation wavelength of 324 nm was used, and the emission spectra were collected from 325 to 675 nm. Excitation slit was set to 2.5 nm and emission slit was set to 5.0 nm. Binding constants were obtained by fitting the integrated fluorescence intensity data between 335 nm and 600 nm as a function of DNA concentration using the least squares equations:

$$KC_b^2 - C_b(KS_0 + KD_0 + 1) + KS_0D_0 = 0$$

$$F = F_0(C_t - C_b) + F_bC_b$$

where K is the association constant in (M^{-1}), C_b is the concentration of bound ligand, S_0 is the total binding site concentration, C_t is the total concentration of small molecule, D_0 is the total ligand concentration, F is observed fluorescence at each titration point, F_0 is fluorescence intensity of the free small molecule, and F_b is the fluorescence of the bound species. Igor Pro software (Wavemetrics Inc, USA) was used in all of our data analysis. Data was obtained as an average of three replicates for each tel24:azacyanine titration.

CHAPTER 3

RESULTS AND DISCUSSION

3.1. Reaction Mechanism of the Synthesis of Azacyanines

The proposed plausible reaction mechanism of the synthesis is presented in Figure 13. There is a 2:1 stoichiometry between the starting materials and the products. First, the lone pairs of amine group induce the lone pair of the upper nitrogen to attack to diiodomethane. This is an S_N2 reaction, and a covalent bond forms between the nitrogen and the carbon, while one of the iodine atom leaves. Second, through the same induction another 1-alkyl-benzimidazole-2-ylamine attacks to the same carbon, and so the other iodine atom leaves. As a result, a bridge bonding two of the starting material compounds, 1-alkyl-benzimidazole-2-ylamine, to each other forms. Third, the free iodine atom in the medium takes a hydrogen from the positively charged nitrogen, and the formal charge on the nitrogen becomes zero. The lone pairs of the nitrogen attack the carbon atom in the imidazole ring resulting in the movement of the double bond electrons to the nitrogen. This step creates a six membered ring between the two starting materials. The amine group takes a proton from the medium and the lone pairs of the upper hydrogen join the ring resulting in the loss of ammonia. The positively charged product coordinates with the negatively charged iodine and forms a salt.

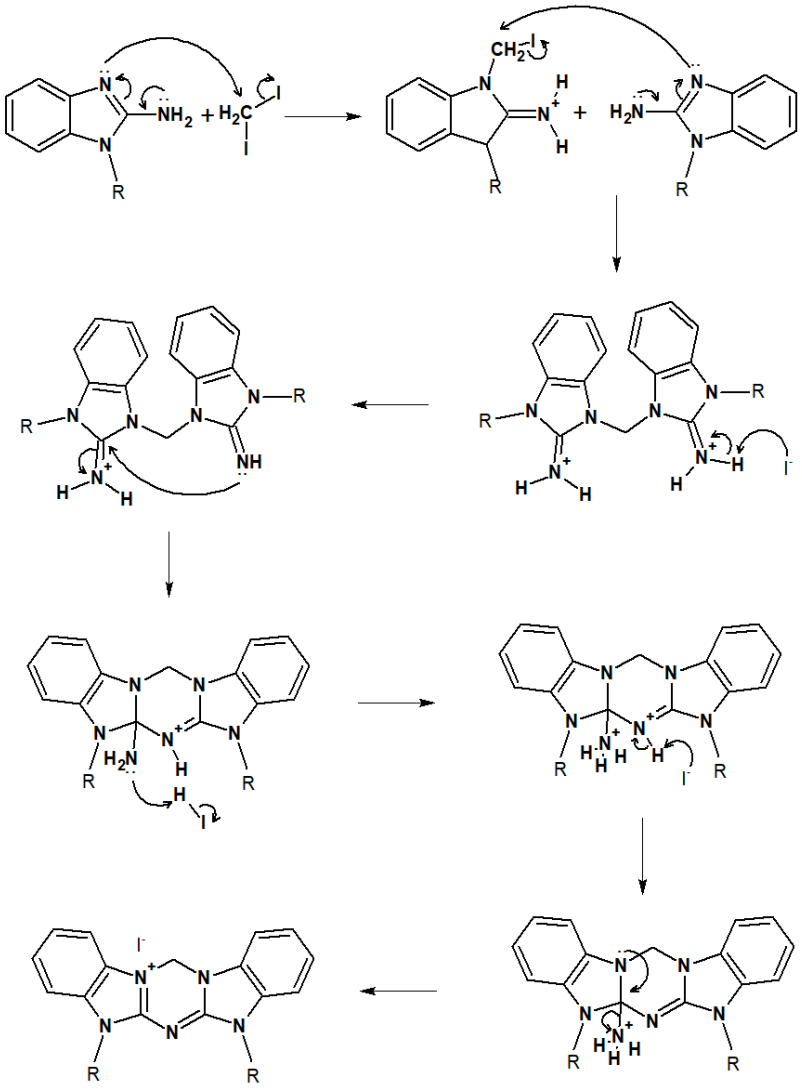

Figure 13: The proposed reaction mechanism of the synthesis.

3.2. The Comparison of 1H-NMR Spectra of Azamethyl and its Starting Material

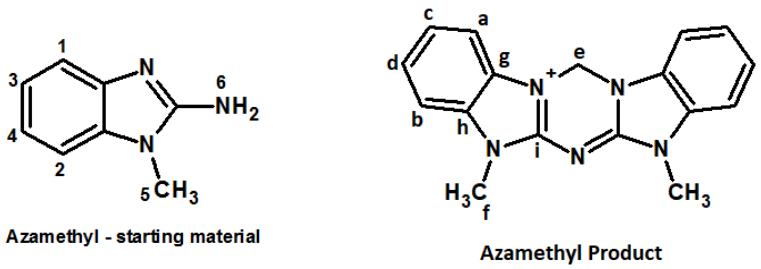

Figure 14: The structure of Azamethyl and its starting material, labeled for ^{13}C and ^{1}H NMR spectra.

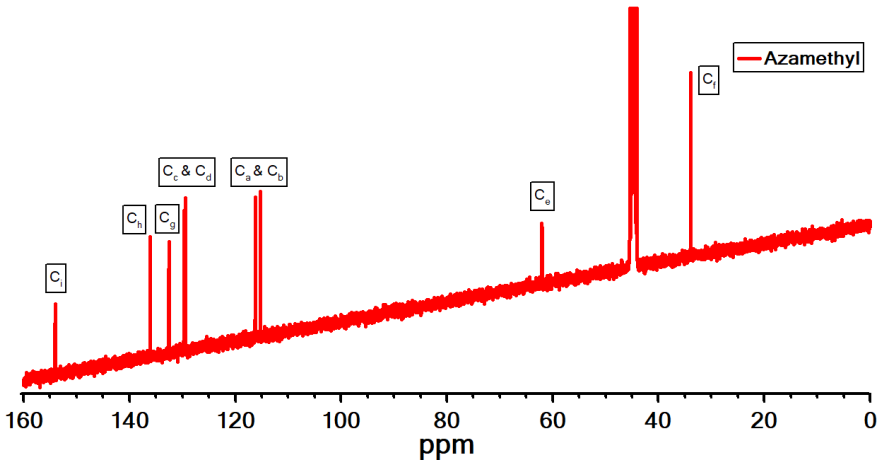

Figure 15: ^{13}C NMR spectrum of Azamethyl product dissolved in DMSO-D_6.

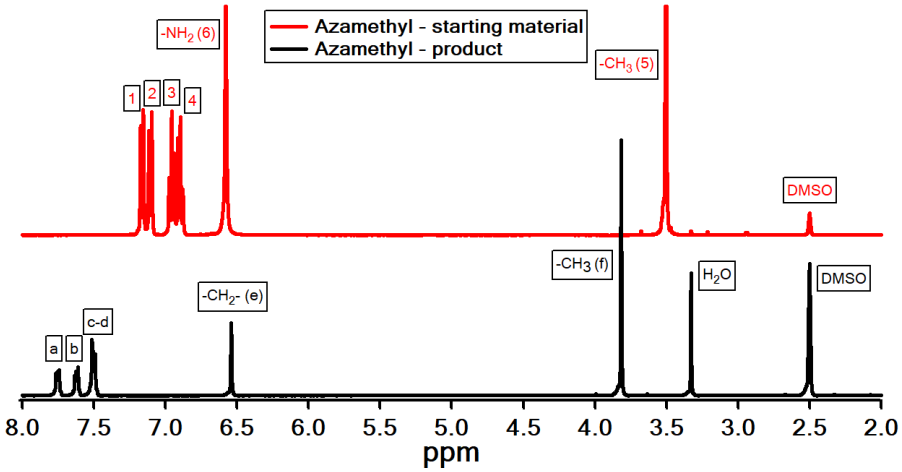

Figure 16: The comparison of ^{1}H NMR spectra of Azamethyl and its starting material dissolved in DMSO-D_6.

In Figure 16, ^{1}H-NMR spectrum of Azamethyl and its starting material were presented. The red line belongs to the starting material of Azamethyl; 1-methyl-1H-benzimidazole-2-ylamine, and the black line belongs to the product, Azamethyl. The hydrogens of the methyl group on the benzimidazole ring of starting material resonate at 3.51 ppm. It is obvious that in the ^{1}H-NMR spectrum of the product, that peak shifts to the downfield from 3.51 to 3.82 ppm, as well as the hydrogens on the aromatic ring shift from 6.9 – 7.1 to 7.5 – 7.7 ppm. These two characteristic shifts indicate the formation of the product. In addition, no peaks belonging to the starting material were observed in the ^{1}H-NMR spectrum of the product, meaning that the product formed was pure and could be isolated from the reaction medium. The ^{13}C and ^{1}H-NMR spectra of all the other products were given in the Appendix A.

3.3. Characterization of Azacyanines

Table 1: Elemental analysis, HRMS, molar absorptivity coefficients and yields of synthesis for Azacyanines.

Compound	*Chemical Formula*	*Elemental Analysis (Theoretical)*	*Elemental Analysis (Experimental)*	*M.Wt. (g/mol)*	*HRMS (50-1000 Da / ES+): m/z (%)*	*Molar Absorptivity Constant (M^{-1} at 343 nm)*	*Yield (%)*
Azamethyl (Aza3)	$C_{17}H_{16}N_5I$		-	417.25	-	42200	34
Azaethyl	$C_{19}H_{20}N_5I$	C 51.24, H 4.53, N 15.73	C 50.57, H 4.43, N 16.16	445.30	319.1789	44700	28
Azapropyl	$C_{21}H_{24}N_5I$	C 53.28, H 5.11, N 14.80	C 52.25, H 5.07, N 14.53	473.35	346.2040	43300	46
Azaisopropyl	$C_{21}H_{24}N_5I$	C 53.28, H 5.11, N 14.80	C 52.34, H 4.90, N 15.11	473.35	347.2105	45100	53
Azabutyl	$C_{23}H_{28}N_5I$	C 55.09, H 5.63, N 13.97	C 53.84, H 5.88, N 14.77	501.41	374.2300	44000	63
Azaisobutyl	$C_{23}H_{28}N_5I$	C 55.09, H 5.63, N 13.97	C 54.18, H 5.80, N 14.04	501.41	375.2410	44700	35

The elemental analysis and HRMS are consistent enough to decide the synthesized compounds are the desired compounds. The experimental and theoretical results of elemental analysis are within the ±5.0 % error range. For example, the experimental findings of the elemental analysis of Azaethyl are 50.57 % C, 4.43 % H, and 16.16 % N, while the theoretical results are 51.24 % C, 4.53 % H, and 15.73 % N, with -1.3%, -2.2%, and 2.7% error accordingly. Similarly, Azapropyl has -1.9% C, -0.8% H, and -1.8% N errors. Azaisopropyl has -1.8% C, -4.1% H, and 2.1% N errors. Azabutyl has -2.3% C, 4.5% H, and 5.7% N errors. Azaisobutyl has -1.7% C, 3.0% H, and 0.5% N errors. The errors of HRMS results are insignificant, <0.001.

3.4. Determination of Binding Using Circular Dichroism Spectroscopy

Circular Dichroism Spectroscopy is a method based on the difference in light absorption of the left and right handed circularly polarized incident light. A compound should be chiral to be CD active. DNA is chiral due to having chiral sugar units and CD Spectroscopy is one of the mostly used technique for investigating the DNA-drug binding interactions, because of the sensitivity of the CD signal to any variations on the conformation of DNA [80, 81].

Therefore, the interaction of azacyanines with tel24 is first investigated using CD spectroscopy in order to reveal the presence of the interactions between tel24 and azacyanines, in addition to reveal the changes in the secondary structure of tel24 (G-quadruplex structure) upon binding to tel24 [82]. The previous structural studies using NMR have shown that one Azamethyl was binding to one tel24 G-quadruplex structure between the top quartet and the A-T base pairing in the loop region. A second binding side was observed at the bottom of the quartet. However, binding to that site was very weak as it has not been observed in Fluorescence or SPR spectroscopy. Only one binding site was determined via fluorescence titrations and SPR measurements [59]. Therefore, in the current studies, first, 1:1 tel24:azacyanine complexes were investigated.

In Figure 17, the dotted black line represents the ellipticity of tel24 structure in the absence of azacyanines, the dotted red line represents the ellipticity of Azamethyl in the absence of tel24, and the straight black, yellow, purple, orange, red and green lines represent the ellipticity of tel24 in the presence of Azamethyl, Azaethyl, Azapropyl, Azaisopropyl, Azabutyl, and Azaisobutyl respectively. For simplicity only the CD spectrum of Azamethyl is given, since all of the other azacyanine compounds are achiral molecules, they do not exhibit any CD bands on the spectrum.

Azamethyl (red dotted line) is not a chiral molecule and as expected do not give rise to any signal in the CD spectrum. On the other hand, tel24 (dotted black line) by itself give rise to a peak between 270 nm and 310 nm in tel24 spectrum. On the other hand, a very weak peak, called the induced CD band , was observed between 320 nm and 360 nm in the CD spectra of all tel24:azacyanine 1:1 complexes. The induced CD band, which is formed due to the induction of chirality in small molecule upon tel24 binding, confirms that all the azacyanines were interacting with tel24 (Figure 17). The shapes of the induced CD bands were similar in all azacyanines with two absorbance maximums at around 330 nm and 342 nm. The intensity of the induced CD band showed slight variation between azacyanines [82].

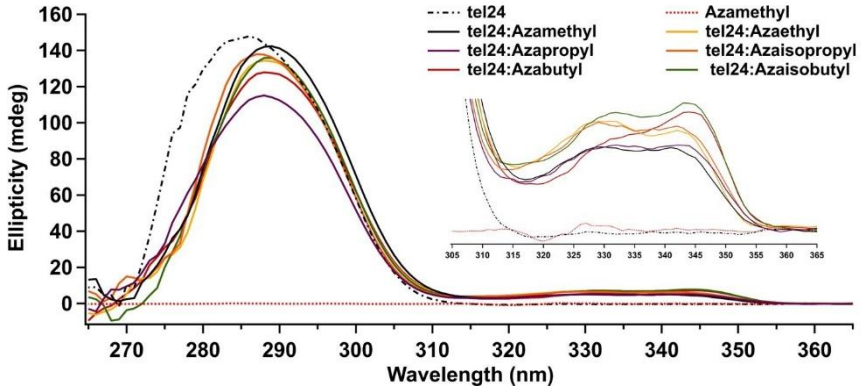

Figure 17: CD spectrum of tel24 (25 μM in strand) in the absence and presence of 25 μM azacyanines (1:1) at 5°C. Insert shows the induced CD band region; all azacyanines gave no CD signal in the absence of DNA. Only Azamethyl was shown in here for the simplicity.

The 1:6 tel24:azacyanine complexes were also investigated via CD spectroscopy (Figure 18). Here again, the dotted black line represents the ellipticity of tel24 in the absence of azacyanines, the dotted red line represents the ellipticity of Azamethyl in the absence of tel24, and the straight black, yellow, purple, orange, red, and green lines represent the ellipticity of tel24 in the presence of Azamethyl, Azaethyl, Azapropyl, Azabutyl, and Azaisobutyl respectively. As also observed for 1:1 samples, a weak induced CD band was also observed for 1:6 samples, confirming the presence of interactions between tel24 and azacyanines. However, the induced CD bands had only one maximum absorbance that is red shifted compared to CD bands observed in 1:1 samples. The change in the shape of the CD bands possibly indicates the change in the main binding mode of azacyanines and/or additional binding sites when azacyanines were present at relatively high concentrations compared to tel24 [82].

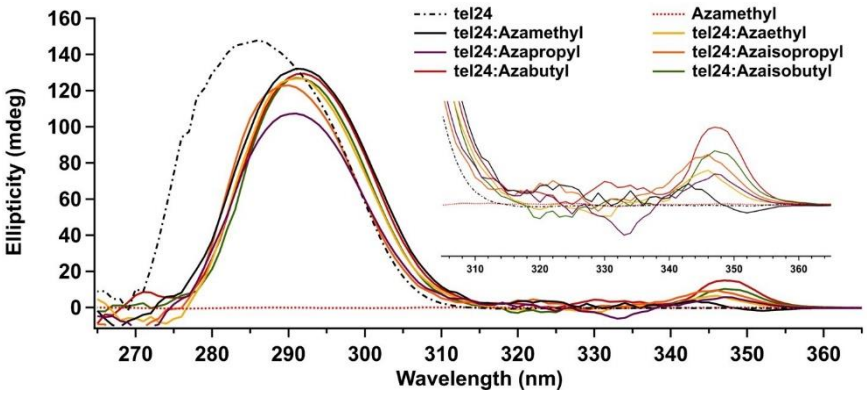

Figure 18: CD spectrum of tel24 (25 μM in strand) in the absence and presence of 150 μM azacyanines (1:6) at 5°C. Insert shows the induced CD band region; all azacyanines gave no CD signal in the absence of DNA. Only Azamethyl was shown in here for the simplicity.

3.5. Determination of Binding Using UV-VIS Spectroscopy

UV-Vis spectroscopy is a widely used method to reveal the formation of a complex between DNA and small molecules. When a small molecule and DNA form a complex, the small molecule causes slight changes on the structure of DNA. These

slight structural differences create hyperchromic/hypochromic changes in the absorption spectrum of DNA. The detection of these changes in the spectrum is an indication of a conformational change in DNA, and the presence of interaction between the small molecules and DNA [80]. Consequently, UV-Vis spectroscopy is one of the commonly used methods in determining of the binding of small molecules to different DNA structures as G-quadruplexes [83, 84].

The interactions of Azamethyl with tel24 were investigated by Persil Çetinkol et. al. using UV-VIS spectroscopy [66]. A hypochromic effect and a red shift in Azametyhl's UV-VIS bands between 305 nm and 360 nm were observed upon binding of Azamethyl to tel24. These changes in UV-VIS spectra are generally associated with the intercalation as the mode of binding and they actually verified that the mode of binding was intercalation via 2D NMR studies [59].

Here, the interactions of 1:1 tel24:azacyanine complexes were also investigated using UV-VIS spectroscopy by comparing the UV-VIS spectra of the samples at 20˚C and 95˚C (Figure 19). At 20˚C, tel24 is in G-quadruplex form and at that low temperature the azacyanines were interacting (bound) to that structure as confirmed by CD. When the temperature was increased to 95˚C, the G-quadruplex unfolds and the small molecules dissociates (unbound) from the folded structure. In other words, the spectrum at 20˚C and 95˚C represents the bound and the unbound state of the corresponding azacyanine to tel24 respectively. First, the spectra of all the azacyanines at 95˚C were very similar and had the same characteristic features. On the other hand, the UV-VIS spectrum of at 20˚C were distinctly different from each other [82]. The comparison of UV-VIS spectra for 1:1 tel24:azacyanine complexes revealed a hypochromic effect similar to Azamethyl's only in Azabutyl's and Azaisobutyl's UV-VIS spectrum (Figure 19) [82]. The hypochromic effect observed upon binding to tel24 was higher in Azabutyl's than any other Azacyanine, which might actually correlate with the tighter binding. Also, the red shift observed upon binding to tel24 was the most obvious in Azabutyl's spectrum. Neither hypochromic effect nor red shift was observed in Azaisopropyl's spectrum in the presence of tel24 [82]. This

indicates that Azaisopropyl has the least stabilization effect on the binding to tel24. There might be a trend on the degree of binding affinity; Azabutyl, Azamethyl, Azaisobutyl, Azaethyl, Azapropyl, Azaisopropyl. The UV-VIS spectra of Azaethyl, Azapropyl, and Azaisopropyl complexes did not show a significant change in between 20˚C and 95˚C, which again might be an indication of weaker binding of these compounds to tel24.

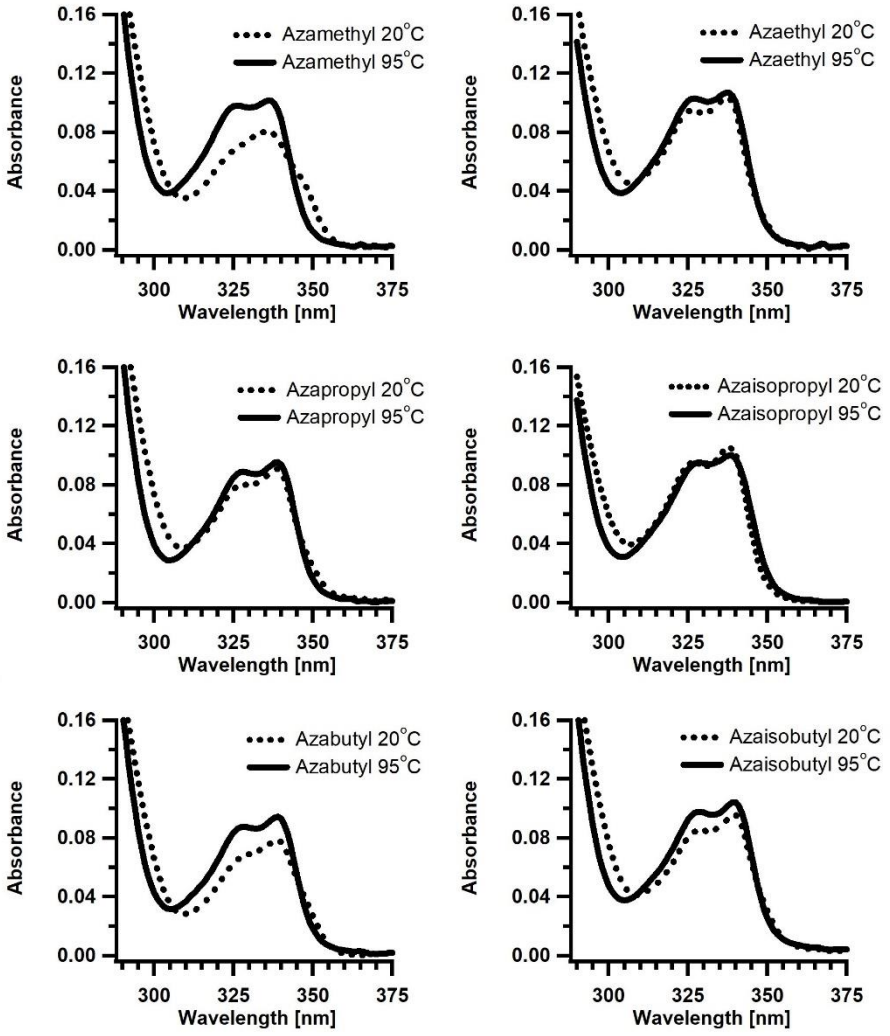

Figure 19: UV-VIS absorbance of 1:1 tel24-azacyanine (2.5 μM tel24 in strand: 2.5 μM azacyanine) complexes at 20ºC and 95ºC.

According to the neighbor-exclusion principle, there must be an unoccupied intercalation site in every second binding site for the planar drugs binding to DNA [85, 86]. From this point of view, we wonder how does increasing the concentration of azacyanines affect the mode of binding to tel24. So, the UV-VIS spectra of 1:6 tel24:azacyanine complexes (prepared based on the nearest neighbor-exclusion principle) were also collected. When the UV-VIS spectra of 1:6 tel24:azacyanine complexes were compared, all of the spectra seemed to be very similar, suggesting that the mode of binding of all the azacyanines at relatively higher concentration have the same effect upon tel24 binding. We believe the stacking of small molecules on the sides of the G-quadruplex might be dominating the intercalative mode of binding in the presence of increased azacyanine concentrations. A very slight hypochromic effect and a red shift were observed only in the UV-VIS spectrum of tel24:Azamethyl sample (Figure 20) [82].

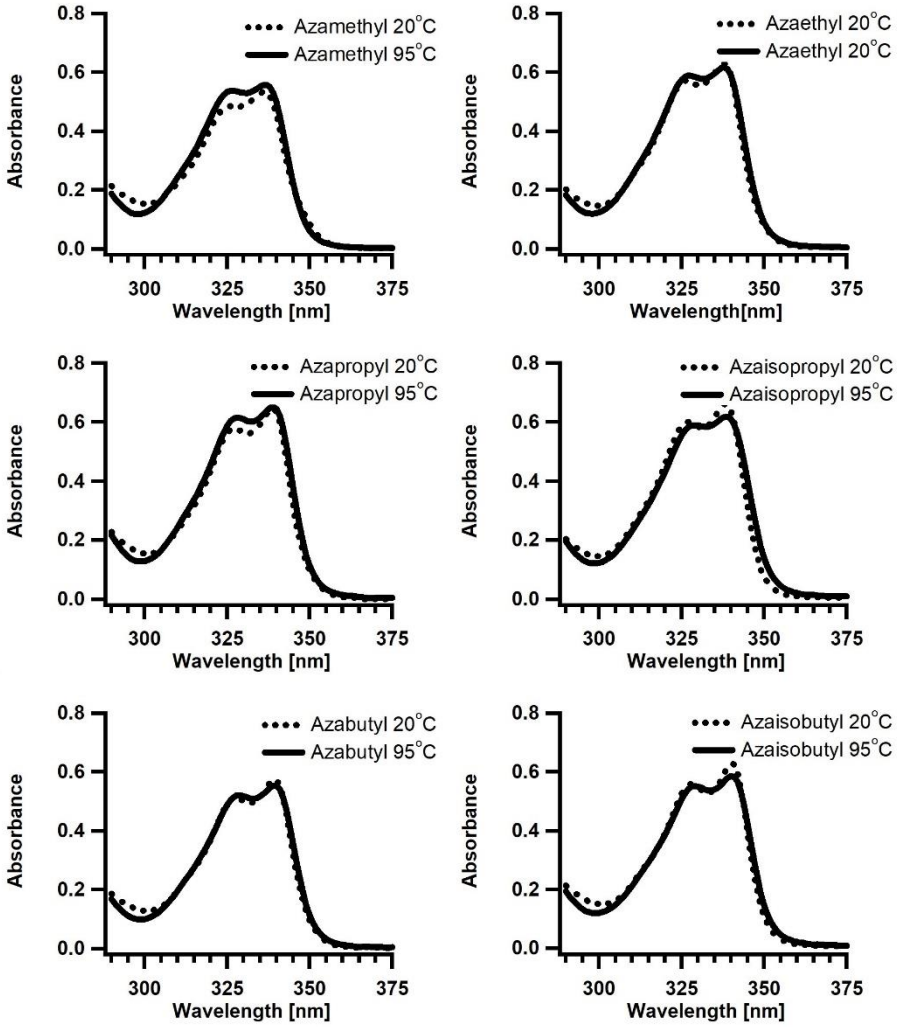

Figure 20: UV-VIS absorbance of 1:6 tel24-azacyanine (2.5 μM tel24 in strand: 15.0 μM azacyanine) complexes at 20ºC and 95ºC.

3.6. Determination of Thermal Denaturation Temperatures Using UV-VIS Spectroscopy

Thermal denaturation studies were performed in order to reveal the effect of azacyanine on tel24's stability. If the compound has a stabilizing effect upon binding to tel24, the tel24-azacyanine complex is expected to denature at a relatively higher temperature. At low temperatures (20˚C), tel24 is folded and azacyanines are bounded to the G-quadruplex structure. When the temperature is raised to 95˚C, G-quadruplex

is denatured and azacyanines are released from the structure. If the compounds are stabilizing the G-quadruplex structure, it will be harder to denature the G-quadruplex structure and so the thermal denaturation temperature increases.

For thermal denaturation studies, the full UV-VIS spectrum between 190 nm and 1100 nm during heating and cooling were collected from 15˚C to 95˚C at each 1˚C intervals for each azacyanine. The UV-VIS spectra collected during denaturation studies for tel24 in the absence and presence of Azamethyl were given in Figure 21 and Figure 22, respectively. The human telomeric DNA, tel24 has a characteristic broad UV-VIS absorbance peak between 230-300 nm in the absence of azacyanines (Figure 21). Azacyanines have also a characteristic broad UV-VIS absorbance peak between 300-360 nm (Figure 22).

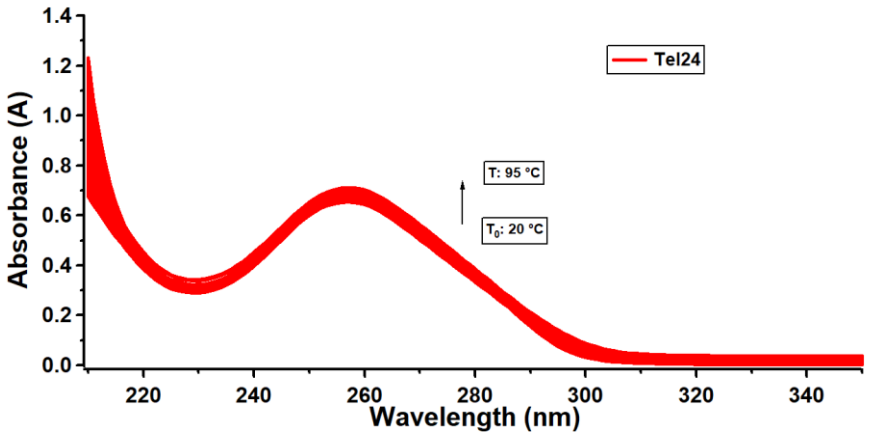

Figure 21: UV-VIS absorbance spectra of tel24 (2.5 μM) in the absence of azacyanines obtained during thermal denaturation experiments.

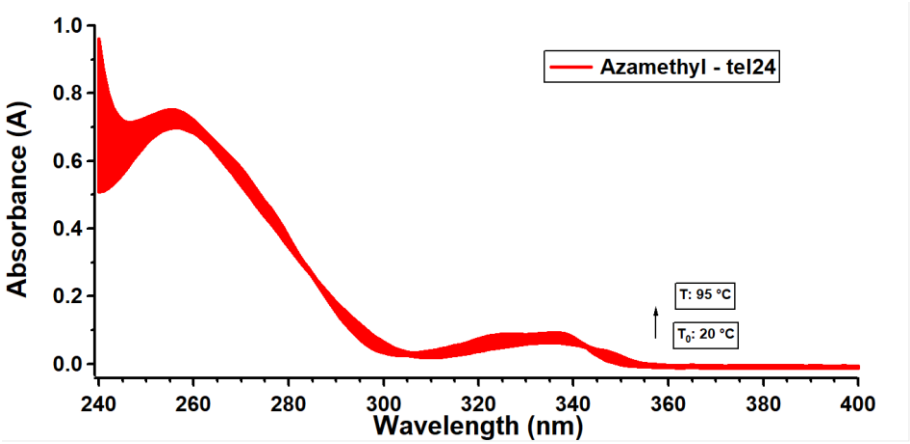

Figure 22: UV-VIS absorbance spectra of 1:1 tel24-Azamethyl (2.5 µM tel24 in strand: 2.5 µM Azamethyl) complexes between 20°C and 95°C.

In literature, the G-quartet formation and dissociation was mentioned to be monitored more precisely by monitoring the change in absorbance at around 290 nm [87]. So that the melting curves were obtained by monitoring the UV-VIS absorbance of tel24 in the absence and presence of azacyanines at 290 nm as a function of Temperature (˚C) (Figure 23). The center of this curve represents the thermal denaturation point, because at this point the complex is 50% denatured. The first derivative of this curve gives the thermal denaturation point of the complex (Appendix B). The UV-VIS spectra of all of the tel24:azacyanine complexes were given in Appendix B.

In Figure 23, the thermal denaturation curves obtained for tel24 by monitoring the change in absorbance at 290 nm with increasing temperature in the presence of Azamethyl were plotted as representative curves. Thermal denaturation temperatures (T_m) were obtained through the first derivative of these thermal denaturation curves (Figure 24).

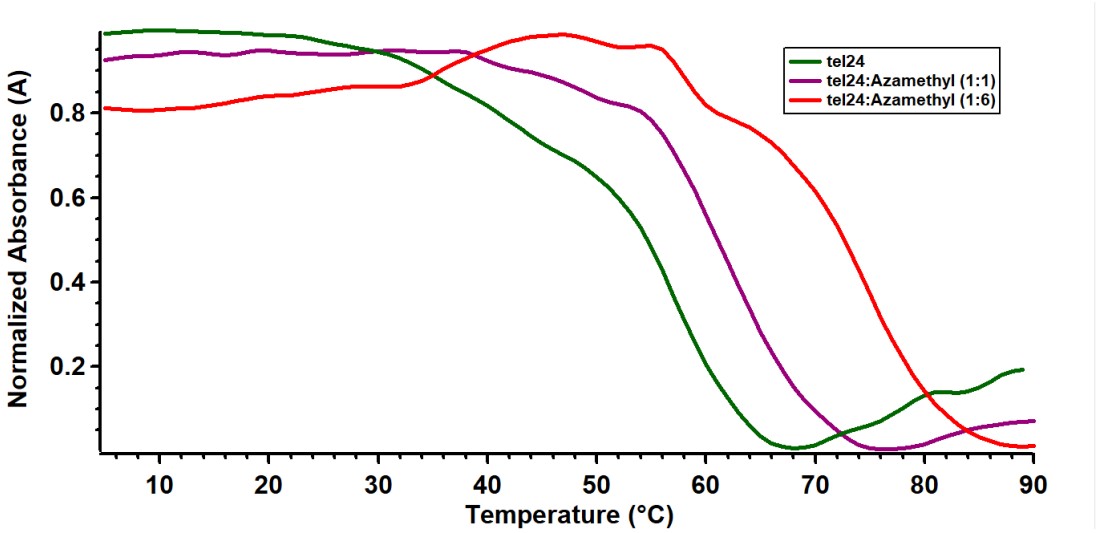

Figure 23: The comparison of the Normalized Absorbance (A) vs. Temperature (˚C) graphs of tel24 in the absence and presence of increasing concentrations of Azamethyl.

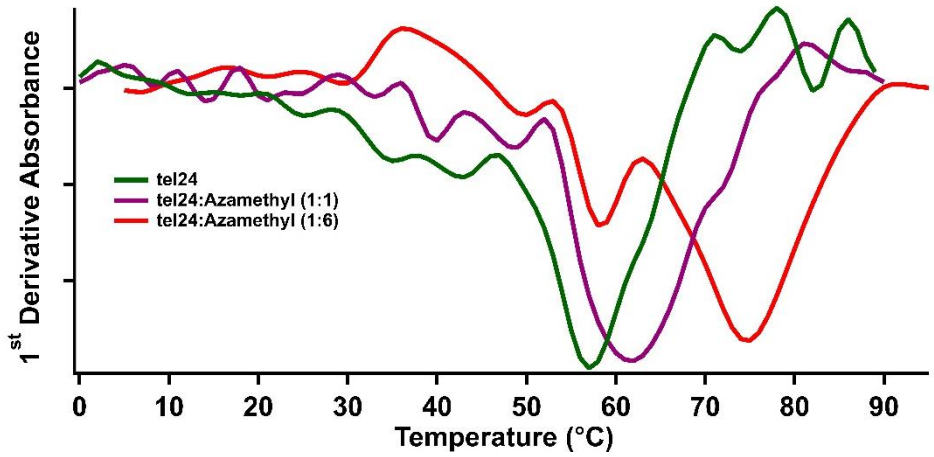

Figure 24: The comparison of the Differentiated Absorbance (dA) vs. Temperature (˚C) graphs of tel24 in the absence and presence of increasing concentrations of Azamethyl.

Table 2 displays the thermal denaturation temperatures of tel24 in the absence and the presence of azacyanines. Thermal denaturation studies of tel24 in the presence of azacyanines revealed that all the azacyanines except the Azaisopropyl were stabilizing the structure slightly in 1:1 tel24:azacyanine complexes (Table 2). T_m of

tel24 by itself was 65˚C. Tel24 was stabilized by Azamethyl and Azabutyl the most, where the thermal denaturation temperature was increased to 68˚C. The T_m of tel24 was 66˚C in the presence of Azaethyl, Azapropyl and Azaisobutyl. The T_m was 65˚C in the presence of Azaisopropyl. It can be deduced from the thermal denaturation temperatures of 1:1 complexes that the degree of stabilization ability of azacyanines from the highest to lowest; Azabutyl = Azamethyl, Azaisobutyl = Azaethyl = Azapropyl, Azaisopropyl. Though, one should be cautious when deliberating about the T_m values obtained for 1:1 complexes since the values are really close to each other.

Table 2: UV-VIS thermal denaturation temperatures obtained from the second heating scans of tel24 in the absence and presence of azacyanines.

Compounds	T_m (˚C), tel24:azacyanine (1:1)	T_m (˚C), tel24:azacyanine (1:6)
Tel 24	65	65
Azamethyl	68	75
Azaethyl	66	72
Azapropyl	66	73
Azaisopropyl	64	68
Azabutyl	68	78
Azaisobutyl	66	77

We wondered whether increasing the azacyanine concentration will stabilize the tel24 structure further and will lead to a discrimination between the azacyanine compounds in terms of their tel24 stabilization ability according to the nearest neighbor-exclusion principle. UV-VIS thermal denaturation studies for 1:6 tel24:azacyanine complexes revealed that the stability of tel24 was increased in the presence of higher azacyanine concentrations. It can be seen from the Figure 23, that increasing the concentration of Azamethyl result in further stabilization of the G-quadruplex structure where the T_m was increased.

When the thermal denaturation temperatures of 1:6 tel24-azacyanine complexes are compared (Table 2), the Azaisopropyl had the least effect again on stability of G-quadruplex, increasing the T_m of tel24 only 3˚C. On the other hand, Azabutyl had the most dramatic effect followed by Azaisobutyl. Azabutyl increased T_m of tel24 to 78˚C and Azaisobutyl increased T_m of tel24 to 77˚C compared to 75˚C of Azamethyl (Table 2). In accordance with the previous results, the trend on stabilization ability of azacyanines is; Azabutyl, Azaisobutyl, Azamethyl, Azapropyl = Azaethyl, Azaisopropyl and the discrimination ability of different azacyanines were more obvious at higher azacyanine.

3.7. Determination of Binding Constants Using Fluorescence Spectroscopy

In order to investigate the effect of molecular structure on the binding affinity of azacyanines to G-quadruplex forming tel24, fluorescence titrations were performed by making incremental additions of 50.0 μM tel24 stock solution containing 1.0 μM azacyanine into the sample containing only 1.0 μM azacyanine, in 25.0 mM $KH_2(PO_4)$ and 70.0 mM KCl at pH 7.0. The spectra obtained for Azamethyl titration was given in Figure 25 and for all the other azacyanines were given in Appendix C.

As displayed in Figure 25, Azamethyl's fluorescence was decreasing with increasing tel24 concentration. Azamethyl has an emission spectrum between 325 nm and 600 nm with the emission maximum around 375 nm. Upon the gradual addition of tel24 into the medium, the intensity of the emission spectra was significantly decreased and eventually remained constant. When Azamethyl molecules are bound

to tel24, the fluorescent ability of azacyanine is quenched by the molecular interactions between azacyanine and tel24.

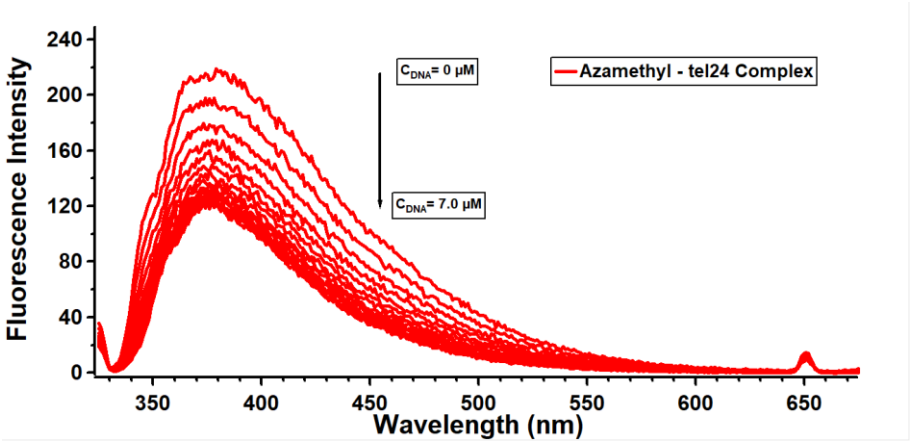

Figure 25: Fluorescence Intensity vs. Wavelength (nm) graph for 1µM Azamethyl solution titrated with increasing volumes of 50 µM tel24 solution from 0 to 7.0 µM of concentrations in titrated solution (1st replicate).

The binding constants were calculated were obtained by fitting the integrated fluorescence intensity data (Figure 25) as a function of DNA concentration by Igor Pro software (Wavemetrics Inc, USA) (Figure 26). One binding site was observed in the fluorescence titrations.

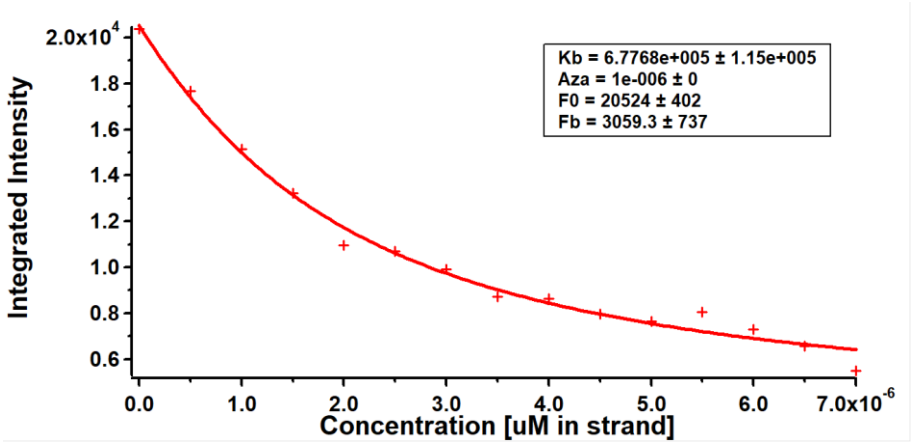

Figure 26: Integrated fluorescence intensity vs. DNA Concentration (μM, in strand) obtained from the Fluorescence Intensity vs. Wavelength (nm) graph 24.

The association constants of azacyanine-tel24 complexes were determined and presented on Table 3. The fluorescence titrations confirmed the results of our thermal denaturation experiments. Tel24:Azabutyl had the highest association constant, $7.84x10^5 \pm (3.44x10^4)$ M^{-1} and tel24:Azaisopropyl had the lowest association constant $2.04x10^5 \pm (5.38x10^4)$ M^{-1}. As an agreement with thermal denaturation studies, tel24:Azamethyl had the second highest association constant $6.61x10^5 \pm (3.74x10^4)$. The trend of the binding strength of azacyanines deduced from the fluorescence titrations is; Azabutyl, Azamethyl, Azaisobutyl, Azapropyl, Azaethyl, and Azaisopropyl.

Table 3: Association constants determined by fluorescence spectroscopy for Azacyanine-tel24 complexes.

Compounds	*Association Constant (M^{-1})*
Azamethyl	$6.61x10^5 \pm (3.74x10^4)$
Azaethyl	$2.57x10^5 \pm (5.40x10^4)$
Azapropyl	$3.63x10^5 \pm (4.06x10^4)$
Azaisopropyl	$2.04x10^5 \pm (5.38x10^4)$
Azabutyl	$7.84x10^5 \pm (3.44x10^4)$
Azaisobutyl	$4.55x10^5 \pm (1.23x10^4)$

CHAPTER 4

CONCLUSION

Here, five new azacyanine molecules (Azaethyl, Azapropyl, Azaisopropyl, Azabutyl, and Azaisobutyl) were synthesized and characterized in addition to the previously synthesized Azamethyl and their interactions with G-quadruplex forming human telomeric DNA, tel24 were investigated. The interactions of Azamethyl with tel24 under the same conditions were also investigated. The newly synthesized azacyanines were characterized by using elemental analysis and High-Resolution Mass Spectroscopy. The molar absorptivity constants of all of the azacyanines were calculated by using UV-VIS Spectroscopy using the Beer-Lambert's Law.

The interactions between azacyanines and tel24 were first investigated by CD Spectroscopy. Our CD results confirmed that all the azacyanines were interacting with G-quadruplex structure. An induced CD band was observed above 300 nm due to the binding of azacyanines to tel24 both in 1:1 and 1:6 tel24:azacyanine complexes. This band had two maximum absorbances at around 330 nm and 345 nm. Although the intensity of the induced CD bands was slightly different in different azacyanine complexes, the shapes of the bands were the same, indicating that all the azacyanines were probably binding to tel24 in the same way. When the concentrations of azacyanines were increased by six times keeping the tel24 concentration same, a different weak induced band was also observed on CD spectrum of all tel24:azacyanine complexes. The induced CD band was red shifted compared to the induced CD band obtained for 1:1 tel24:azacyanine complexes with only one maximum absorbance at 350 nm. This difference in the shape of the CD bands at different concentrations of azacyanines might be indicating that the modes of binding were different in each case, or there might be additional binding sites when higher concentrations of azacyanines were present.

The binding interactions were also investigated by UV-VIS Spectroscopy. The spectrum of tel24:azacyanine complexes at 20˚C represents the bound state and 95˚C the unbound state of azacyanines to tel24 structure respectively. When two spectra are compared, a hypochromic affect and a red shift was noticeable upon binding of azacyanines to tel24. According to literature, these changes on the spectrum of G-quadruplex at 20˚C (bound state) indicate that the drug molecules are binding to the structure via intercalation (ref). In addition, for 1:1 tel24:azacyanine complex, the mode of binding was proved to be as intercalation via 2D NMR studies previously [57]. Here, since the mode of binding in 1:1 complexes looks similar based on our CD results, we believe the intercalation is also the dominant mode of binding for all other 1:1 tel24:azacyanine complexes. When the azacyanine concentration were increased by six times, the UV-VIS spectra at 20˚C and 95˚C spectra were almost the same. We think that the stacking of azacyanine molecules on the sides of the G-quadruplex structure dominates the intercalative mode of binding in the presence of increased azacyanine concentrations.

The thermal denaturation temperatures of tel24 structure were determined in the absence and presence of azacyanine molecules. UV-VIS thermal denaturation studies revealed that all of azacyanine molecules were stabilizing the tel24 structure and the stability of tel24 was increasing in the presence of increased azacyanine concentrations.

The binding constants of all tel24:azacyanine complexes were determined by using Fluorescence spectroscopy. In accordance with the results of CD, and UV-VIS spectroscopy, the results of Fluorescence spectroscopy also indicated that all of the azacyanines were binding to tel24 structure. Also, one tight binding site was observed in the fluorescence titrations. As an agreement with thermal denaturation studies, Azabutyl has the most dramatic effect upon stabilizing the G-quadruplex structure, on the contrary, Azaisobutyl is the least stabilizing molecule.

In conclusion, it was found that all the azacyanines were interacting with tel24 and stabilizing the G-quadruplex structure as evident by CD, UV-VIS and Florescence

spectroscopy. The stabilization degree was not directly related to the alkyl chain length or the branching on the benzimidazole ring. Azabutyl was stabilizing the tel24 structure the most, followed by Azamethyl, Azaisobutyl, Azapropyl, and Azaethyl. Azaisopropyl was the least stabilizing molecule as evident both from the UV-VIS thermal denaturation experiments and Florescence titrations. Previously, Azamethyl was found to be intercalating between the top G-quartet and A-T base pairing in the loop region. It was suspect that the short bulky isopropyl group might be preventing the slide of the azacyanine as an intercalator between the base pairs. On the other hand, having a longer alkyl chain on the benzimidazole ring might also be interfering with such interactions since Azaethyl and Azapropyl were stabilizing the G-quadruplex structure less compared to Azamethyl. But once the length of the alkyl chain is long and flexible enough as in the case of Azabutyl, the long chain still be interfering with the intercalation but the increased hydrophobic interactions between the butyl chain and the quadruplex structure might be compensating for that. The studies also demonstrated that while the degree of red shift and the hypochromic effect might be an indication of tighter binding in the same class of small molecules binding to nucleic acids, the intensity of induced CD band was not. We believe the stacking of small molecules on the sides of the G-quadruplex dominates the intercalative mode of binding in the presence of increased azacyanine concentration in 1:6 tel24:azacyanine complexes.

Benzimidazole scaffold, the one step synthesis and the ease of purification of azacyanines makes them plausible candidates in the development of new G-guadruplex binding small molecules. Here it was found that Azabutyl was binding to tel24 more tightly compared to Azamethyl. The significance of these derivatives arises from its selectivity and high binding affinity to telomeric DNA. Their selectivity to G-quadruplex DNA is 200 times more than that to dsDNA. The benzimidazole ring structure in the system sets the π-π stacking interactions with the Guanine bases, and help to the small molecule to be intercalated between the base pairs. Such an interaction increases the stability of the G-quadruplex structure. When these

molecules are compared in the existing drug molecules used in the cancer treatment, their large surface area provides themselves to be selective towards G-quadruplex DNA than to dsDNA, which leads them to specifically target the cancer cells other than the normal cells. Also, these derivatives can be considered as potential drug molecules due to having small size, low molecular weight, significant number of H-bond donors and acceptors, and moderate lipophilicity. The future experiments will continue with decorating Azabutyl benzimidazole ring with additional H-bonding donor and acceptor functional groups to increase binding affinity towards G-quadruplex structures.

REFERENCES

[1] Huang, C. Y., Ju, D. T., Chang, C. F., Reddy, P. M., & Velmurugan, B. K. (2017). A Review on the Effects of Current Chemotherapy Drugs and Natural Agents in Treating Non-Small Cell Lung Cancer. *BioMedicine, 7*(4), 12-23. Doi: 10.1051/bmdcn/2017070423.

[2] Galluzzi, L., Buque, A., Kepp, O., Zitvogel, L. & Kroemer, G. (2015). Immunological Effects of Conventional Chemotherapy and Targeted Anticancer Agents. *Cancer Cell, 28*(6), 690-714. Doi: 10.1016/j.ccell.2015.10.012.

[3] Cheung-Ong, K., Giaever, G. & Nislow, C. (2013). DNA-Damaging Agents in Cancer Chemotherapy: Serendipity and Chemical Biology. *Chemistry & Biology, 20*. Doi: 10.1016/j.chembiol.2013.04.007.

[4] O'Connor, M. J. (2015). Targeting the DNA Damage Response in Cancer. *Molecular Cell, 60*(4), 547-560. Doi: 10.1016/j.molcel.2015.10.040.

[5] Bischoff, G., Hoffmann, S. (2012). DNA-binding of Drugs Used in Medicinal Therapies. *Current Medicinal Chemistry, 9*, 321-348.

[6] Martinez, R., & Chacon-Garcia, L. (2005). The Search of DNA-intercalators as Antitumoral Drugs: What It Worked and What Did Not Work. *Current Medicinal Chemistry, 12*(2), 127-151.

[7] Palchaudhuri, R., Hergenrother, J. (2007). DNA as a Target for Anticancer Compounds: Methods to Determine the Mode of Binding and the Mechanism of Action. *Current Opinion in Biotechnology, 18,* 497-503.

[8] Luedtke, N. W. (2009). Targeting G-quadruplex DNA with Small Molecules. *Chimia, 63*, 134-139.

[9] Martinez, R., Chacon-Garcia, L. (2005). The Search of DNA-intercalators as Antitumoral Drugs: What It Worked and What did not Work. *Current Medicinal Chemistry, 12*, 127-151.

[10] Rizzo, A., Salvati, E., Porru, M., D'Angelo, C., Stevens, M.F., D'Incalci, M., Leonetti, C., Gilson, E., Zupi, G., Biroccio, A. (2009). Stabilization of Quadruplex DNA Perturbs Telomere Replication Leading to the Activation of an ATR-dependent ATM Signalling Pathway. *Nucleic Acids Research, 37*, 5353-5364.

[11] Shalaby, T., Fiaschetti, G., Nagasawa, K., Shin-ya, K., Baumgartner, M., Grotzer, M. (2013). G-quadruplexes as Potential Therapeutic Targets for Embryonal Tumors. *Molecules, 18*(10), 12500-12537.

[12] Ochnmacht, S. A., Neidle, S. (2014). Small-molecule Quadruplex-targeted Drug Discovery. *Bioorganic & Medicinal Chemistry Letters, 24*, 2602-2612.

[13] Chen, M., Song, G., Wang, C., Hu, D., Ren, J., Qu, X. (2009). Small-Molecule Selectively Recognizes Human Telomeric G-Quadruplex DNA and Regulates Its

Conformational Switch. *Biophysical Journal, 97,* 2014-2023; doi:10,1016/j.bpj.2009.07.025.

[14] Rhodes, D. & Lipps, H. J. (2015). G-quadruplexes and Their Regulatory Roles in Biology. *Nucleic Acids Research, 43*(18), 8627-8637.

[15] Burchett, K. M., Yan, Y., Ouellette, M. M. (2014). Telomerase Inhibitor Imetelstat (GRN163L) Limits the Lifespan of Human Pancreatic Cancer Cells. *Plos One, 9*(1), e85155; doi:10.1371/journal.pone.0085155.

[16] Arthanari, H. & Bolton, P. H. (2001). Functional and Dysfunctional Roles of Quadruplex DNA in Cells. *Chemistry & Biology, 8*, 221-230.

[17] Li, Y. & Tergaonkar, V. (2014). Nancanonical Functions of Telomerase: Implications in Telomerase-Targeted Cancer Therapies. *American Association for Canser Research.* Doi: 10.1158/0008-5472.CAN-13-3568.

[18] Marchand, A., Granzhan, A., Iida, K., Tsushima, Y., Ma, Y., Nagasawa, K., Teulade-Fichou, M., & Gabelica, V. (2015). Ligand-induced Conformational Changes with Cation Ejection upon Binding to Human Telomeric DNA G-quadruplexes. *Journal of the American Chemical Society, 137*(2), 750-756.

[19] Maciejowski, J. & Langei T. (2017). Telomeres in Cancer: Tumuor Suppression and Genome Instability. *Nature Reviews Molecular Cell Biology, 18*(3), 175. Doi: 10.1038/nrm.2016.171.

[20] Agarwala, P., Pandey, S., & Maiti, S. (2015). The tale of RNA G-quadruplex. *Organic & Biomolecular Chemistry, 13*(20), 5570-5585.

[21] Ivancich, M., Schrank, Z., Wojdyla, L., Leviskas, B., Kuckovic, A., Sanjali, A., Puri, N. (2017). Treating Cancer by Targeting Telomeres and Telomerase. *Antioxidants, 6*(15); doi:10.3390/antiox6010015.

[22] Jafri, M. A., Ansari, S. A., Alqahtani, M. H., Shay, J. W. (2016). Roles of Telomeres and Telomerase in Cancer, and Advances in Telomerase-targeted Therapies. *Genome Medicine, 8*(69). Doi: 10.1186/s13073-016-0324-x.

[23] Maji, B. & Bhattacharya, S. (2014). Advances in the Molecular Design of Potential Anticancer Agents via Targeting of Human Telomeric DNA. *The Royal Society of Chemistry*. Doi: 10.1039/c4cc00611a.

[24] Andrews, L. G., Tollefsbol, T. O. (2008). Methods of Telomerase Inhibition. *Methods Mol Biol., 405*, 1-8.

[25] Jäger, K., Walter, M. (2016). Therapeutic Targeting of Telomerase. *Genes, 7*(39); doi: 10.3390/genes7070039.

[26] Zvereva, M. I., Schherbakova, D. M., Dontsova, O. A. (2010). Review: Telomerase: Structure, Functions, and Activity Regulation. *Biochemistry Moscow, 75*, 1563. https://doi.org/10,1134/S0006297910130055.

[27] Zahler, A. M., Williamson, J. R., Cech, T. R., Prescott, D. M. (1991). Inhibition of Telomerase by G-quartet DNA Structures. *Nature, 350*, 718-720.

[28] Siddiqui-Jain, A., Grand, C. L., Bearss, D. J., Hurley, L. H. (2002). Direct Evidence for a G-quadruplex in a Promoter Region and its Targeting with a Small Molecule to Repress c-MYC Transcription. *Proceedings of the National Academy of Sciences USA, 99*, 11593-11598.

[29] Neidle, S. (2009). Human Telomeric G-quadruplex: The Current Status of Telomeric G-quadruplexes as Therapeutic Targets in Human Cancer. *Federation of European Biochemical Societies Journal, 277*(5), 1118-1125.

[30] Wright, W.E., Shay, J. W. (2011). Role of Telomeres and Telomerase in Cancer. *Seminars in Cancer Biology, 21*(6), 349-353.

[31] Hänsel-Hertsch, R., Antonio, M. D., Balasubramanian, S. (2017). DNA G-quadruplexes in The Human Genome: Detection, Functions and Therapeutic Potential. *Nature Reviews Molecular Cell Biology, 18*(5), 279-284, doi:10.1038/nrm.2017.3.

[32] Gomez-Marquez, J. (2010). DNA G-quadruplex: Structure, Function and Human Disease. *Federation of European Biochemical Societies Journal, 277*, 3451. Doi: 10.1111/j.1742-4658.2010.07757.x

[33] Chen, Y. & Yang, D. (2012). Sequence, Stability, Structure of G-Quadruplexes and Their Drug Interactions. *Current Protocols in Nucleic Acid Chemistry*, Chapter: 17.5. Doi: 10.1002/0471142700.nc1705s50.

[34] Fukuhara, M., Ma, Y., Nagasawa, K. & Toyoshima, F. (2017). A G-quadruplex Structure at the 5' End of the H19 Coding Region Regulates H19 Transcription. *Scientific Reports, 7*, 45815. Doi: 10.1038/srep45815.

[35] Murat, P. & Balasubramanian, S. (2014). Existence and Consequences of G-quadruplex Structures in DNA. *Current Opinion in Genetics and Development, 25*, 22-29.

[36] Kota, S., Dhamodharan, V., Pradeepkumar, P. I. & Misra, H. S. (2015). G-quadruplex Forming Structural Motifs in the Genome of Deinococcus Radiodurans and Their Regulatory Roles in Promoter Functions. *Applied Microbial and Cell Physiology, 99,* 9761-9769. Doi: 10.1007/s00253-015-6808-6.

[37] Biswas, B., Kandpal, M. & Vivekanandan, P. (2017). A G-quadruplex Motif in an Envelope Gene Promoter Regulates Transcription and Virion Secretion in HBV Genotype B. *Nucleic Acids Research, 45*(19, 11268-11280. Doi: 10.1093/nar/gkx823.

[38] Chen, B. J., Wu, Y. L., Tanaka, Y. & Zhang, W. (2014). Small Molecules Targeting c-Myc Oncogene: Promising Anti-Cancer Therapeutics. *International Journal of Biological Sciences, 10*(10), 1084-1096. Doi: 10.7150/ijbs.10190.

[39] Mengual Gomez, D. L., Armando, R. G., Cerrudo, C. S., Ghiringhelli, P. D., Gomez, D. E. (2015). Telomerase as a Cancer Target. Development of New Molecules. *Current Topics in Medicinal Chemistry, 16*, 2432-2440.

[40] Bryan, C., Rice, C., Hoffman, H., Harkisheimer, M., Sweeney, M., & Skordalakes, E. (2015). Structural Basis of Telomerase Inhibition by the Highly Specific BIBR1532. *Structure, 23*(10), 1934-1942.

[41] Xu, H., Di Antonio, M., McKinney, S., Mathew, V., Ho, B., O'Neil, N. J., ... & Kabeer, F. (2017). CX-5461 is a DNA G-quadruplex Stabilizer with Selective Lethality in BRCA1/2 Deficient Tumours. *Nature Communications, 8*, 14432.

[42] De Cian, A., Cristofari, G., Reichenbach, P., De Lemos, E., Monchaud, D., Teulade-Fichou, Marie-Paule, Shin-ya, Kazuo, Lacroix, L., Lingner, J., Mergny, J. (2007). Reevaluation of Telomerase Inhibition by Quadruplex Ligands and their Mechanisms of Action. *Proceedings of the National Academy of Sciences of the United States of America, 104*(44), 17347-17352.

[43] Ruggiero, E. & Richter, S. N. (2018). G-quadruplexes and G-quadruplex Ligands: Targets and Tools in Antiviral Therapy. *Nucleic Acids Research, 46*(7), 3270-3283. Doi: 10.1093/nar/gky187.

[44] Islam, M. K., Jackson, P. J. M., Rahman, K. M., & Thurston, D. E. (2016). Recent Advances in Targeting the Telomeric G-quadruplex DNA Sequence with Small Molecules as a Strategy for Anticancer Therapies. *Future Medicinal Chemistry, 8*(11), 1259-1290. Doi: 10.4155/fmc-2016-0017.

[45] Bryan, C., Rice, C., Hoffman, H., Harkisheimer, M., Sweeny, M. & Skordalakes, E. (2015). Structural Basis of Telomerase Inhibition by the Highly Specific BIBR1532. *Structure, 23*(10), 1934-1942. Doi: 10.1016/j.str.2015.08.006.

[46] Bashash, D., Zareii, M., Safaroghli-Azar, A., Omrani, M. D., & Ghaffari, S. H. (2016). Inhibition of Telomerase Using BIBR1532 Enhances Dozorubicin-induced Apoptosis in Pre-B Acute Lymphoblastic Leukemia Cells. *Hematology, 22*(6), 330-340. Doi: 10.1080/10245332.2016.1275426.

[47] Shi, Y., Sun, L., Chen, G., Zheng, D., Li, L., & Wei, W. (2014). A Combination of The Telomerase Inhibitor, BIBR1532, and Paclitaxel Synergistically Inhibit Cell Proliferation in Breast Cancer Cell Lines. *Targeted Oncology, 10*(4), 565-573. Doi: 10.1007/s11523-015-0364-y.

[48] Xu, H., Di Antonio, M., McKinney, S., Mathew, V., Ho, B., O'Neil, N. J. … & Balasubramanian, S. (2017). CX-5461 is a DNA G-quadruplex Stabilizer with Selective Lethality in BRCA1/2 Deficient Tumours. *Nature Communications, 8*, 14432. Doi: 10.1038/ncomms14432.

[49] Lee, H. C., Wang, H., Baladandayuthapani, V., Lin, H., He, J., Jones, R. J., ... & Orlowski, R. Z. (2017). RNA Polymerase I Inhibition with CX-5461 as a Novel Therapeutic Strategy to Target MYC in Multiple Myeloma. *British Journal of Haematology, 177*(1), 80-94. Doi: 10.1111/bjh.14525.

[50] Harrison, S. J., George, A., & Hannan, R. (2015). A New Window on Cancer Therapy? Targeting The Nucleolus and Ribosome Biogenesis Using the Small Molecule Inhibitor of Polymerase I Transcription, CX-5461. *Internal Journal of Hematologic Oncology*, 61-65. Doi: 10.2217/ijh.15.9.

[51] Hojjat-Farsangi, M. (2017). Small Molecule Inhibitors: Suitable Drugs for Targeted-Based Cancer Therapy. *American Journal of Leukemia Research, 1*(1), 1005.

[52] Mostafa A S, Gomaa R M, Elmorsy M A. Design and synthesis of 2-phenyl benzimidazole derivatives as VEGFR-2 inhibitors with anti-breast cancer activity. Chemical Biology & Drug Design 2019; 93: 454-463. doi:10.1111/cbdd.13433.

[53] Maji B, Kumar K, Kaulage M, Muniyappa K, Bhattacharya S. Design and synthesis of new benzimidazole-carbazole conjugates for the stabilization of human telomeric DNA, Telomerase inhibition, and their selective action on cancer cells. Journal of Medicinal Chemistry 2014; 57: 6973-6988. doi: 10.1021/jm500427n.

[54] Shimomura I, Yokoi A, Kohama I, Kumazaki M, Tada Y, et al. Drug library screen reveals benzimidazole derivatives as selective cytotoxic agents for KRAS-mutant lung cancer. Cancer Letters 2019; 451: 11-22. doi: 10.1016/j.canlet.2019.03.002.

[55] Sur S, Tiwari V, Sinha D, Kamran M Z, Dubey K D, et al. Naphthalenediimide-linked bisbenzimidazole derivatives as telomeric G-quadruplex-stabilizing ligands with improved anticancer activity. Omega 2017; 2: 966-980. doi: 10.1021/acsomega.6b00523.

[56] Maji B, Kumar K, Muniyappa K, Bhattacharya S. New dimeric carbazole-benzimidazole mixed ligands for the stabilization of human telomeric G-quadruplex DNA and as telomerase inhibitors. A remarkable influence of the spacer. Organic & Biomolecular Chemistry 2015; 13: 8335-8348. doi: 10.1039/c5ob00675a.

[57] Kaulage M H, Maji B, Pasadi S, Ali A, Bhattacharya S, et al. Targeting G-quadruplex DNA structures in the telomere and oncogene promoter regions by benzimidazole-carbazole ligands. European Journal of Medicinal Chemistry 2018, 148: 178-194. doi: 10.1016/j.ejmech.2018.01.091.

[58] Yadav K, Meka P N R, Sadhu S, Guggilapu S D, Kovvuri J, et al. Telomerase inhibition and human telomeric G-quadruplex DNA stabilization by a β-carboline-benzimidazole derivative at low concentrations. Biochemistry 2017; 56: 4392-4404. doi: 10.1021/acs.biochem.7b00008.

[59] Hernández-Luis, F., Hernández-Campos, A., Castillo, R., Navarrete-Vázquez, G., Soria-Arteche, O., Hernández-Hernández, M., Yépez-Mulia, L. (2010). Synthesis and Biological Activity of 2-(trifluoromethyl)-1H-benzimidazolee Derivatives Against

Some Protozoa and Trichinella Spiralis. *European Journal of Medicinal Chemistry, 45*, 3135-3141.

[60] Khokra, S. L., Choudhary, D. (2011). Benzimidazolee an Important Scaffold in Drug Discovery. *Asian Journal of Biochemical and Pharmaceutical Research, 3*(1), 476-486.

[61] Tantawy, A., Barghash, A., Badr, S., Gomaa, R. (2013). Synthesis of New Heterocyclic Compounds Containing Benzimidazolee Moiety as Inhibitors of Breast Cancer Cell Growth. *Heterocyclic Communications, 19*(12), 125-131.

[62] Velik, J., Baliharova, V., Fink-Gremmels, J., Bull, S., Lamka, J., Skalova, L. (2004). Benzimidazolee Drugs and Modulation of Biotransformation Enzymes. *Research in Veterinary Science, 79*, 95-108.

[63] Kim, H. J., Heo, C. H., Kim, H. M. (2013). Benzimidazole-based Ratiometric Two-photon Fluorescent Probes for Acidic pH in Live Cells and Tissues. *Journal of American Chemical Society, 135*, 17969-17977.

[64] Shao, J., Qiao, Y., Lin, H., Lin, H. (2009). Rational Design of Novel Benzimidazole-based Sensor Molecules that Display Positive and Negative Fluorescence Responses to Anions. *Journal of Fluorescence, 19*(1), 183-188.

[65] Wang, Y., Liu, L., Pan, Y., Wang, H. (2011). Synthesis of a Dehydroabietyl Derivative Bearing a 2-(2'-Hydroxyphenyl) Benzimidazole Unit and its Selective Cu^{2+} Chemosensing. *Molecules, 16,* 100-106.

[66] Persil Çetinkol, Ö., Engelhart, A. E., Nanjunda, R. K., Wilson, W. D., Hud, N. V. (2008). Submicromolar, Selective G-Quadruplex Ligands from One Pot: Thermodynamic and Structural Studies of Human Telomeric DNA Binding by Azacyanines. *ChemBioChem, 9*(12), 1889-1892.

[67] Haddadin, M. J., Kurth, M. J., Olmstead, M. M. (2000). One-step Synthesis of New Heterocyclic Azacyanines. *Tetrahedron Letters, 41 (30)*, 5613-5616.

[68] Huang, K. S., Haddadin, M. J., Olmstead, M. M., Kurth, M. J. (2001). Synthesis and Reactions of Some Heterocyclic Azacyanines. *Journal of Organic Chemistry, 66,* 1310-1315.

[69] Leung, C. H., Chan, D. S. H., Ma, V. P. Y., & Ma, D. L. (2013). DNA-Binding Small Molecules as Inhibitors of Transcription Factors. *Medicinal Research Reviews, 33*(4), 823-846.

[70] Lipinski, C. A. (2015). Rule of five in 2015 and beyond: Target and Ligand Structural Limitations, Ligand Chemistry Structure and Drug Discovery Project Decisions. *Advanced Drug Delivery Reviews, 101,* 34-41. Doi: 10.1016/j.addr.2016.04.029.

[71] Hoelder, S., Clarke, P. A., & Workman, P. (2012). Discovery of Small Molecule Cancer Drugs: Successes, Challenges and Opportunities. *Molecular Oncology, 6*, 155-176.

[72] Lavanya, V., Mohamed Adil, A. A., Neesar, A., Arun, K. R., & Shazia, J. (2014). Small Molecule Inhibitors as Emerging Cancer Therapeutics. *Integrative Cancer Science and Therapeutics, 1*(3), 39-46. Doi: 10.15761/ICST.1000109.

[73] Pradeep T P, Barthwal R. A 4:1 stoichiometric binding and stabilization of mitoxantrone-parallel stranded G-quadruplex complex established by spectroscopy techniques. Journal of Photochemistry & Photobiology, B: Biology 2016; 162: 106-114. doi: 10.1016/j.jphotobiol.2016.06.019

[74] Tariq Z, Barthwal R. Binding of anticancer drug daunomycin to parallel G-quadruplex DNA [d-(TTGGGT)]$_4$ leads to thermal stabilization: A multispectroscopic investigation. International Journal of Biological Macromolecules 2018; 120: 1965-1974. doi: 10.1016/j.ijbiomac.2018.09.154.

[75] Das R N, Chevret E, Desplat V, Rubio S, Mergny J L, et al. Design, synthesis and biological evaluation of new substituted diquinolinyl-pyridine ligands as anticancer drug agents by targeting G-quadruplex. Molecules 2017; 23 (1), 81. doi: 10.3390/molecules23010081.

[76] Maiti S, Saha P, Das T, Bessi I, Schwalbe H, et al. Human telomeric G-quadruplex selective fluoro-isoquinolines induce apoptosis in cancer cells. Bioconjugate Chemistry 2018; 29: 1141-1154. doi: 10.1021/acs.bioconjchem.7b00781.

[77] Kumar P, Barthwal R. Structural and biophysical insight into dual site binding of the protoberberine alkoloid palmatine to parallel G-quadruplex DNA using NMR, fluorescence and circular dichroism spectroscopy. Biochimie 2018; 147: 153-169. doi: 10.1016/j.biochi.2018.02.002.

[78] Jha N S, Mishra S, Mamidi A S, Mishra A, Jha S K, et al. Targeting human telomeric G-quadruplex DNA with curcumin and its synthesized analogues under molecular crowding conditions. RSC Advances 2016; 6: 7474-7487. doi: 10.1039/c5ra17390f.

[79] Tutuncu, S., Guloglu, S., Kucukakdag, A. & Cetinkol, O. P. (2018). Selective High Binding Affinity of Azacyanines to polyd(A).polyd(T).polyd(T) Triplex: The Effect of Chain Length and Branching on Stabilization, Selectivity and Affiinity. *Chemistry Select, 3*(45), 12878-12887. Doi: 10/1002/slct.201802802.

[80] Shabadi, N. & Hashempour, S. (2019). DNA Binding Studies of Antibiotic Drug Cephalexin Using Spectroscopic and Molecular Docking Techniques. *Nucleosides, Nucleotides and Nucleic Acids*, *38*(6), 428-447. Doi: 10.1080/15257770.2018.1562071.

[81] Kerwin, S. M. (2000). Nucleic Acids: Structures, Properties, and Functions By Victor A. Bloomfield, Donald M. Crothers, and Ignacio Tinoco, Jr., with contributions from John E. Hearst, David E. Wemmer, Peter A. Kollman, and Douglas H. Turner. University Science Books, Sausalito, CA. 2000. ix+ 794 pp. 17× 25 cm. ISBN 0-935702-49-0.

[82] Doğu, A. K. & Çetinkol, Ö. P. (2019). Targeting Human Telomeric DNA with Azacyanines. *Turkish Journal of Chemistry, Doi:* 10.3906/kim-1903-6.

[83] Wumaier, M., Shi, J. J., Yao, T. M., Hu, X. C., Gao, R. R., et. al. (2019). G. quadruplex and Duplex DNA Binding Studies of Novel Ruthenium (II) Complexes Containing Ascididemin Ligands. *Journal of Inorganic Biochemistry, 126,* 110681. Doi: 10.1016/j.jinorgbio.2019.03.021.

[84] Zhou, K., Liu, J., Xiong, X., Cheng, M., Hu, X., et. al. (2019). Design, Synthesis of 4,5-diazafluorene Derivatives and Their Anticancer Activity via Targeting Telomeric DNA G-quadruplex. *European Journal of Medicinal Chemistry, 178,* 484-499. Doi: 10.1016/j.ejmech.2019.06.012.

[85] Crothers, D. M. (1968). Calculation of Binding Isotherms for Heterogeneous Polymers. *Biopolymers, 6,* 575-584.

[86] Rao, S. N. & Kolmann, P. A. (1987). Molecular Mechanical Simulations on Double Intercalation of 9-amino acridine into d(CGCGCGC.d(GCGCGCG): Analysis

of the Physical Basis for the Neighbor-Exclusion Principle. *Proceedings of the National Academy of Sciences of the United States of America, 84,* 5735-5739.

[88] Mergny, J. L., Phan, A. T. & Lacroix, L. (1998). Following G-quartet Formation by UV-spectroscopy. *FEBS Letters, 435,* 74-78.

APPENDICES

A. NMR SPECTRA

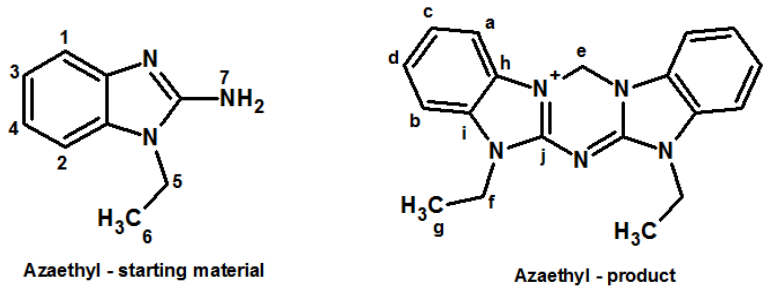

Figure 27: The structure of Azaethyl and its starting material, labeled for ^{13}C and ^{1}H NMR spectra dissolved in DMSO-D_6.

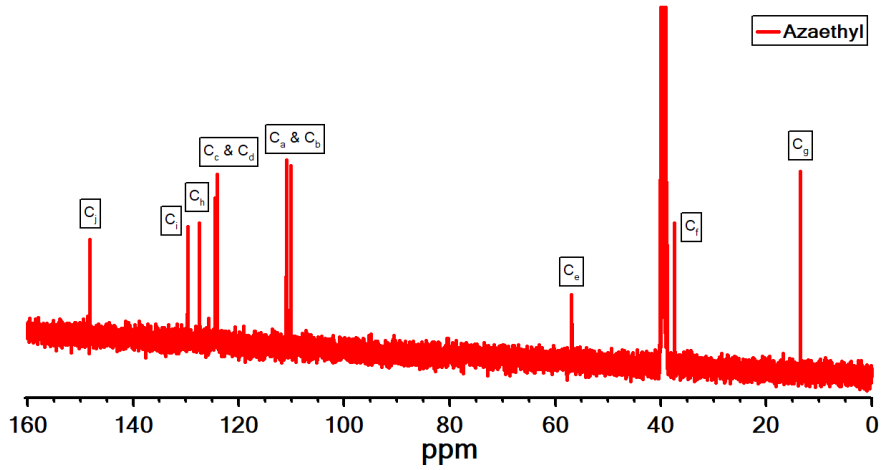

Figure 28: ^{13}C NMR spectrum of Azaethyl product dissolved in DMSO-D_6.

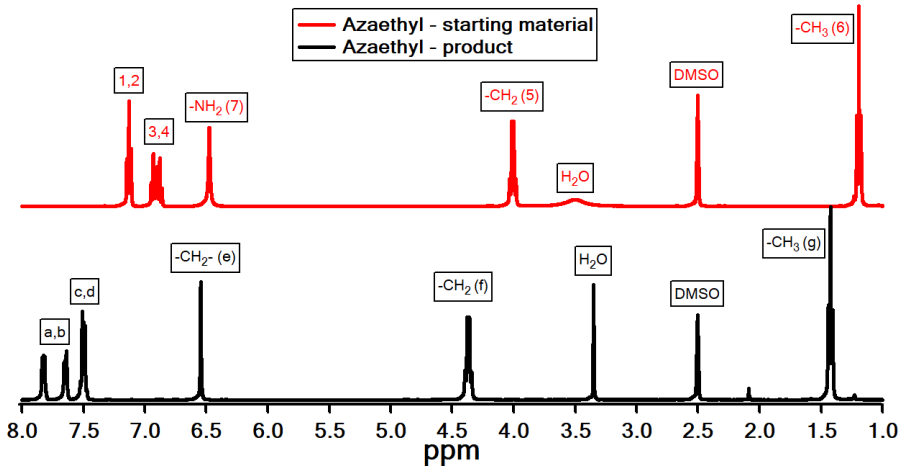

Figure 29: The comparison of ^{1}H NMR spectra of Azaethyl and its starting material dissolved in DMSO-D_6.

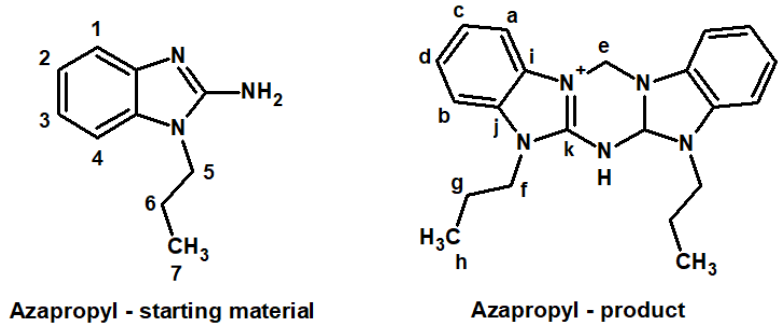

Figure 30: The structure of Azapropyl and its starting material, labeled for ^{13}C and ^{1}H NMR spectra.

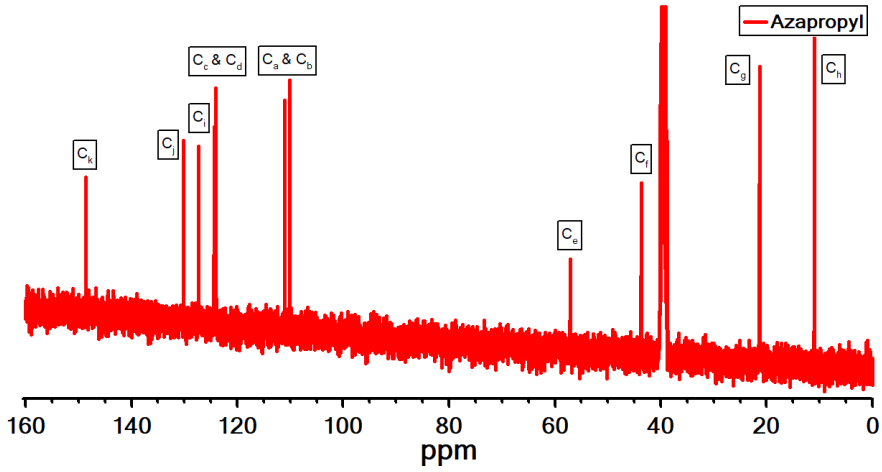

Figure 31: ^{13}C NMR spectrum of Azapropyl product dissolved in DMSO-D_6.

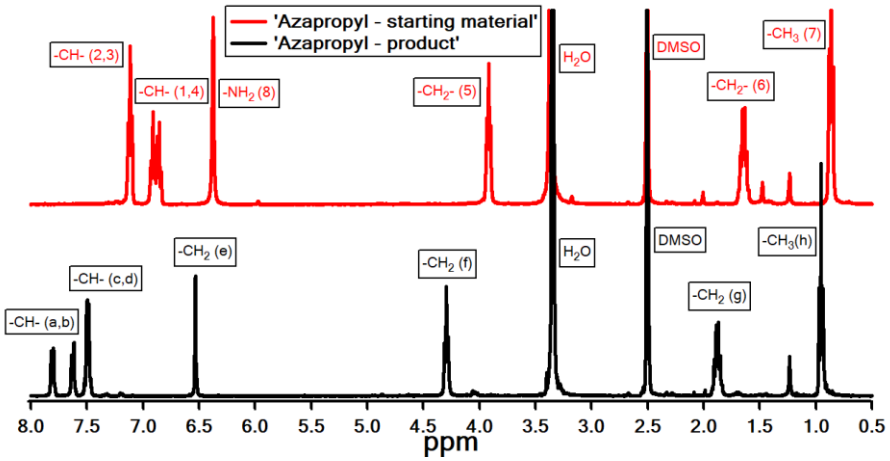

Figure 32: The comparison of ^{1}H NMR spectra of Azapropyl and its starting material dissolved in DMSO-D_6.

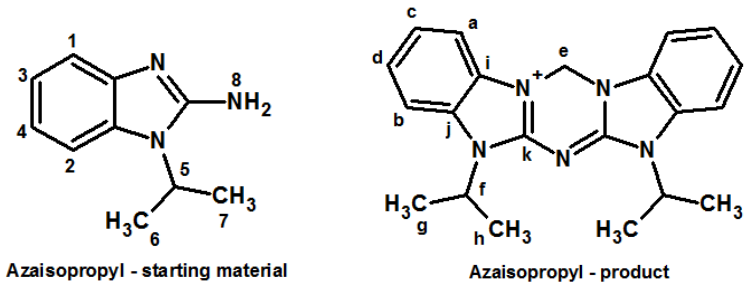

Figure 33: The structure of Azaisopropyl and its starting material, labeled for ^{13}C and ^{1}H NMR spectra.

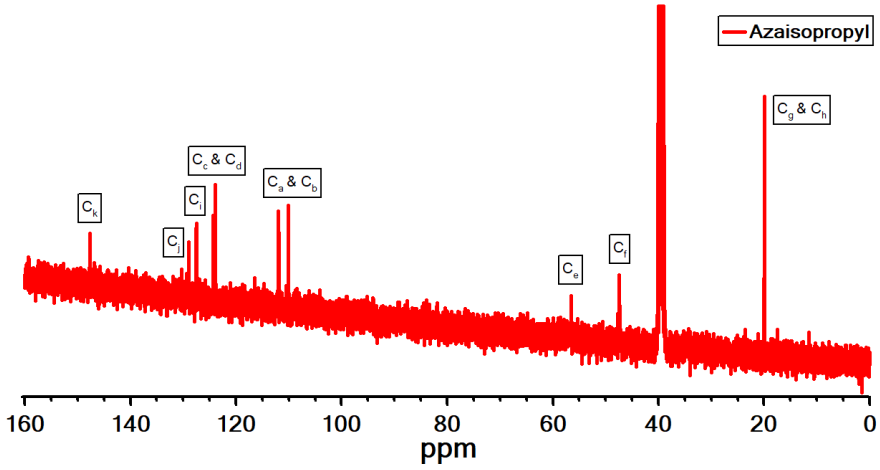

Figure 34: ^{13}C NMR spectrum of Azaisopropyl product dissolved in DMSO-D_6.

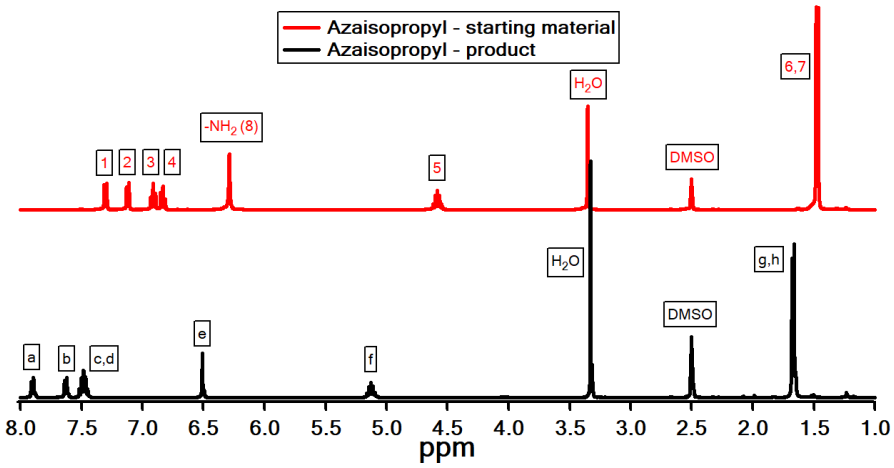

Figure 35: The comparison of [1]H NMR spectra of Azaisopropyl and its starting material dissolved in DMSO-D6.

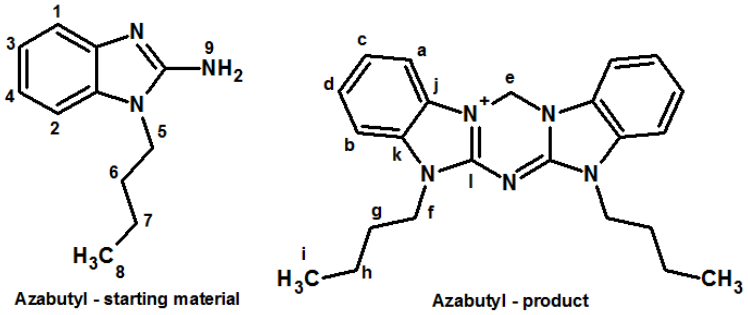

Figure 36: The structure of Azabutyl and its starting material, labeled for [13]C and [1]H NMR spectra.

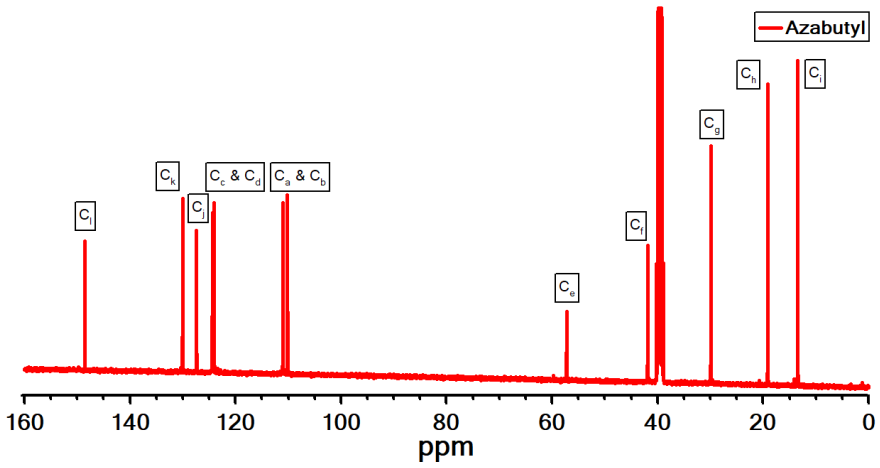

Figure 37: ^{13}C NMR spectrum of Azabutyl product dissolved in DMSO-D_6.

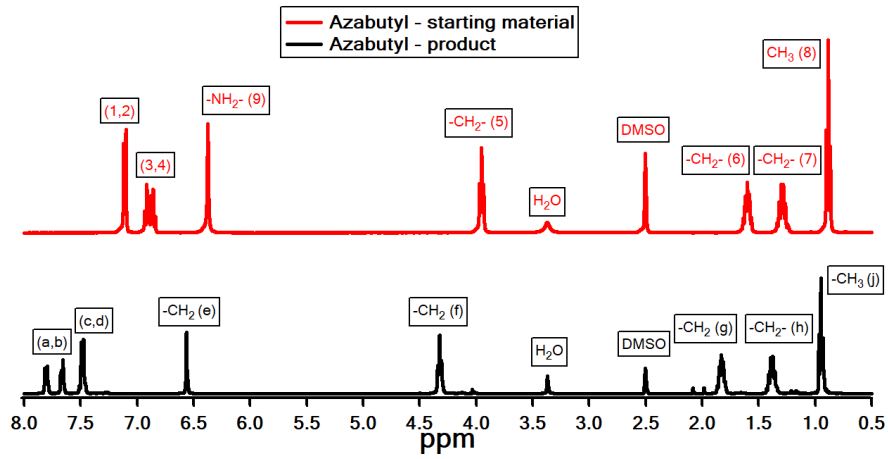

Figure 38: The comparison of ^{1}H NMR spectra of Azabutyl and its starting material dissolved in DMSO-D_6.

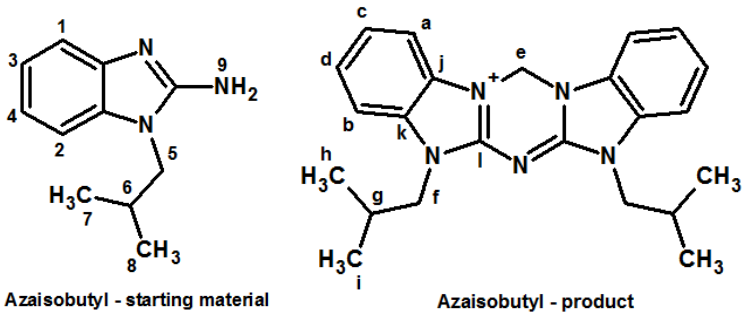

Figure 39: The structure of Azaisobutyl and its starting material, labeled for ^{13}C and ^{1}H NMR spectra.

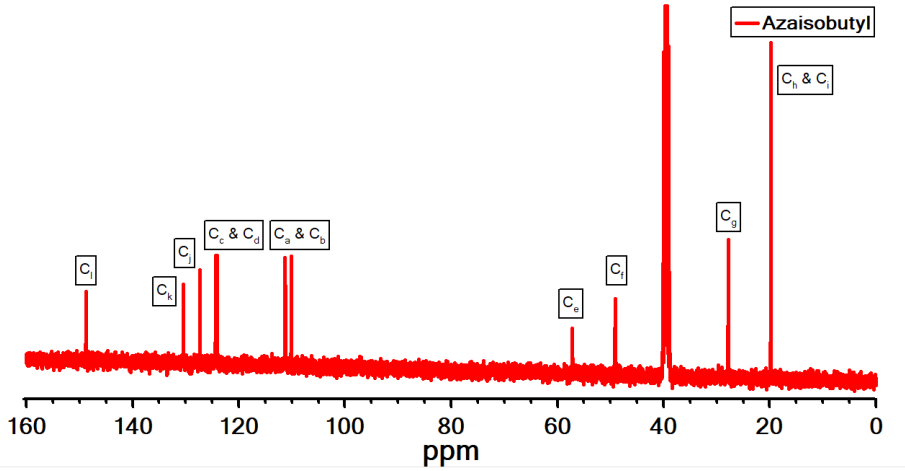

Figure 40: ^{13}C NMR spectrum of Azaisobutyl product dissolved in DMSO-D_6.

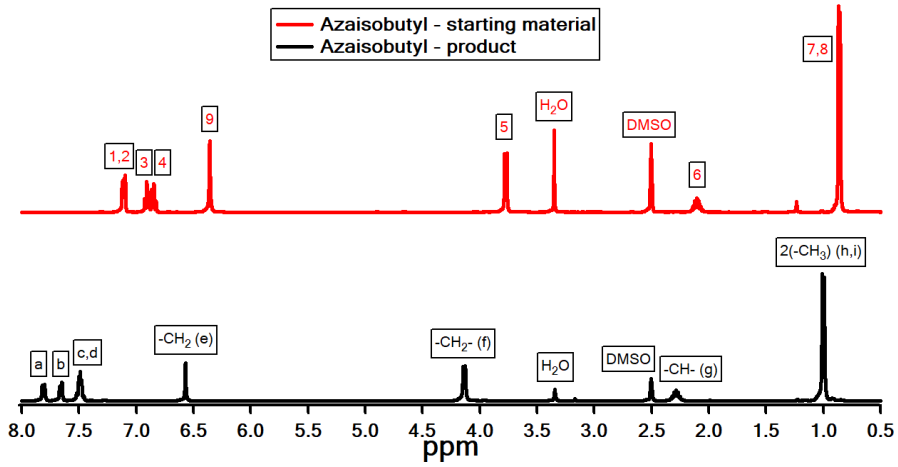

Figure 41: The comparison of ^{1}H NMR spectra of Azaisobutyl and its starting material dissolved in DMSO-D_6.

B. UV-VIS ABSORBANCE SPECTRA

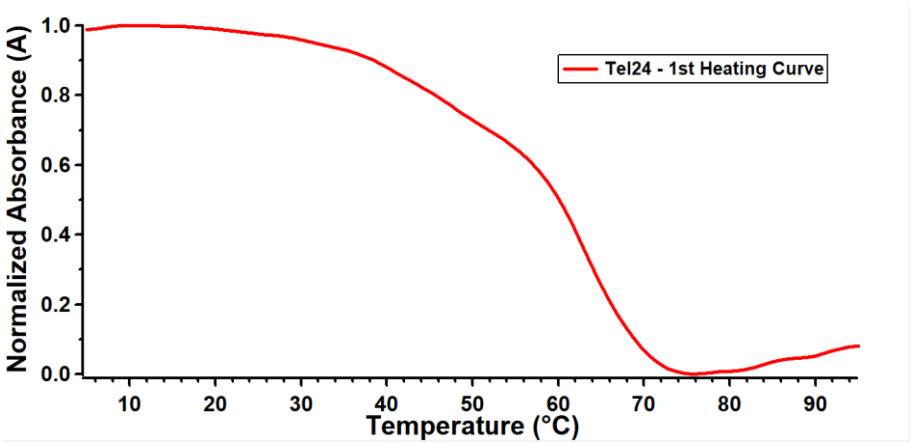

Figure 42: Thermal denaturation curve for tel24 (2.5 µM) in the absence of azacyanines obtained by monitoring the UV-VIS absorbance at 290 nm.

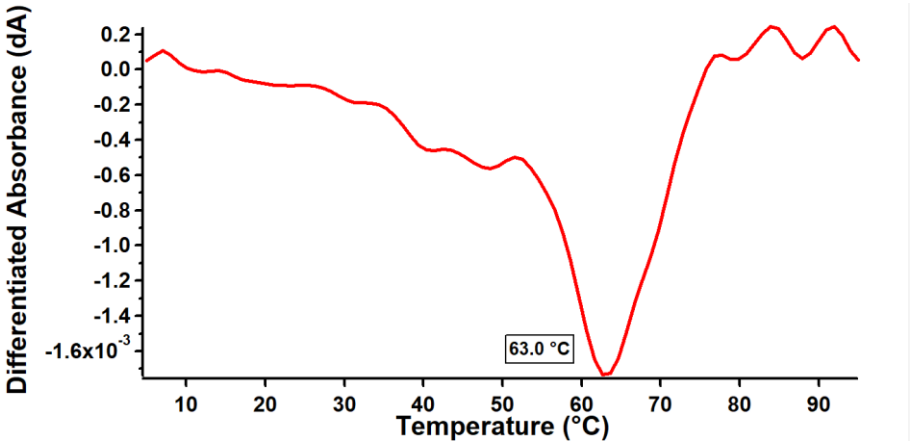

Figure 43: First derivative spectrum of the thermal denaturation curve in Figure 36.

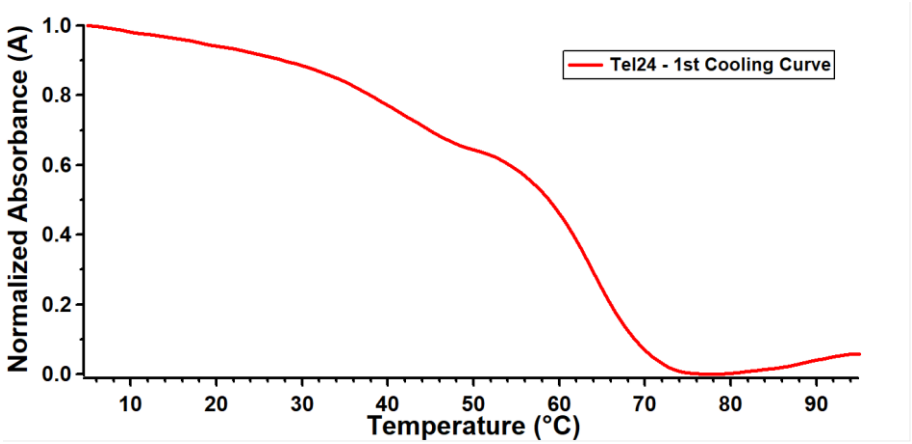

Figure 44: Thermal denaturation curve for tel24 (2.5 μM) in the absence of azacyanines obtained by monitoring the UV-VIS absorbance at 290 nm.

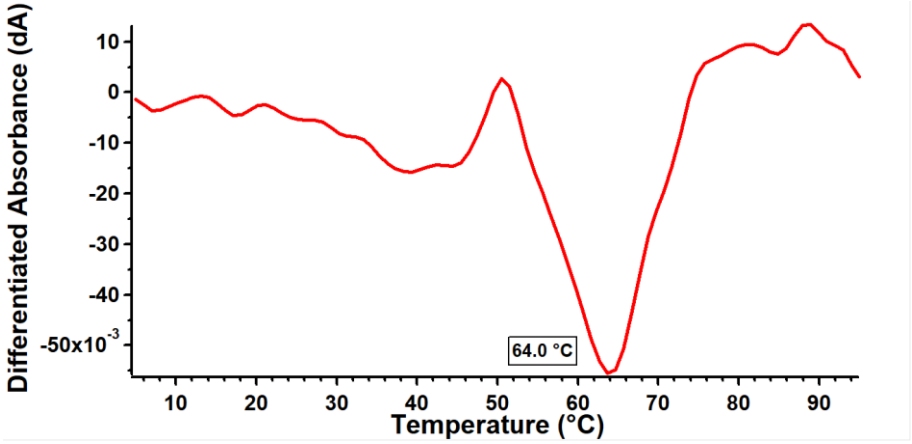

Figure 45: First derivative spectrum of the thermal denaturation curve in Figure 38.

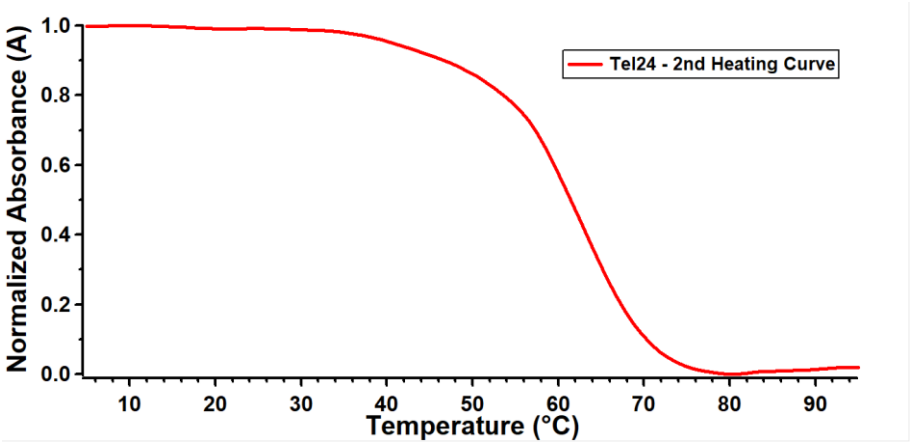

Figure 46: Thermal denaturation curve for tel24 (2.5 µM) in the absence of azacyanines obtained by monitoring the UV-VIS absorbance at 290 nm.

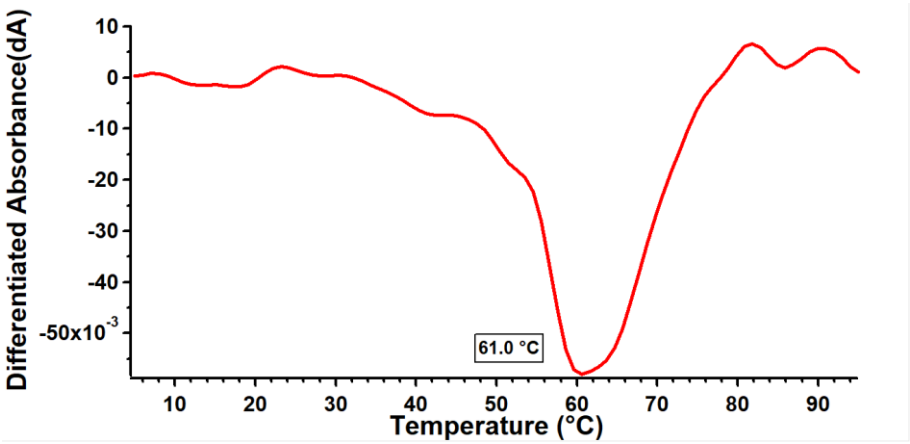

Figure 47: First derivative spectrum of the thermal denaturation curve in Figure 40.

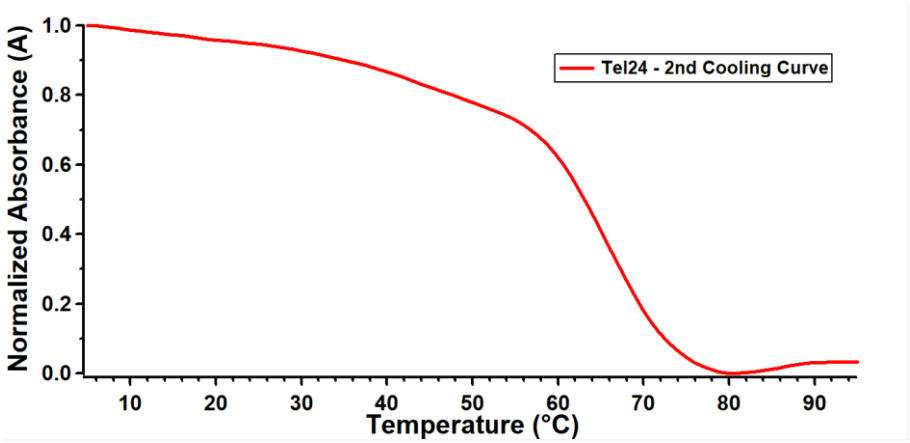

Figure 48: Thermal denaturation curve for tel24 (2.5 μM) in the absence of azacyanines obtained by monitoring the UV-VIS absorbance at 290 nm.

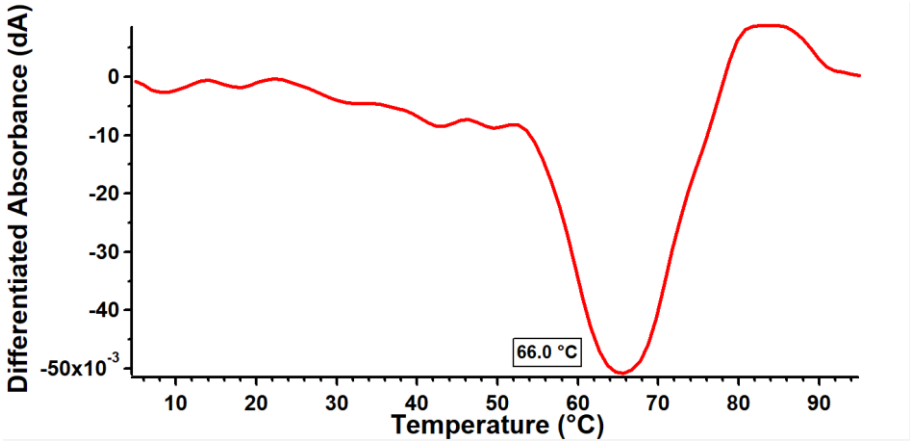

Figure 49: First derivative spectrum of the thermal denaturation curve in Figure 42.

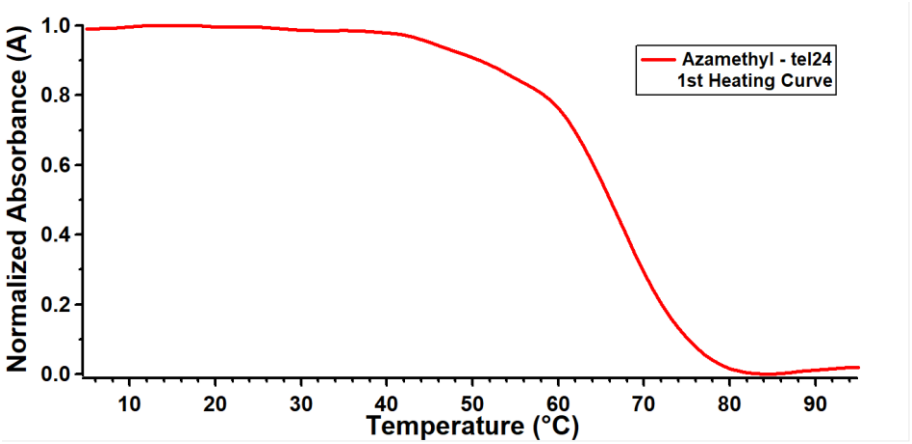

Figure 50: Thermal denaturation curve for tel24 (2.5 µM) in the presence of Azamethyl (2.5 µM) obtained by monitoring the UV-VIS absorbance at 290 nm.

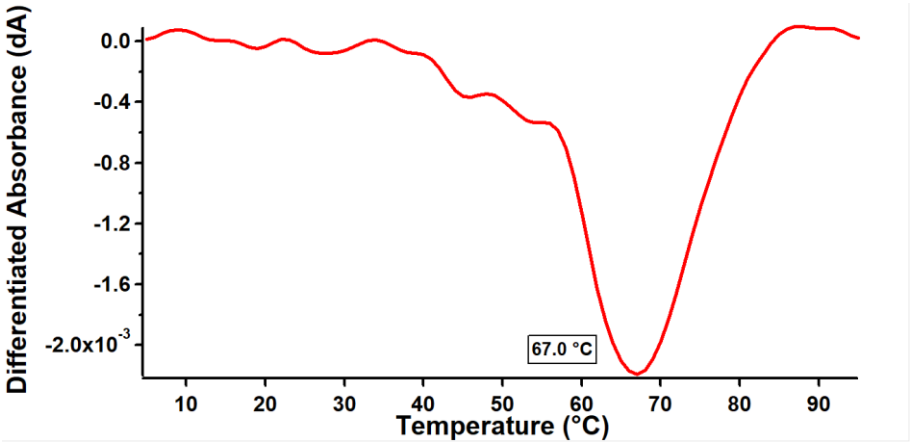

Figure 51: First derivative spectrum of the thermal denaturation curve in Figure 45.

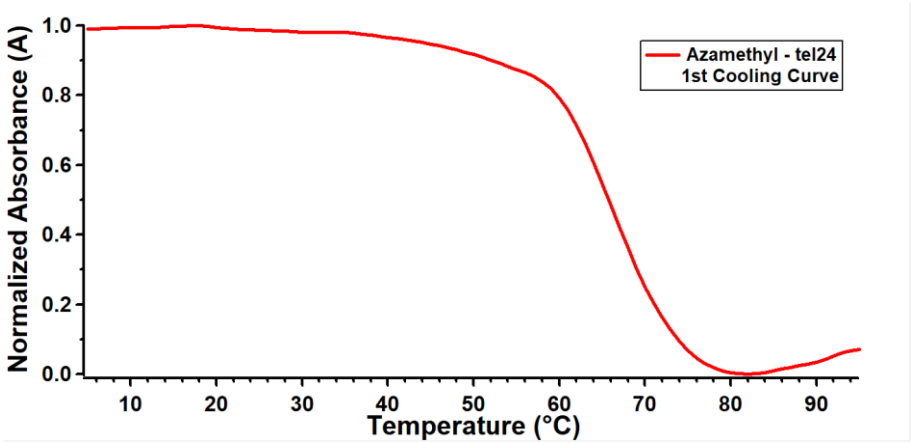

Figure 52: Thermal denaturation curve for tel24 (2.5 µM) in the presence of Azamethyl (2.5 µM) obtained by monitoring the UV-VIS absorbance at 290 nm.

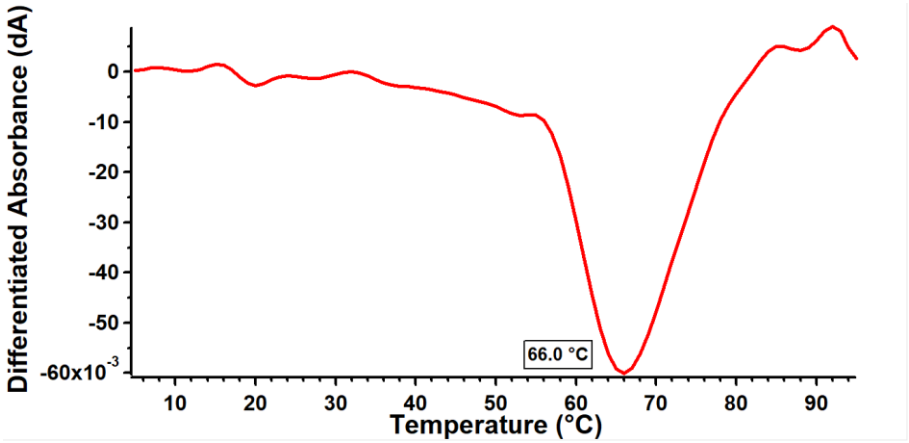

Figure 53: First derivative spectrum of the thermal denaturation curve in Figure 47.

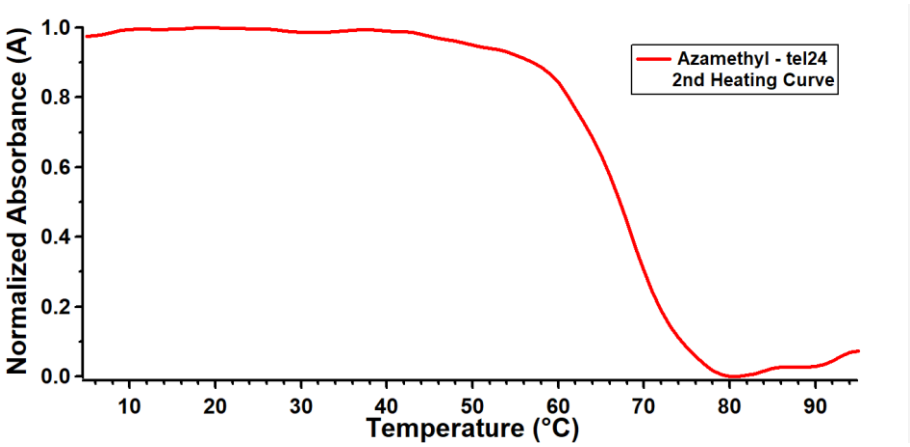

Figure 54: Thermal denaturation curve for tel24 (2.5 µM) in the presence of Azamethyl (2.5 µM) obtained by monitoring the UV-VIS absorbance at 290 nm.

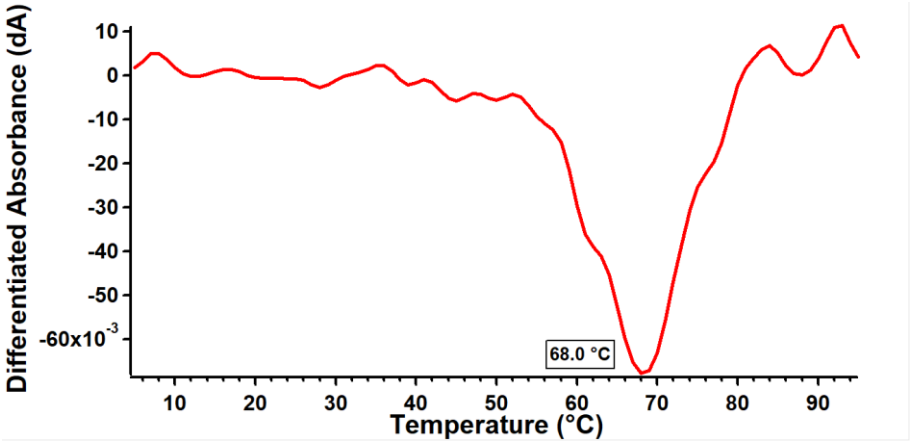

Figure 55: First derivative spectrum of the thermal denaturation curve in Figure 49.

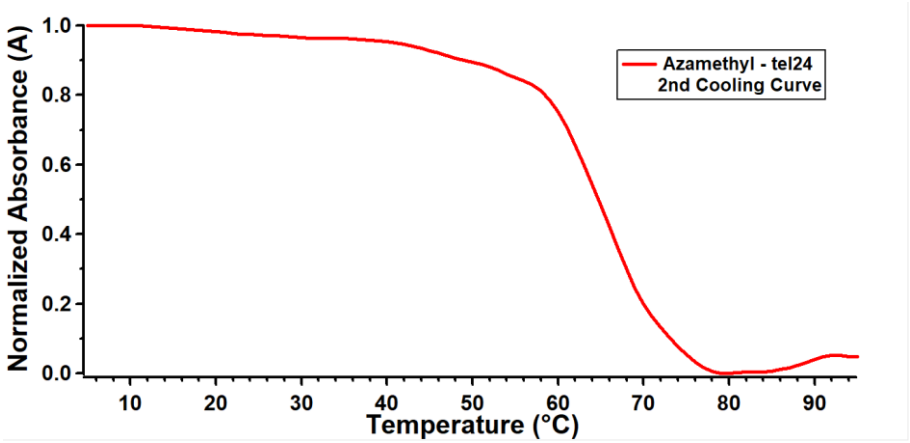

Figure 56: Thermal denaturation curve for tel24 (2.5 µM) in the presence of Azamethyl (2.5 µM) obtained by monitoring the UV-VIS absorbance at 290 nm.

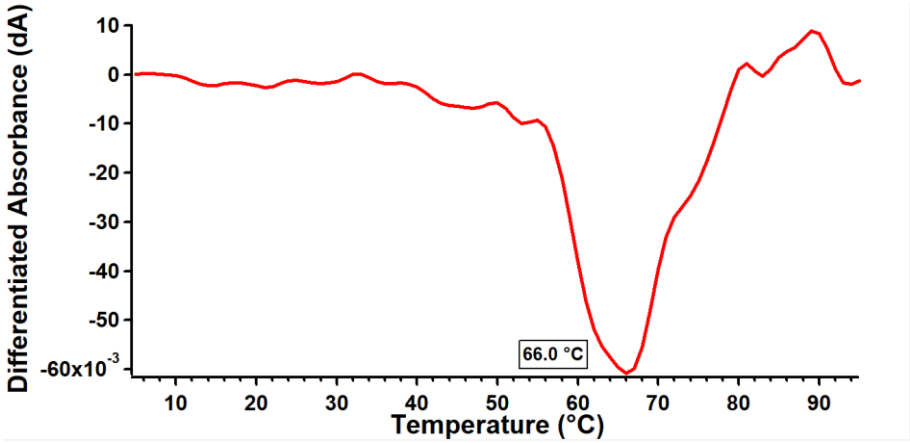

Figure 57: First derivative spectrum of the thermal denaturation curve in Figure 51.

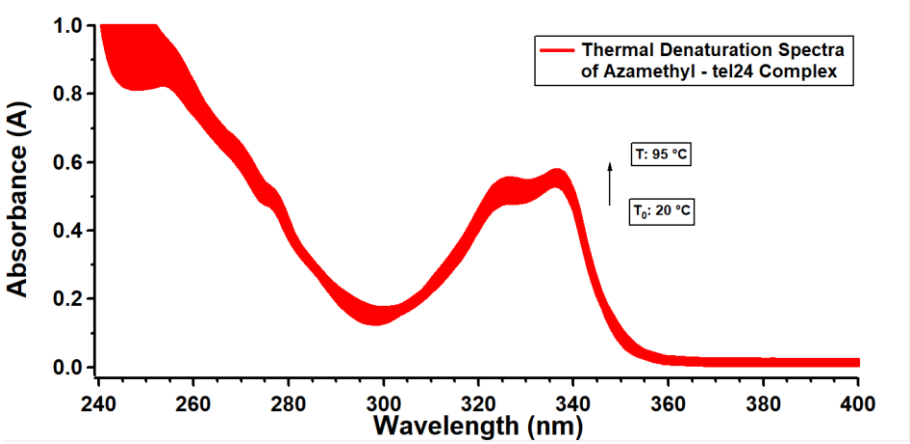

Figure 58: UV-VIS absorbance spectra of tel24 (2.5 µM) in the presence of Azamethyl (15.0 µM) obtained during thermal denaturation experiments.

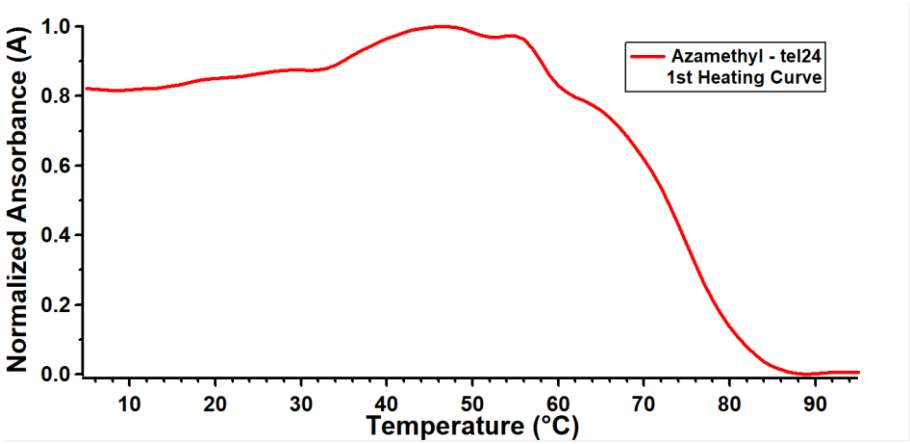

Figure 59: Thermal denaturation curve for tel24 (2.5 µM) in the presence of Azamethyl (15.0 µM) obtained by monitoring the UV-VIS absorbance at 290 nm.

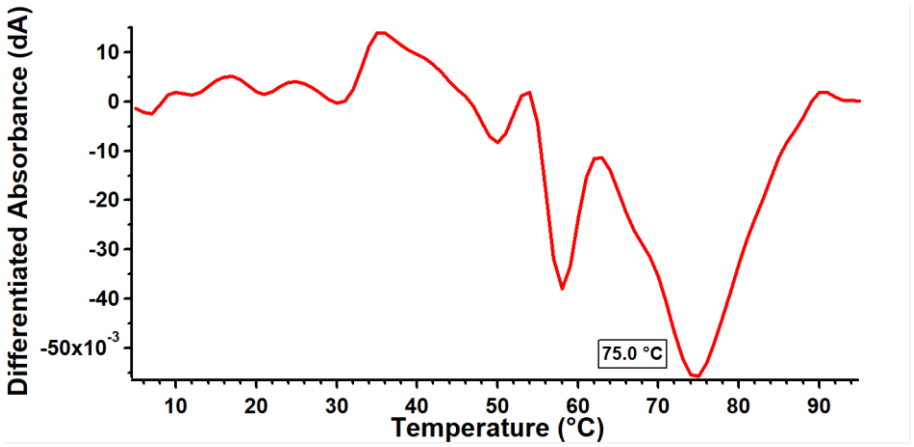

Figure 60: First derivative spectrum of the thermal denaturation curve in Figure 54.

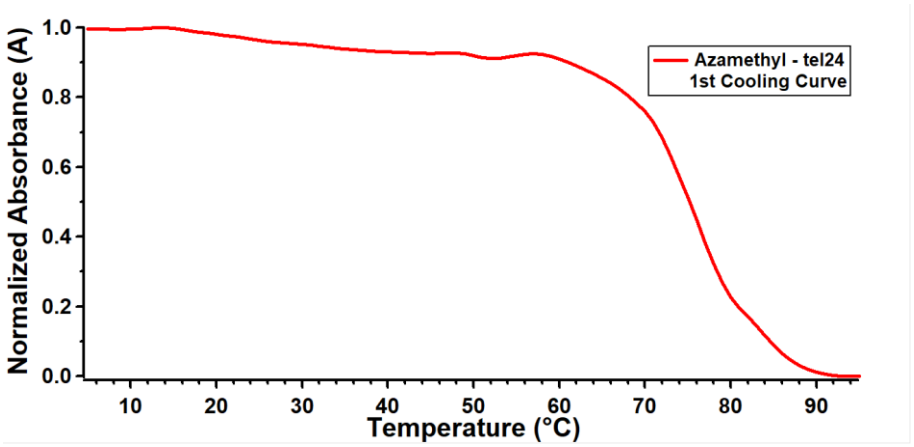

Figure 61: Thermal denaturation curve for tel24 (2.5 µM) in the presence of Azamethyl (15.0 µM) obtained by monitoring the UV-VIS absorbance at 290 nm.

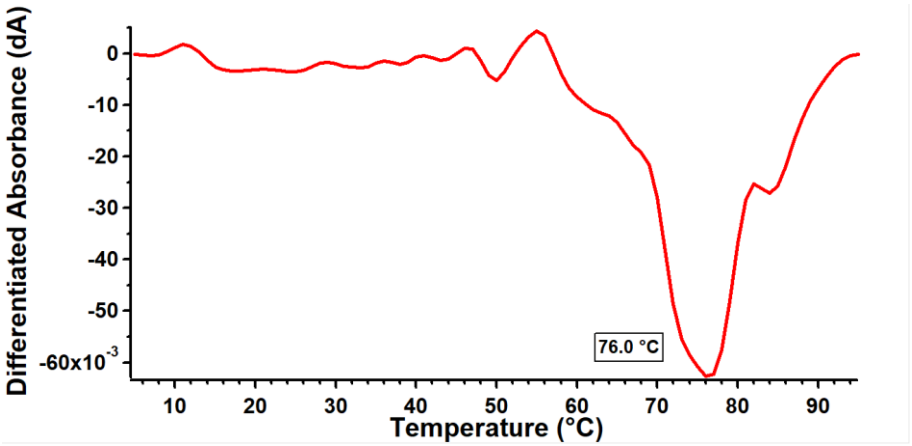

Figure 62: First derivative spectrum of the thermal denaturation curve in Figure 56.

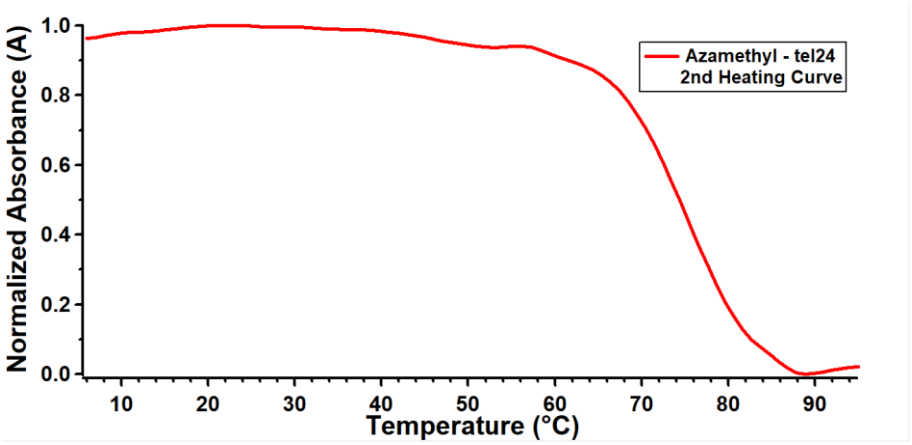

Figure 63: Thermal denaturation curve for tel24 (2.5 µM) in the presence of Azamethyl (15.0 µM) obtained by monitoring the UV-VIS absorbance at 290 nm.

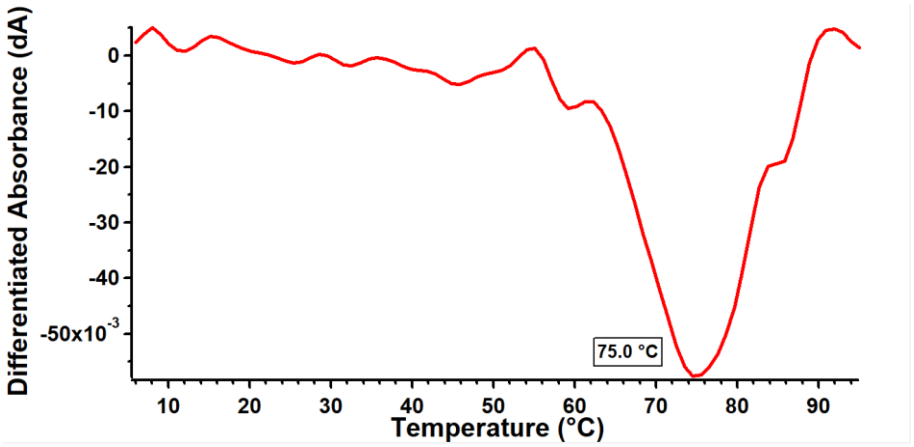

Figure 64: First derivative spectrum of the thermal denaturation curve in Figure 58.

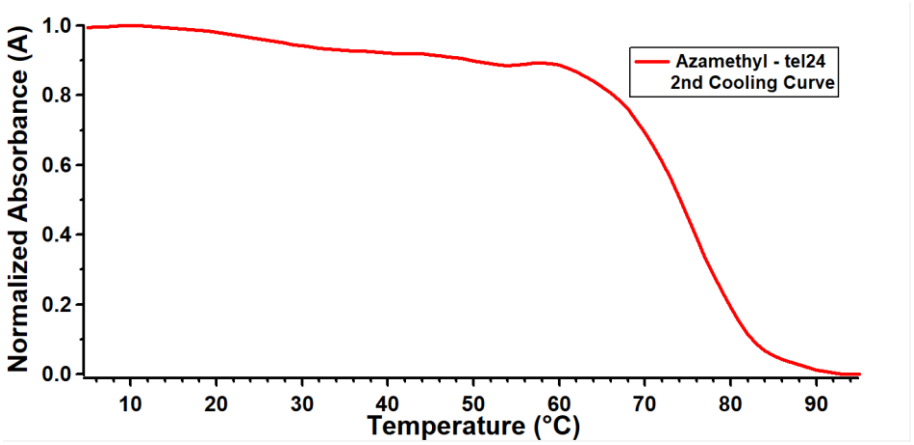

Figure 65: Thermal denaturation curve for tel24 (2.5 µM) in the presence of Azamethyl (15.0 µM) obtained by monitoring the UV-VIS absorbance at 290 nm.

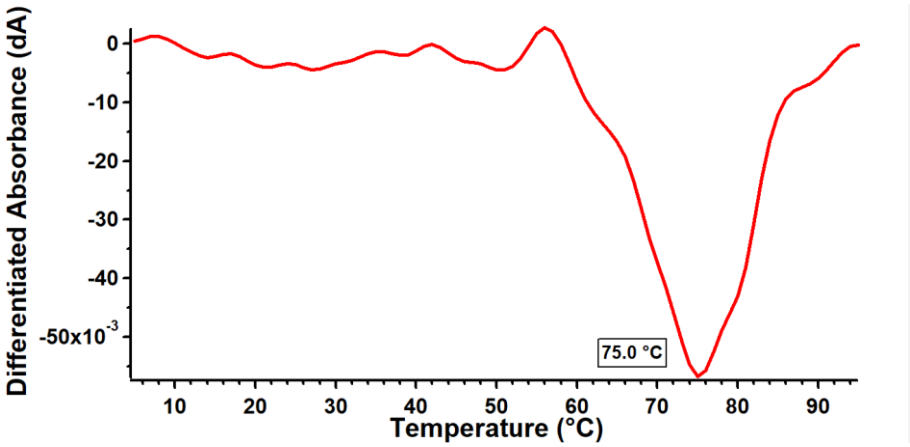

Figure 66: First derivative spectrum of the thermal denaturation curve in Figure 60.

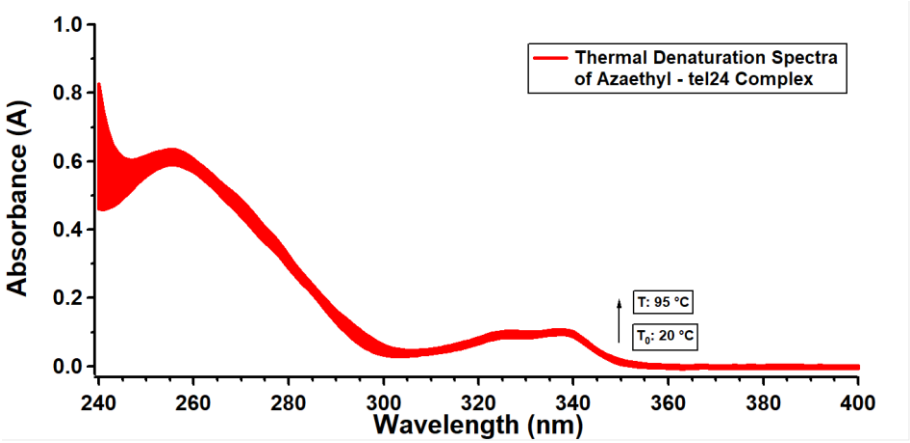

Figure 67: UV-VIS absorbance spectra of tel24 (2.5 µM) in the presence of Azaethyl (2.5 µM) Azacyanines obtained during thermal denaturation experiments.

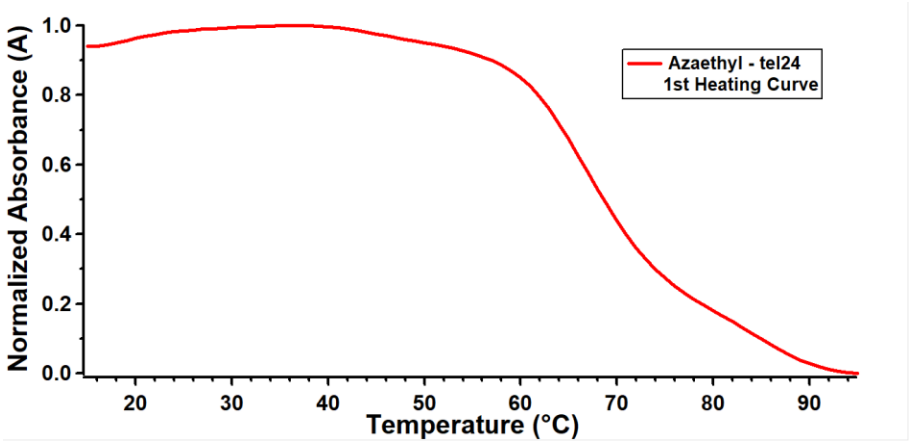

Figure 68: Thermal denaturation curve for tel24 (2.5 µM) in the presence of Azaethyl (2.5 µM) obtained by monitoring the UV-VIS absorbance at 290 nm.

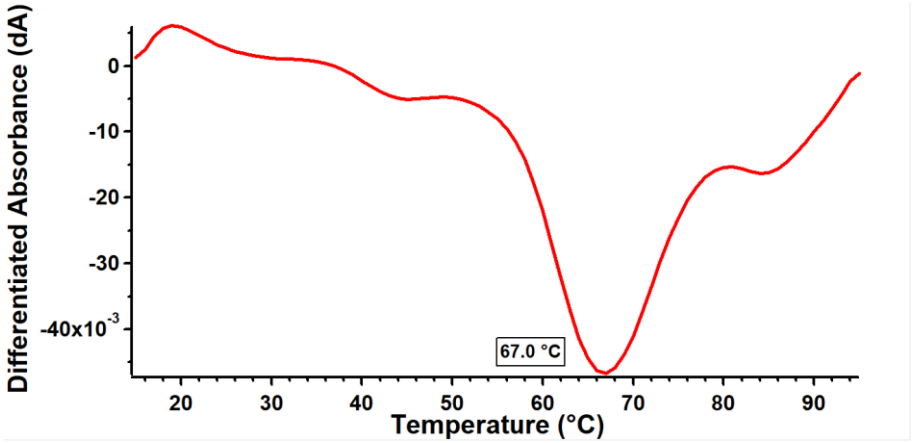

Figure 69: First derivative spectrum of the thermal denaturation curve in Figure 63.

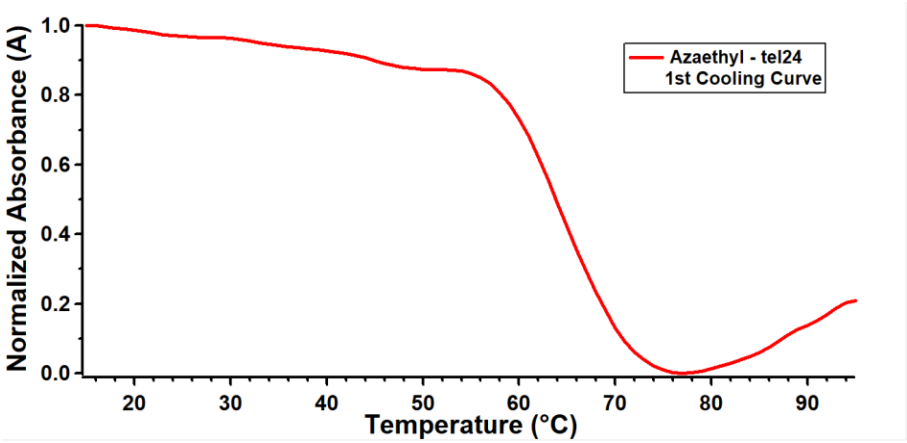

Figure 70: Thermal denaturation curve for tel24 (2.5 µM) in the presence of Azaethyl (2.5 µM) obtained by monitoring the UV-VIS absorbance at 290 nm.

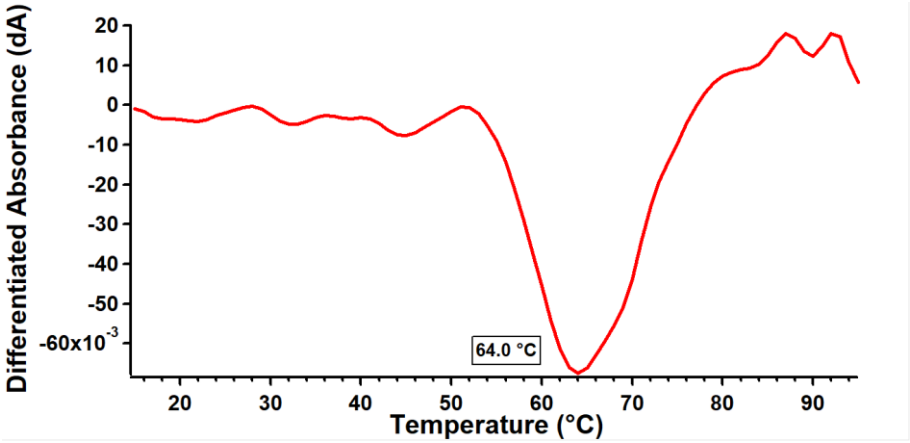

Figure 71: First derivative spectrum of the thermal denaturation curve in Figure 65.

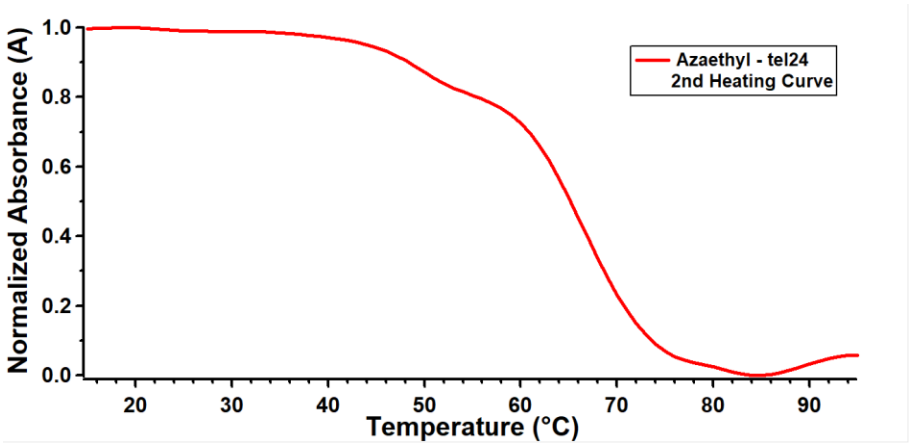

Figure 72: Thermal denaturation curve for tel24 (2.5 µM) in the presence of Azaethyl (2.5 µM) obtained by monitoring the UV-VIS absorbance at 290 nm.

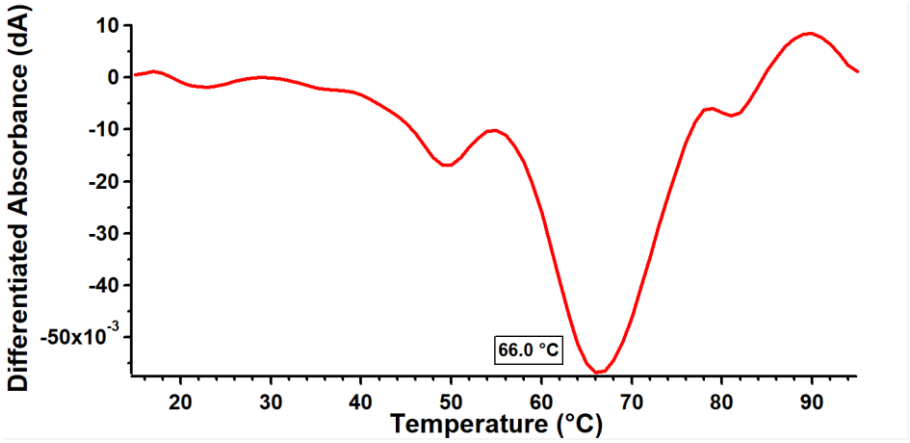

Figure 73: First derivative spectrum of the thermal denaturation curve in Figure 67.

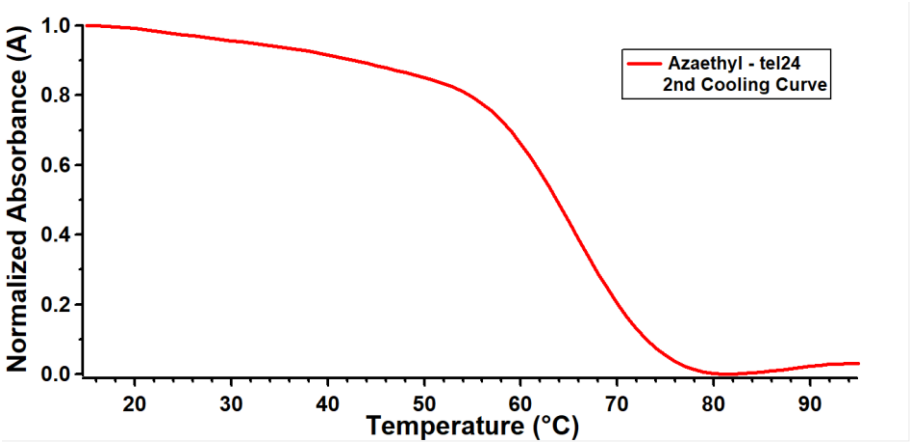

Figure 74: Thermal denaturation curve for tel24 (2.5 µM) in the presence of Azaethyl (2.5 µM) obtained by monitoring the UV-VIS absorbance at 290 nm.

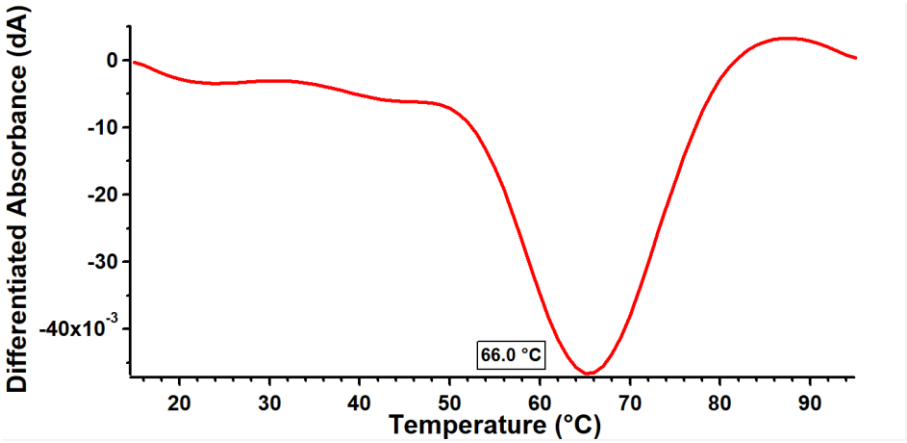

Figure 75: First derivative spectrum of the thermal denaturation curve in Figure 69.

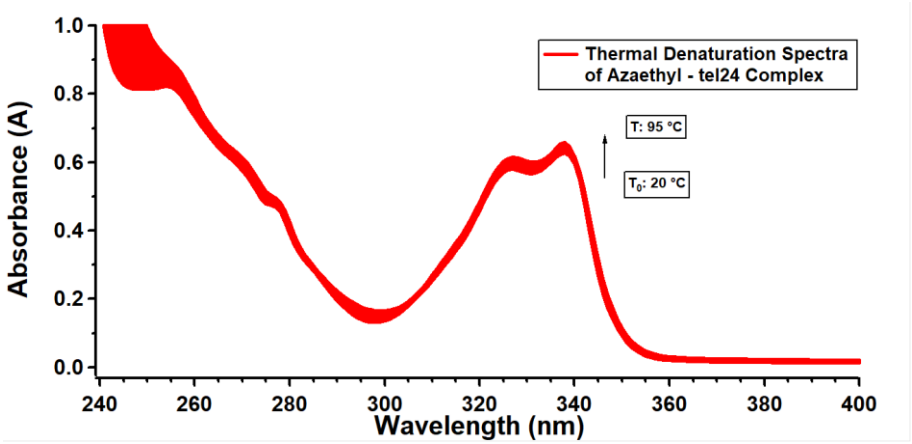

Figure 76: UV-VIS absorbance spectra of tel24 (2.5 μM) in the presence of Azaethyl (15.0 μM) obtained during thermal denaturation experiments.

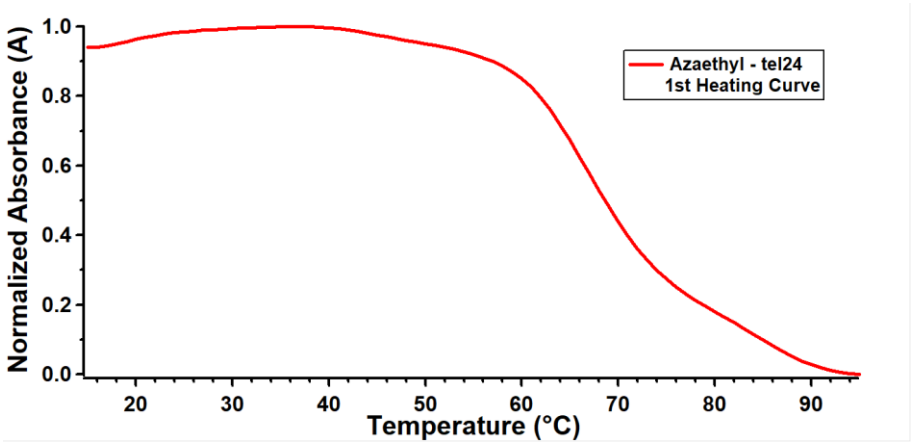

Figure 77: Thermal denaturation curve for tel24 (2.5 μM) in the presence of Azaethyl (15.0 μM) obtained by monitoring the UV-VIS absorbance at 290 nm.

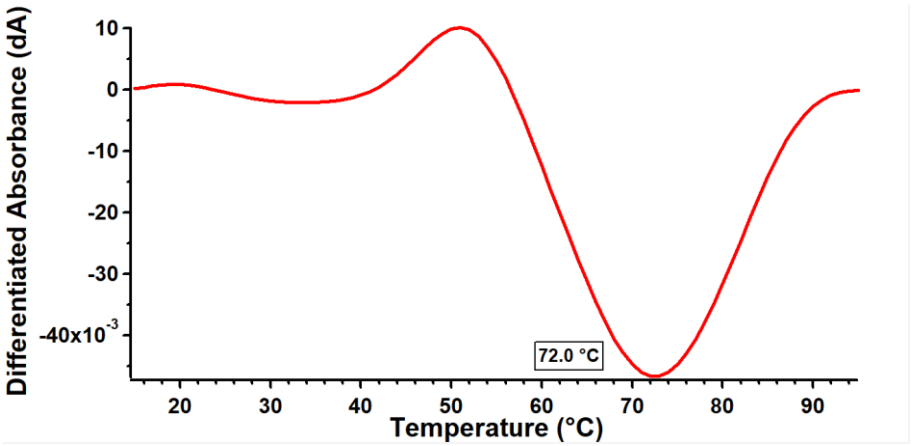

Figure 78: First derivative spectrum of the thermal denaturation curve in Figure 72.

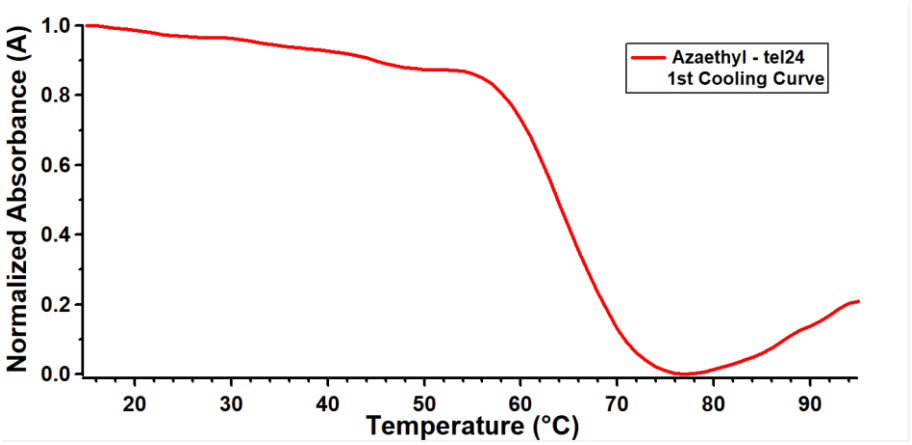

Figure 79: Thermal denaturation curve for tel24 (2.5 μM) in the presence of Azaethyl (15.0 μM) obtained by monitoring the UV-VIS absorbance at 290 nm.

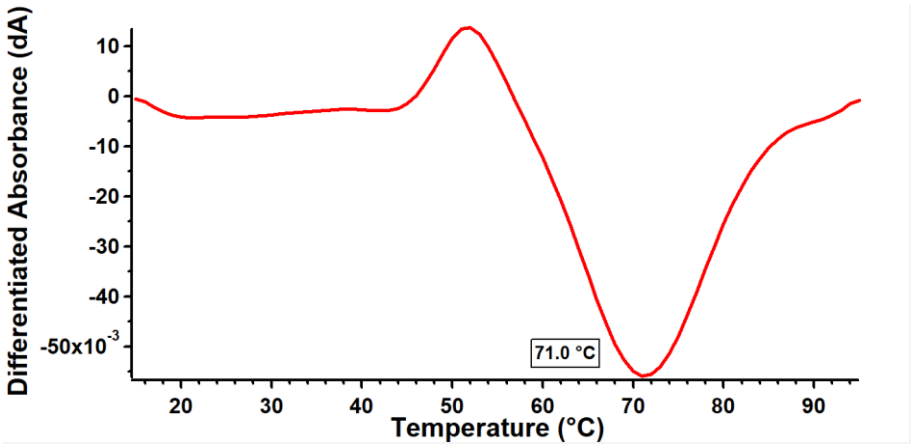

Figure 80: First derivative spectrum of the thermal denaturation curve in Figure 74.

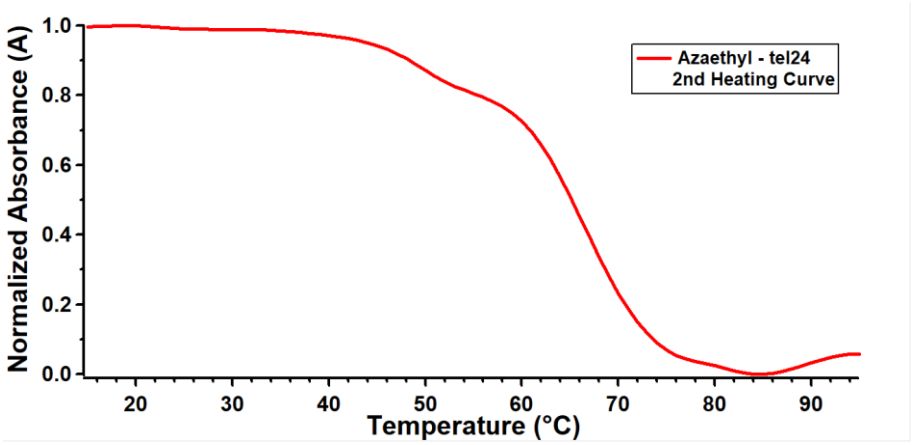

Figure 81: Thermal denaturation curve for tel24 (2.5 μM) in the presence of Azaethyl (15.0 μM) obtained by monitoring the UV-VIS absorbance at 290 nm.

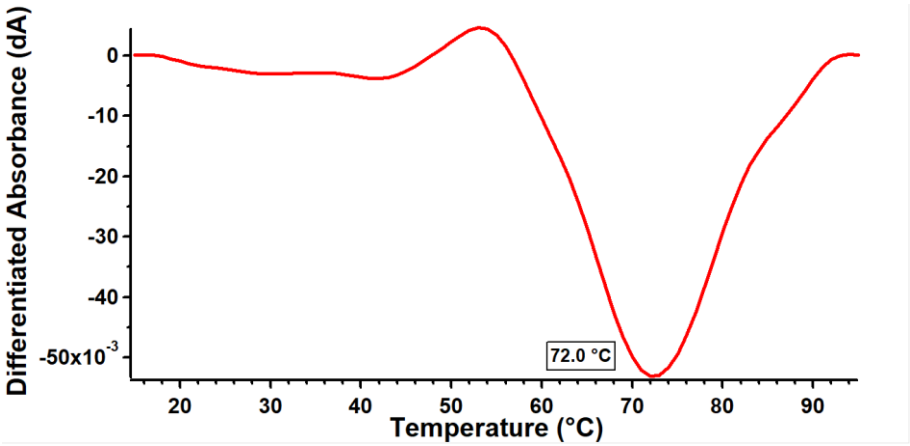

Figure 82: First derivative spectrum of the thermal denaturation curve in Figure 76.

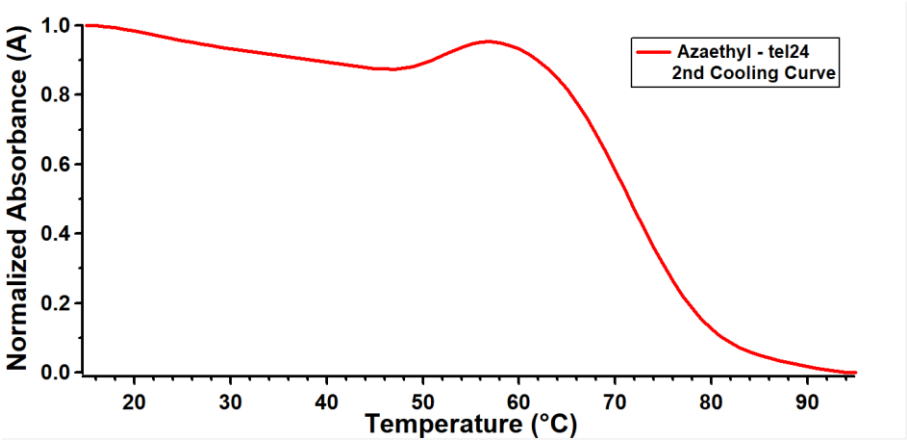

Figure 83: Thermal denaturation curve for tel24 (2.5 µM) in the presence of Azaethyl (15.0 µM) obtained by monitoring the UV-VIS absorbance at 290 nm.

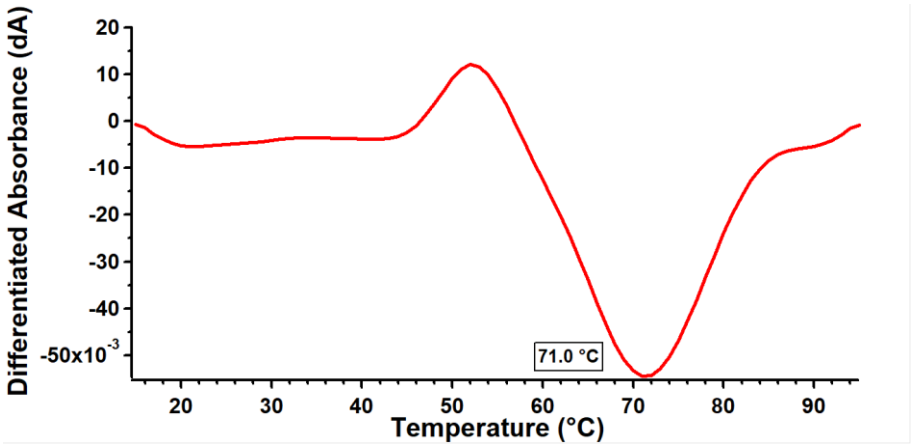

Figure 84: First derivative spectrum of the thermal denaturation curve in Figure 78.

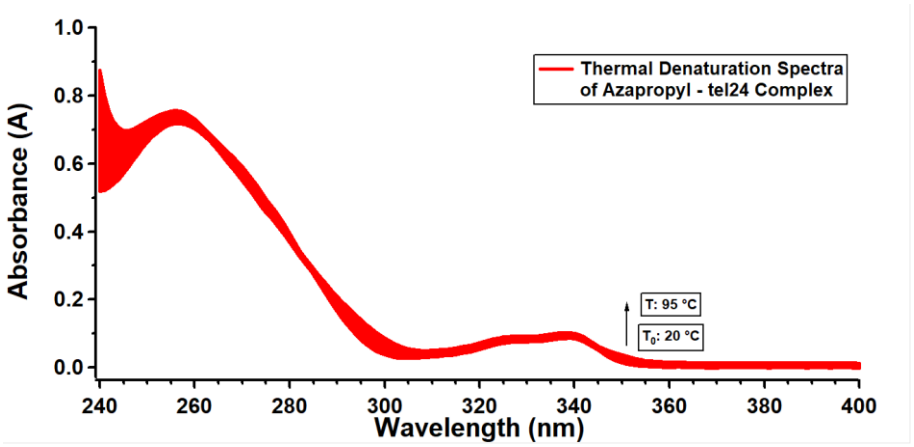

Figure 85: UV-VIS absorbance spectra of tel24 (2.5 µM) in the presence of Azapropyl (2.5 µM) obtained during thermal denaturation experiments.

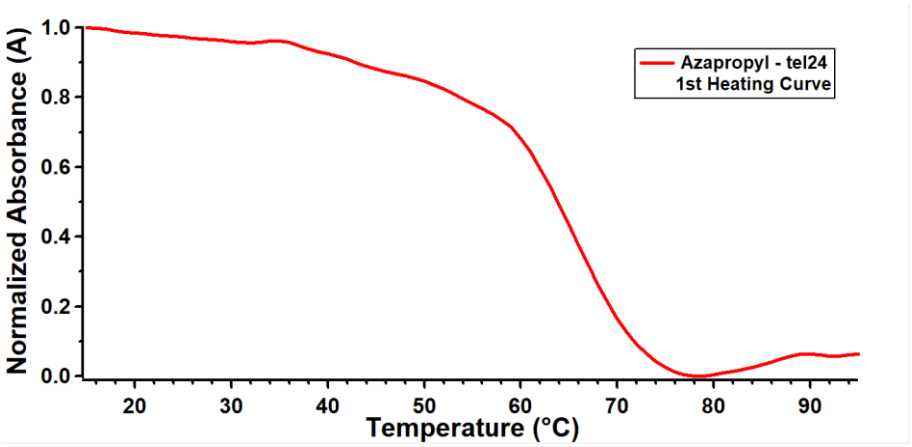

Figure 86: Thermal denaturation curve for tel24 (2.5 µM) in the presence of Azapropyl (2.5 µM) obtained by monitoring the UV-VIS absorbance at 290 nm.

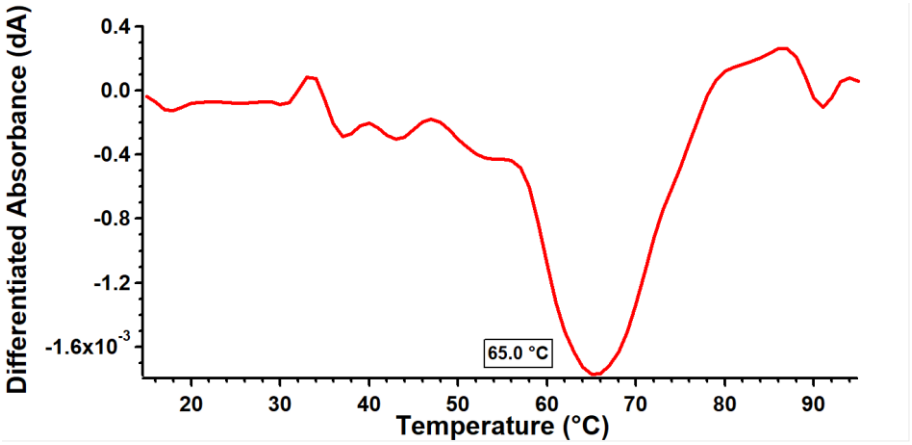

Figure 87: First derivative spectrum of the thermal denaturation curve in Figure 81.

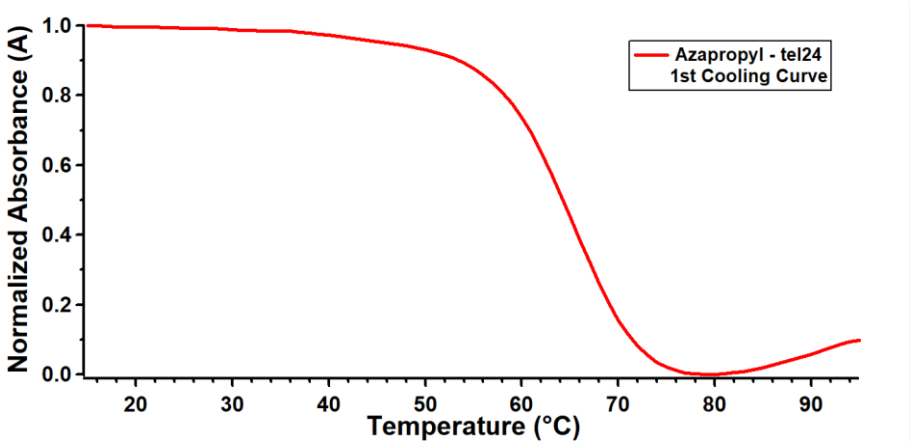

Figure 88: Thermal denaturation curve for tel24 (2.5 µM) in the presence of Azapropyl (2.5 µM) obtained by monitoring the UV-VIS absorbance at 290 nm.

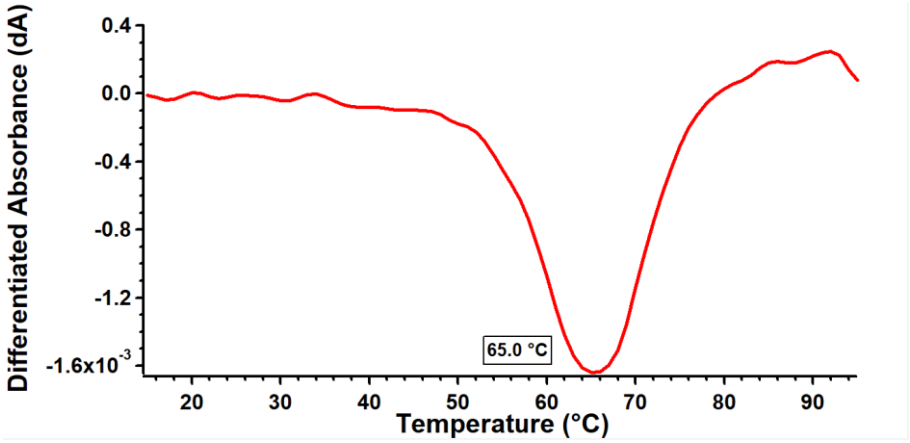

Figure 89: First derivative spectrum of the thermal denaturation curve in Figure 83.

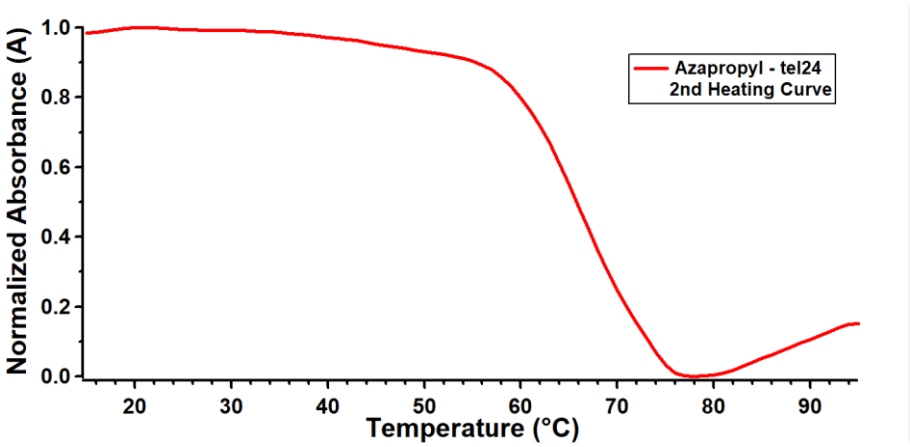

Figure 90: Thermal denaturation curve for tel24 (2.5 µM) in the presence of Azapropyl (2.5 µM) obtained by monitoring the UV-VIS absorbance at 290 nm.

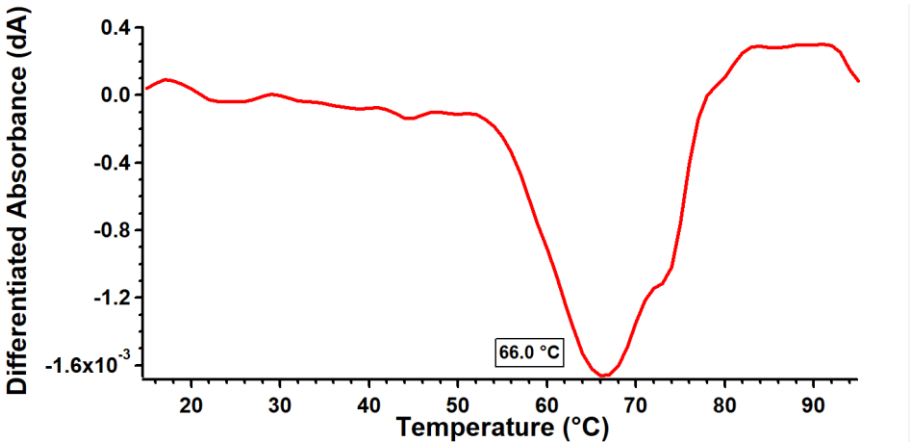

Figure 91: First derivative spectrum of the thermal denaturation curve in Figure 85.

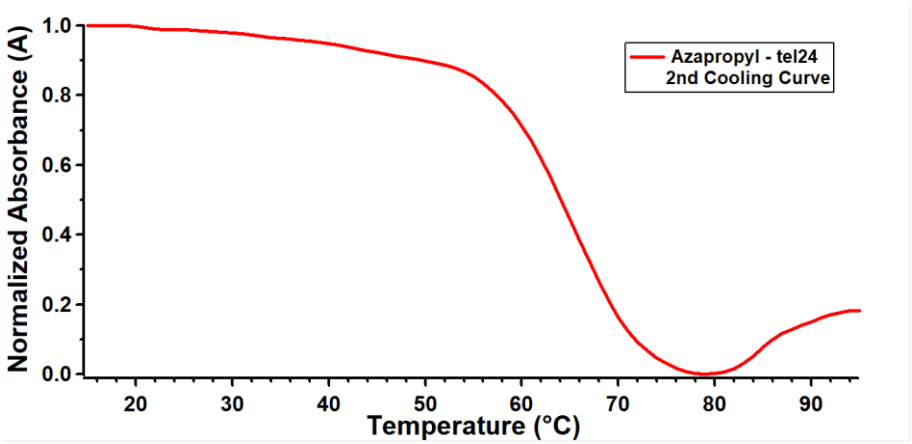

Figure 92: Thermal denaturation curve for tel24 (2.5 µM) in the presence of Azapropyl (2.5 µM) obtained by monitoring the UV-VIS absorbance at 290 nm.

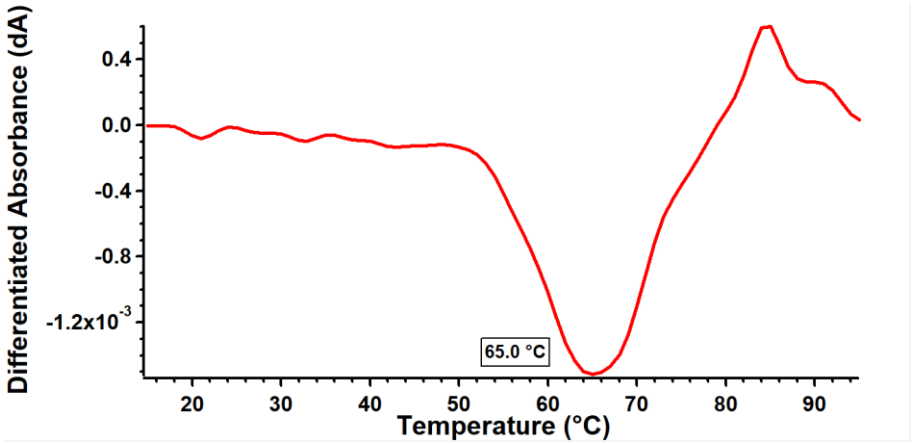

Figure 93: First derivative spectrum of the thermal denaturation curve in Figure 87.

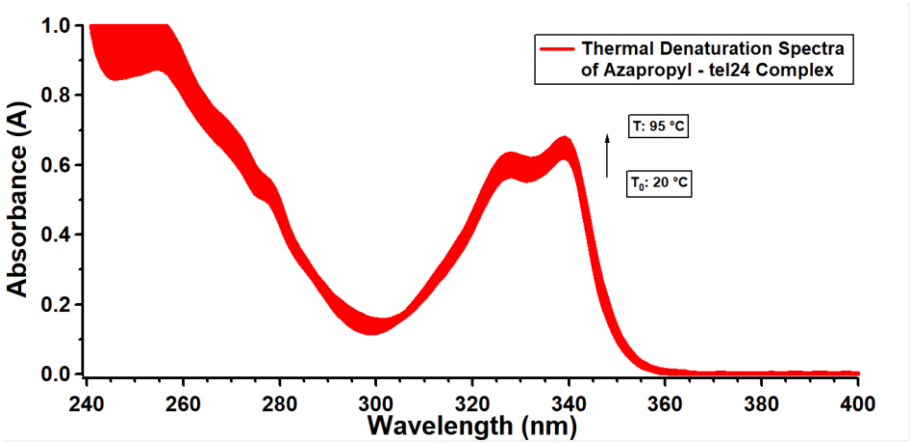

Figure 94: UV-VIS absorbance spectra of tel24 (2.5 µM) in the presence of Azapropyl (15.0 µM) obtained during thermal denaturation experiments.

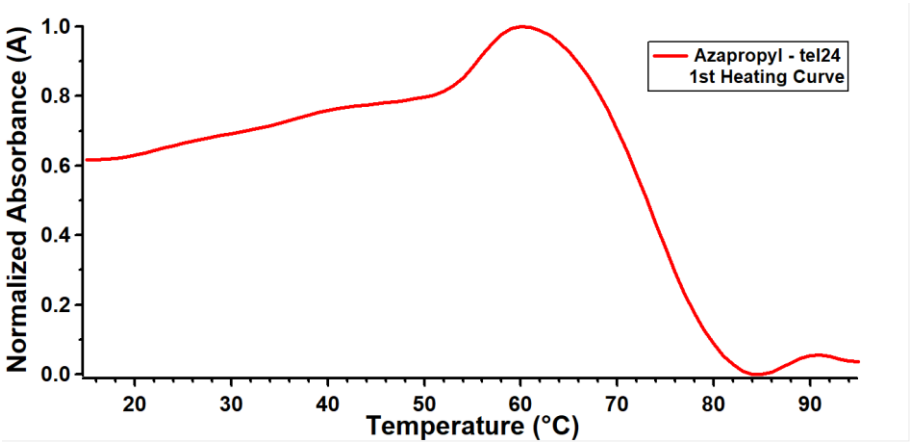

Figure 95: Thermal denaturation curve for tel24 (2.5 µM) in the presence of Azapropyl (15.0 µM) obtained by monitoring the UV-VIS absorbance at 290 nm.

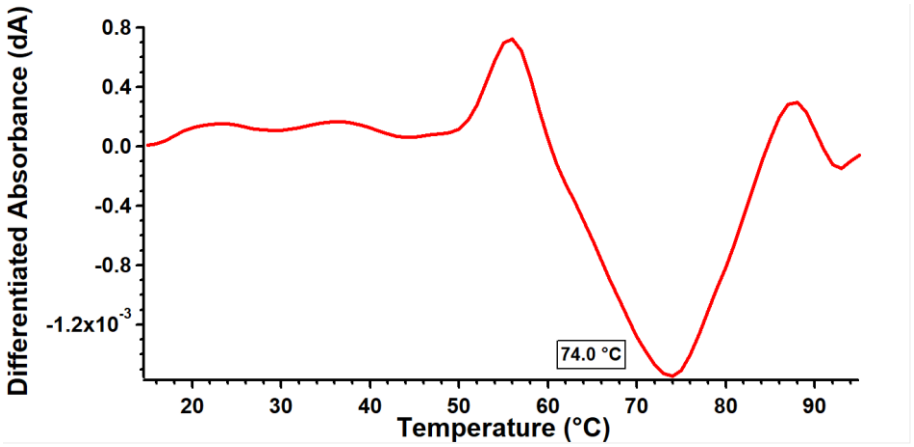

Figure 96: First derivative spectrum of the thermal denaturation curve in Figure 90.

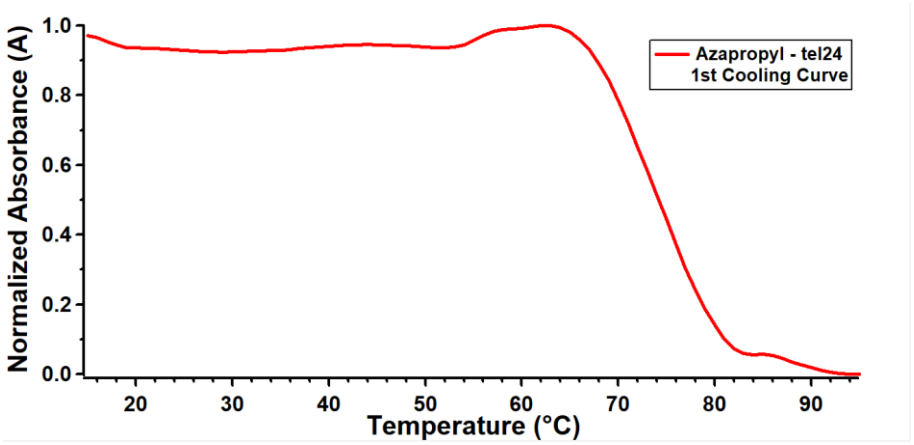

Figure 97: Thermal denaturation curve for tel24 (2.5 µM) in the presence of Azapropyl (15.0 µM) obtained by monitoring the UV-VIS absorbance at 290 nm.

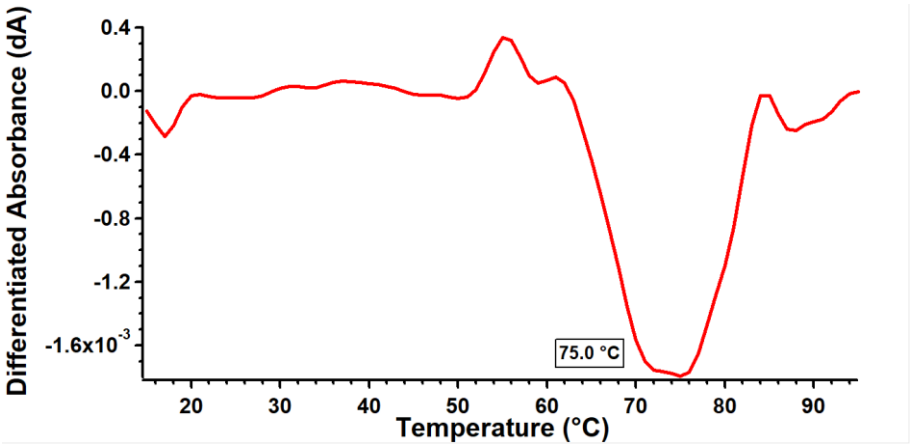

Figure 98: First derivative spectrum of the thermal denaturation curve in Figure 92.

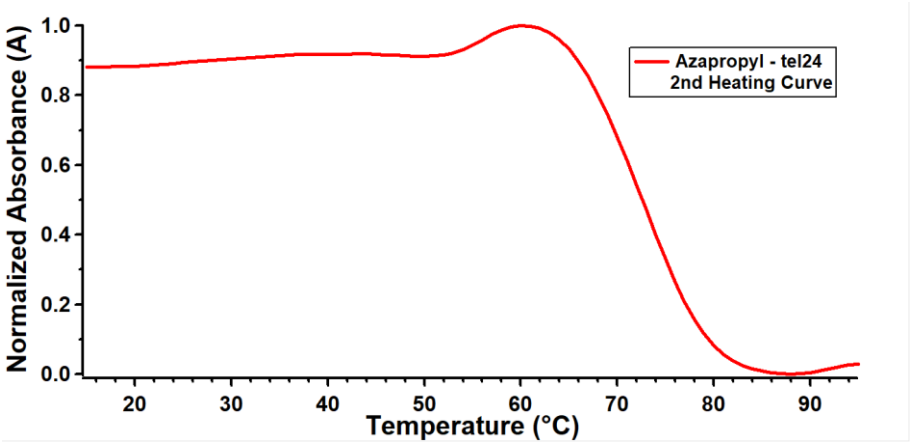

Figure 99: Thermal denaturation curve for tel24 (2.5 μM) in the presence of Azapropyl (15.0 μM) obtained by monitoring the UV-VIS absorbance at 290 nm.

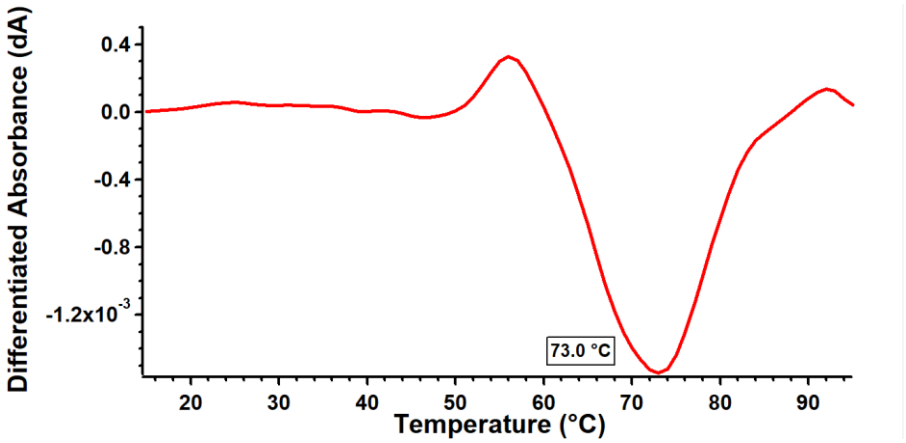

Figure 100: First derivative spectrum of the thermal denaturation curve in Figure 94.

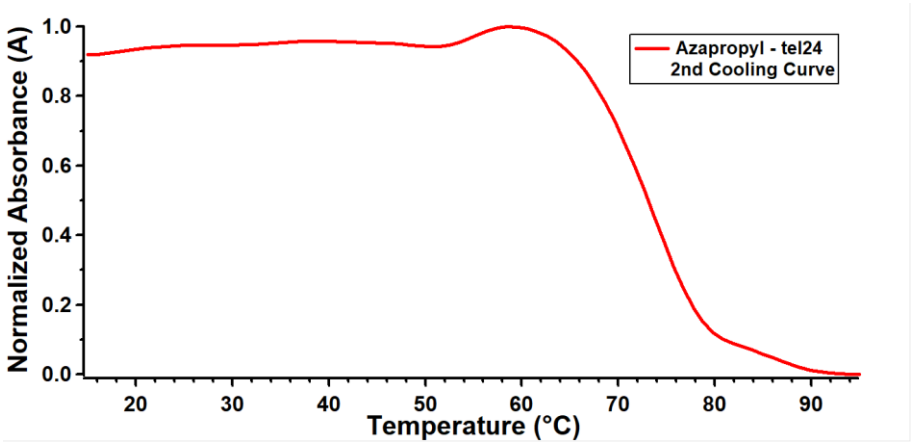

Figure 101: Thermal denaturation curve for tel24 (2.5 μM) in the presence of Azapropyl (15.0 μM) obtained by monitoring the UV-VIS absorbance at 290 nm.

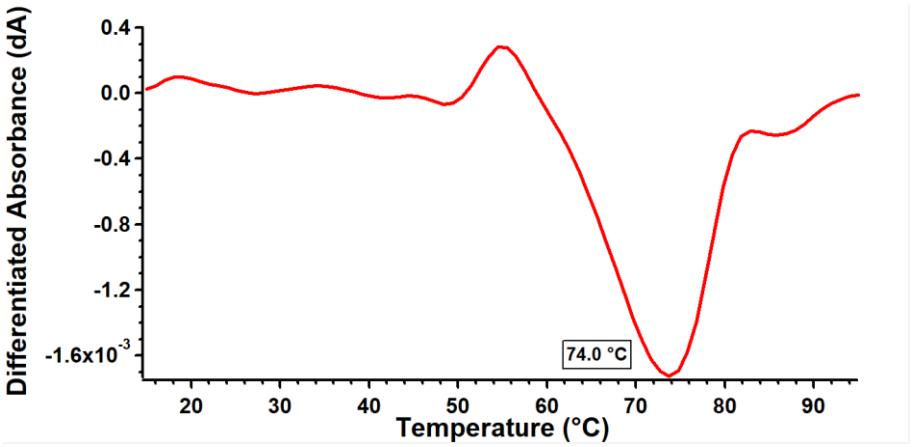

Figure 102: First derivative spectrum of the thermal denaturation curve in Figure 96.

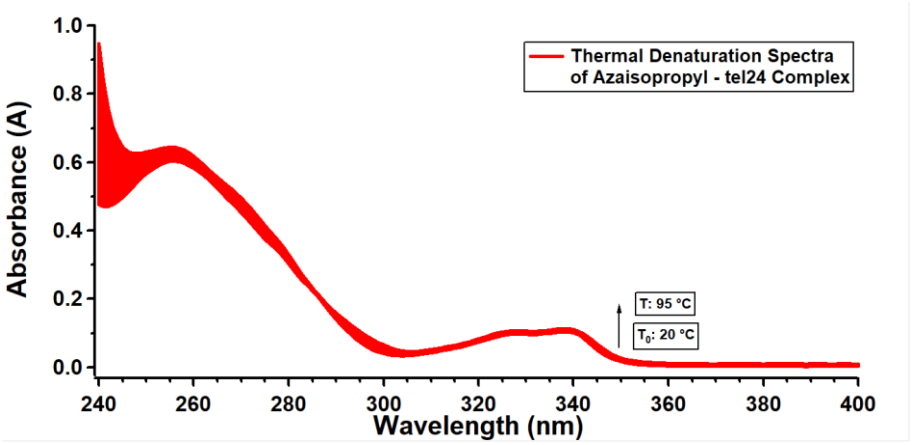

Figure 103: UV-VIS absorbance spectra of tel24 (2.5 μM) in the presence of Azaisopropyl (2.5 μM) obtained during thermal denaturation experiments.

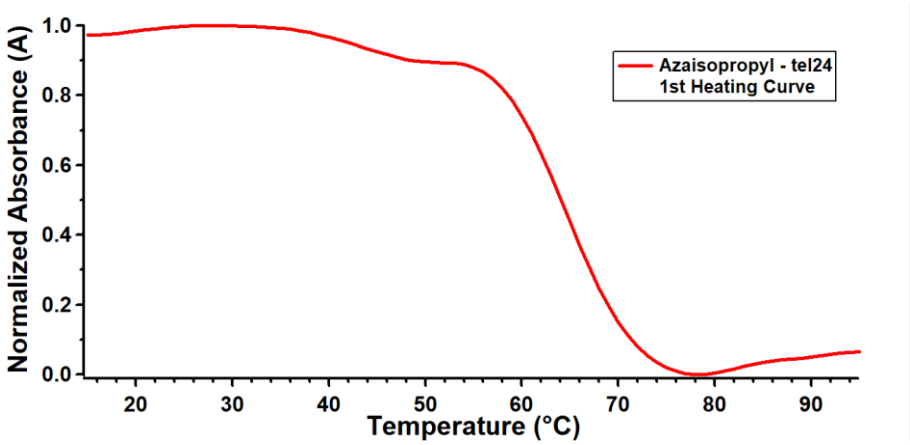

Figure 104: Thermal denaturation curve for tel24 (2.5 µM) in the presence of Azaisopropyl (2.5 µM) obtained by monitoring the UV-VIS absorbance at 290 nm.

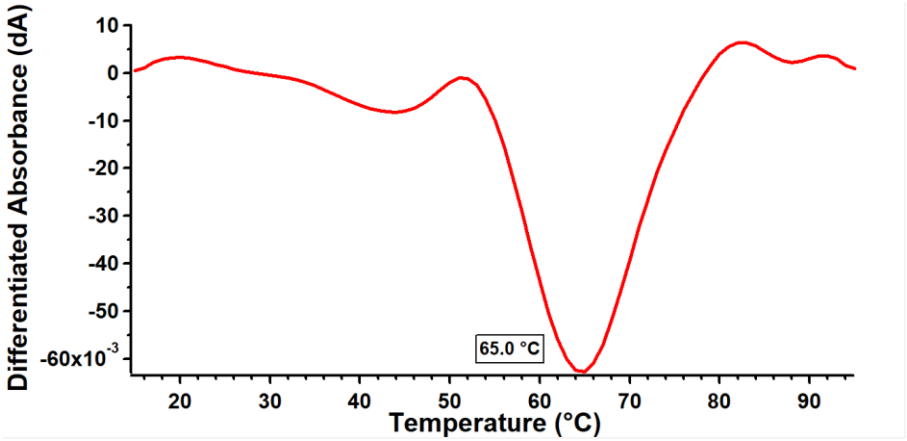

Figure 105: First derivative spectrum of the thermal denaturation curve in Figure 99.

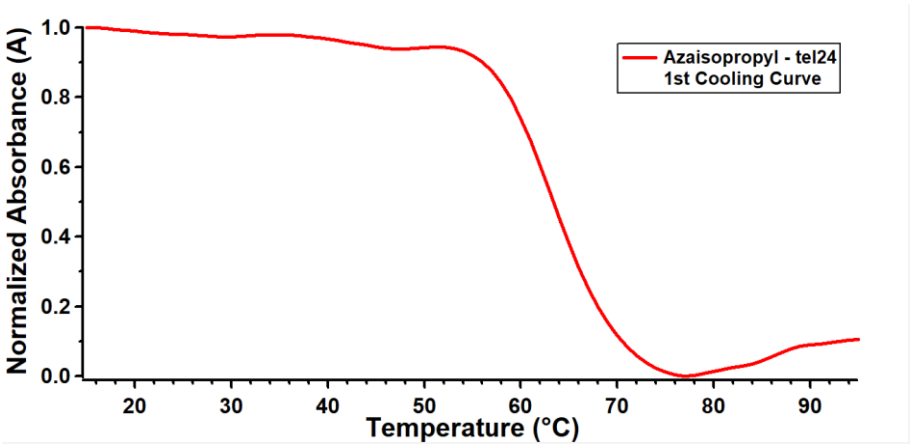

Figure 106: Thermal denaturation curve for tel24 (2.5 µM) in the presence of Azaisopropyl (2.5 µM) obtained by monitoring the UV-VIS absorbance at 290 nm.

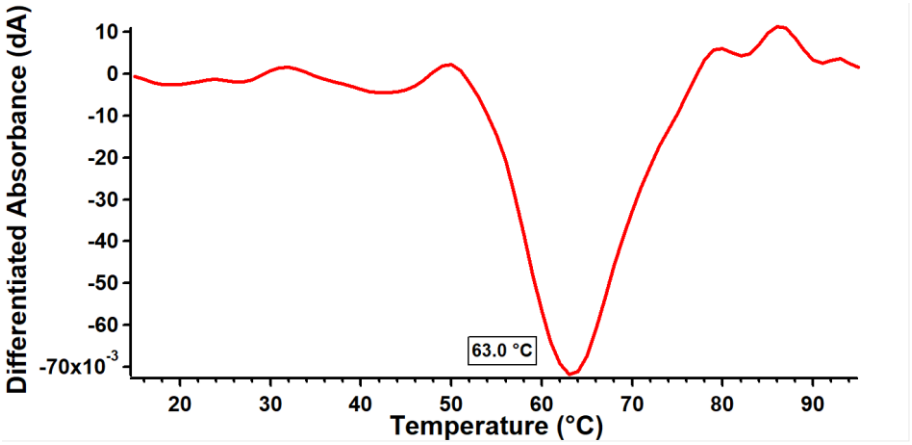

Figure 107: First derivative spectrum of the thermal denaturation curve in Figure 101.

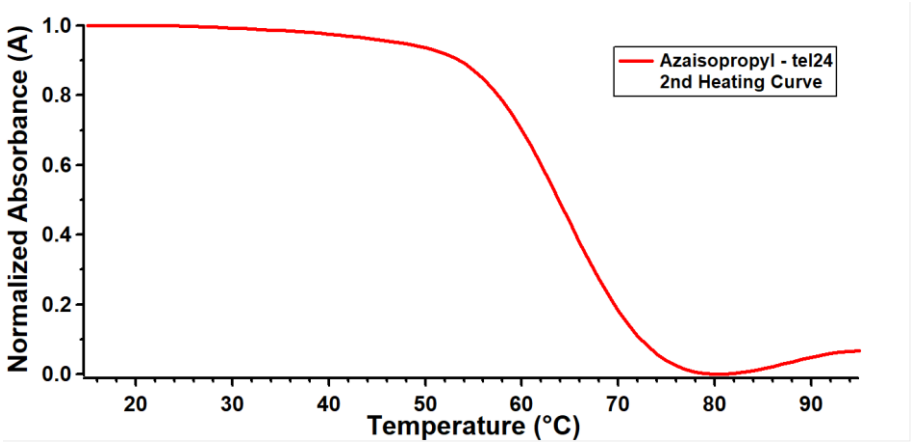

Figure 108: Thermal denaturation curve for tel24 (2.5 µM) in the presence of Azaisopropyl (2.5 µM) obtained by monitoring the UV-VIS absorbance at 290 nm.

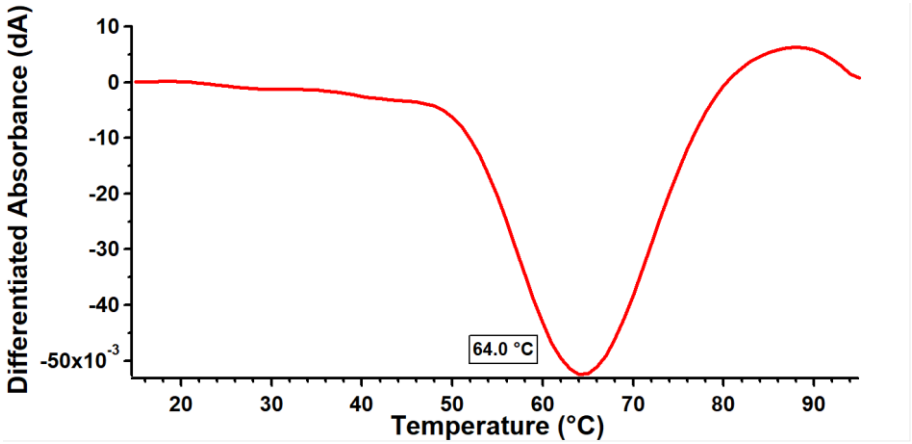

Figure 109: First derivative spectrum of the thermal denaturation curve in Figure 103.

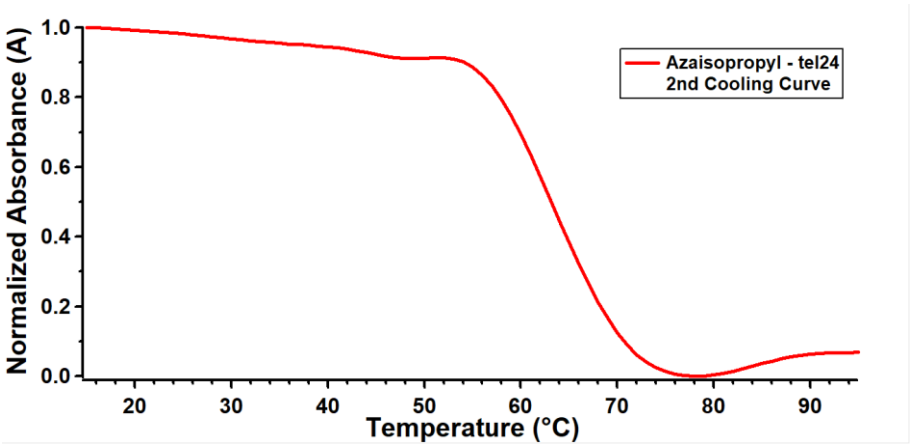

Figure 110: Thermal denaturation curve for tel24 (2.5 µM) in the presence of Azaisopropyl (2.5 µM) obtained by monitoring the UV-VIS absorbance at 290 nm.

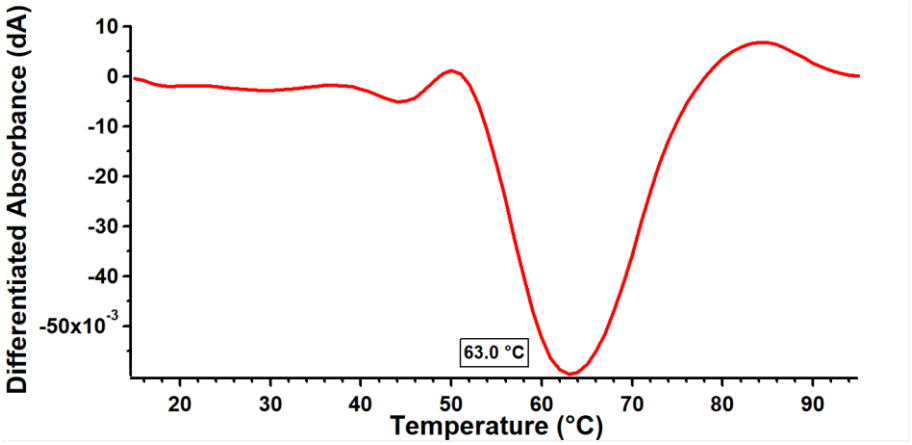

Figure 111: First derivative spectrum of the thermal denaturation curve in Figure 105.

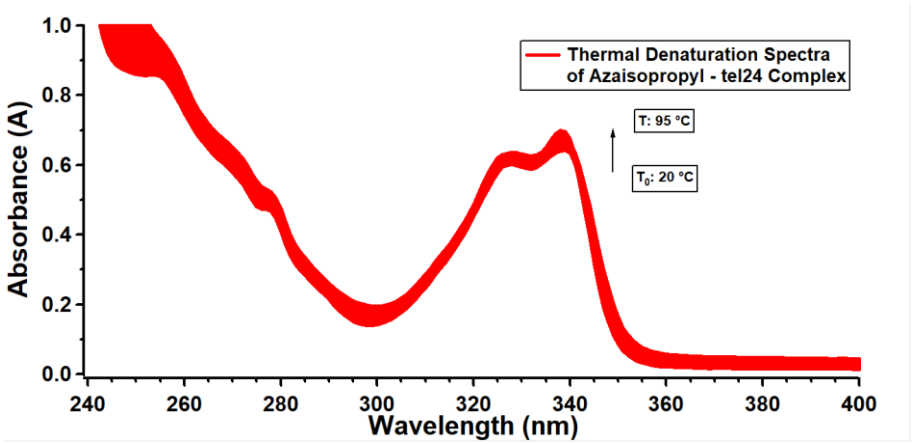

Figure 112: UV-VIS absorbance spectra of tel24 (2.5 µM) in the presence of Azaisopropyl (15.0 µM) obtained during thermal denaturation experiments.

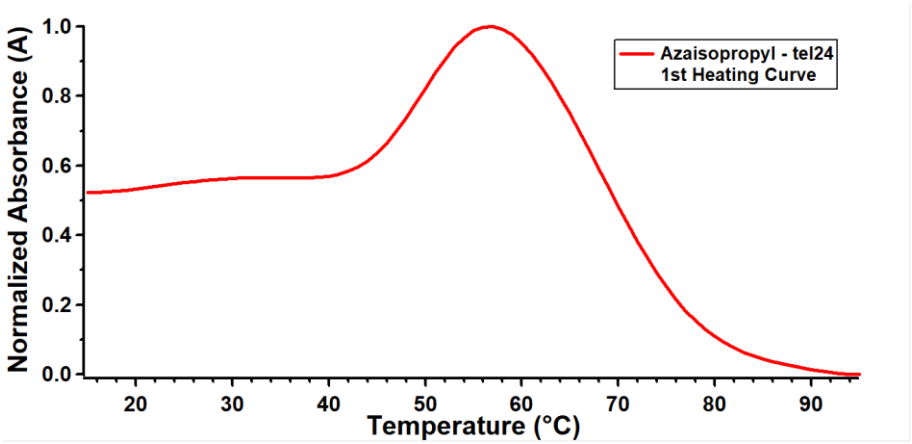

Figure 113: Thermal denaturation curve for tel24 (2.5 µM) in the presence of Azaisopropyl (15.0 µM) obtained by monitoring the UV-VIS absorbance at 290 nm.

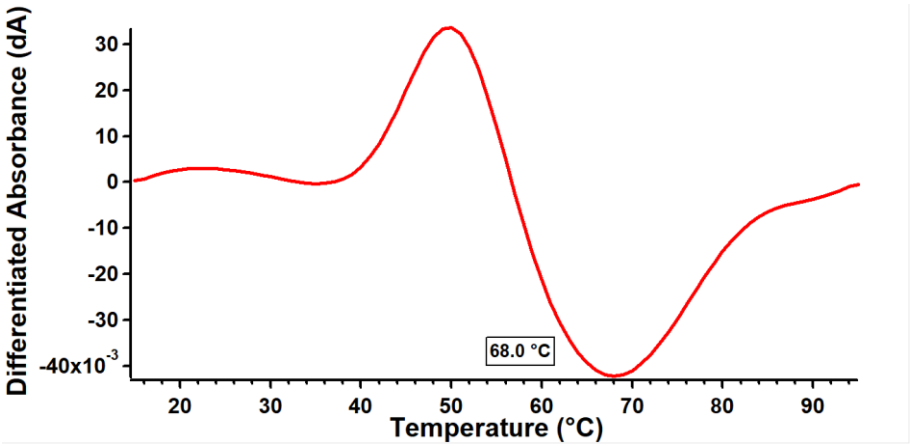

Figure 114: First derivative spectrum of the thermal denaturation curve in Figure 108.

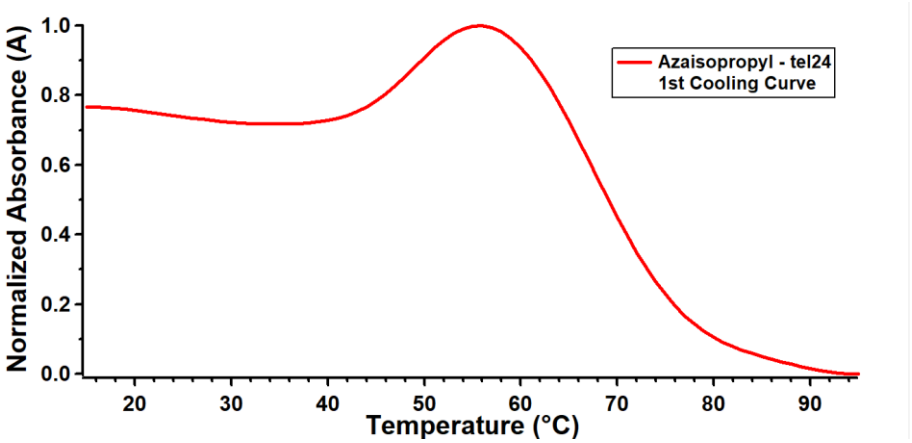

Figure 115: Thermal denaturation curve for tel24 (2.5 μM) in the presence of Azaisopropyl (15.0 μM) obtained by monitoring the UV-VIS absorbance at 290 nm.

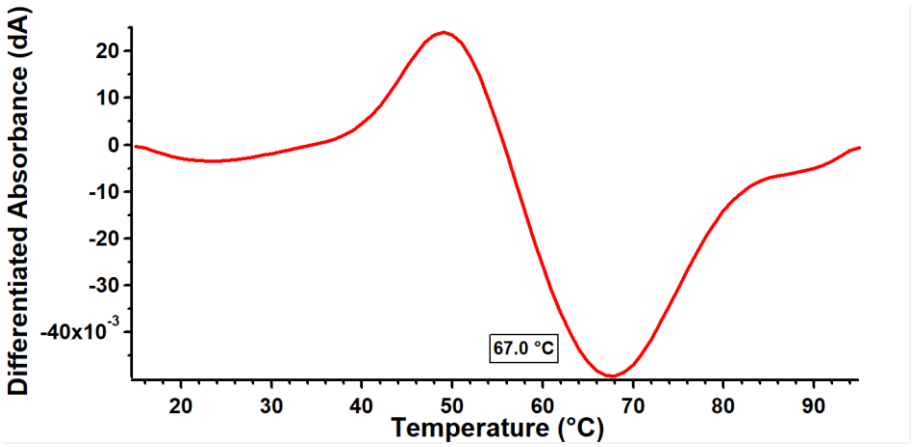

Figure 116: First derivative spectrum of the thermal denaturation curve in Figure 110.

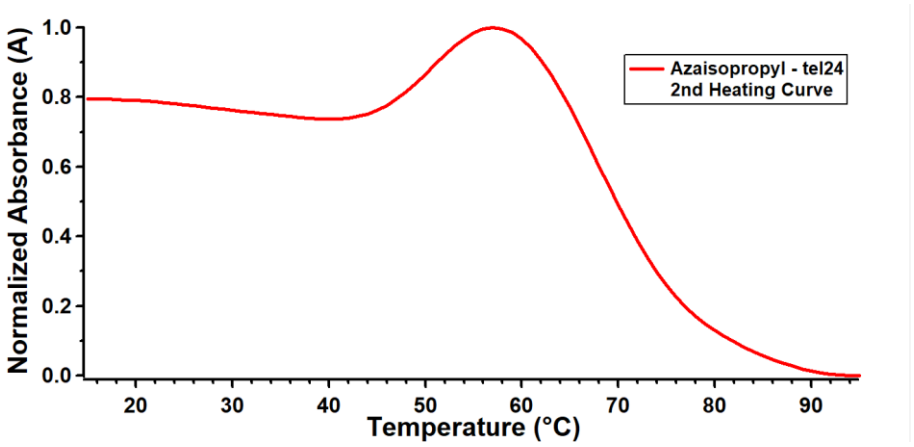

Figure 117: Thermal denaturation curve for tel24 (2.5 µM) in the presence of Azaisopropyl (15.0 µM) obtained by monitoring the UV-VIS absorbance at 290 nm.

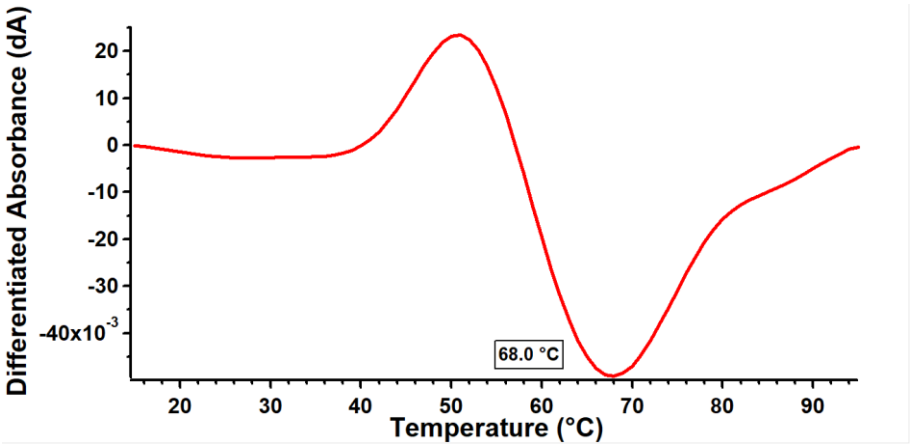

Figure 118: First derivative spectrum of the thermal denaturation curve in Figure 112.

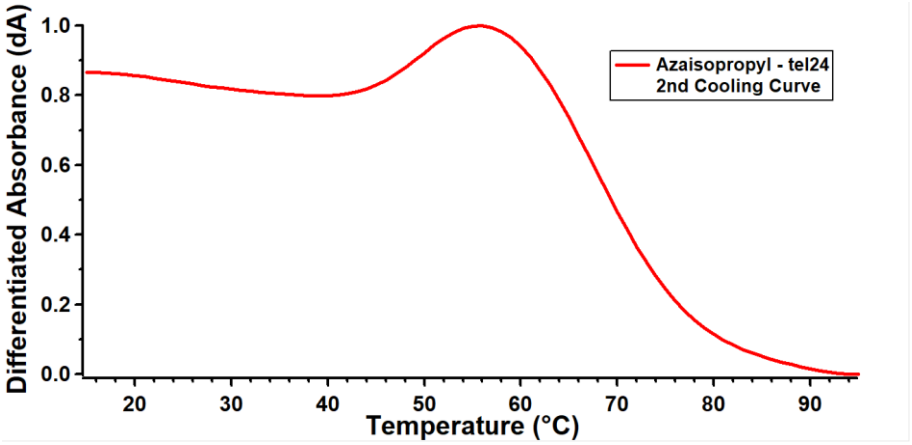

Figure 119: Thermal denaturation curve for tel24 (2.5 μM) in the presence of Azaisopropyl (15.0 μM) obtained by monitoring the UV-VIS absorbance at 290 nm.

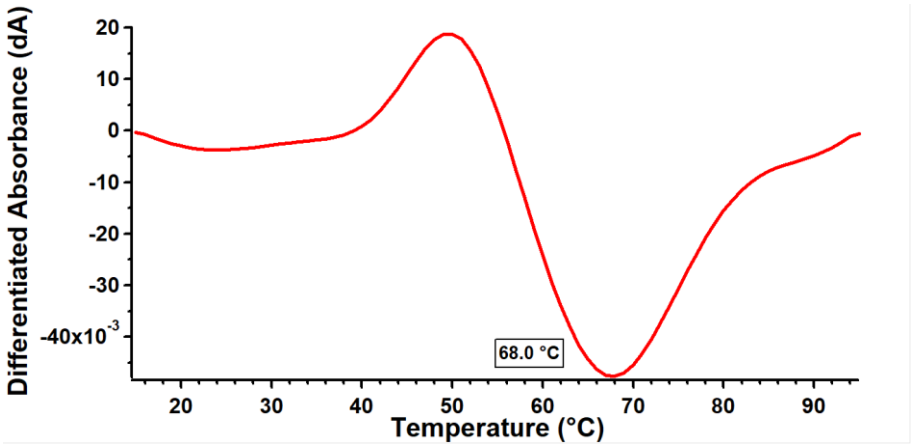

Figure 120: First derivative spectrum of the thermal denaturation curve in Figure 114.

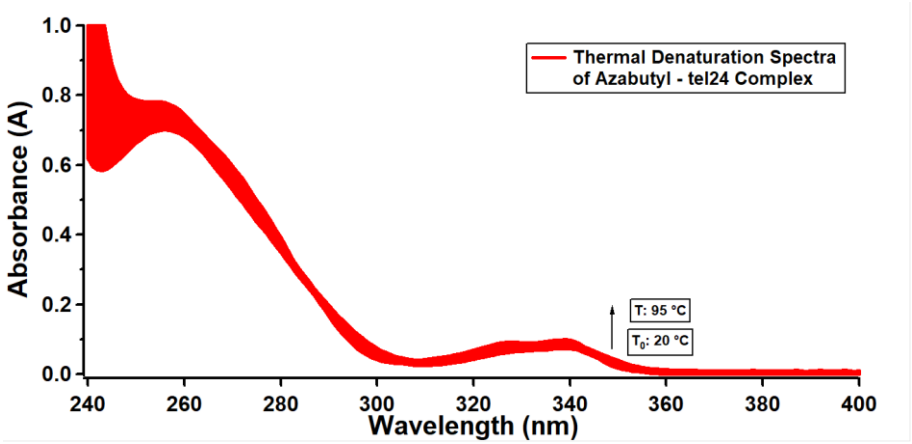

Figure 121: UV-VIS absorbance spectra of tel24 (2.5 µM) in the presence of Azabutyl (2.5 µM) obtained during thermal denaturation experiments.

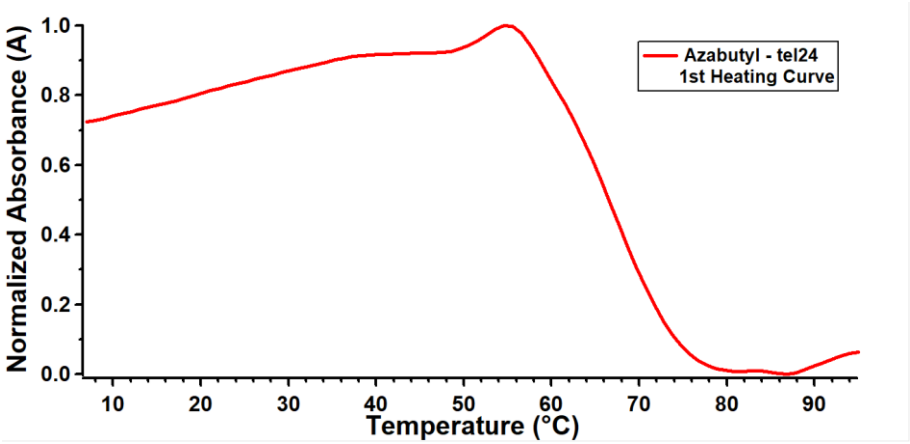

Figure 122: Thermal denaturation curve for tel24 (2.5 µM) in the presence of Azabutyl (2.5 µM) obtained by monitoring the UV-VIS absorbance at 290 nm.

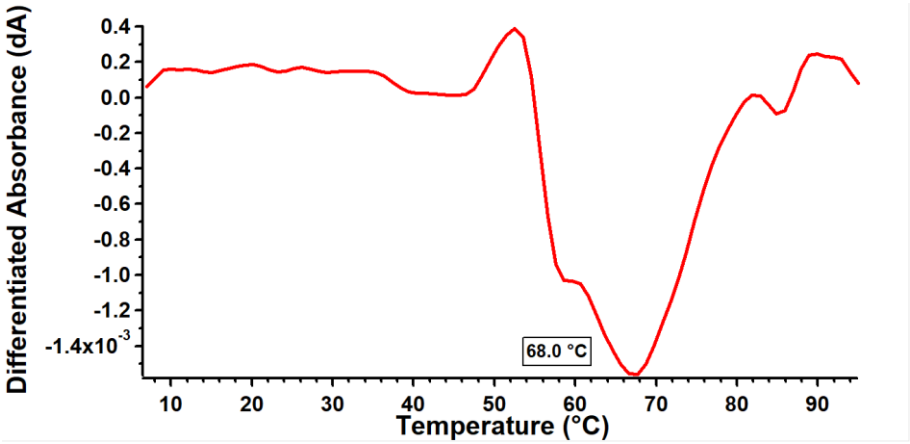

Figure 123: First derivative spectrum of the thermal denaturation curve in Figure 117.

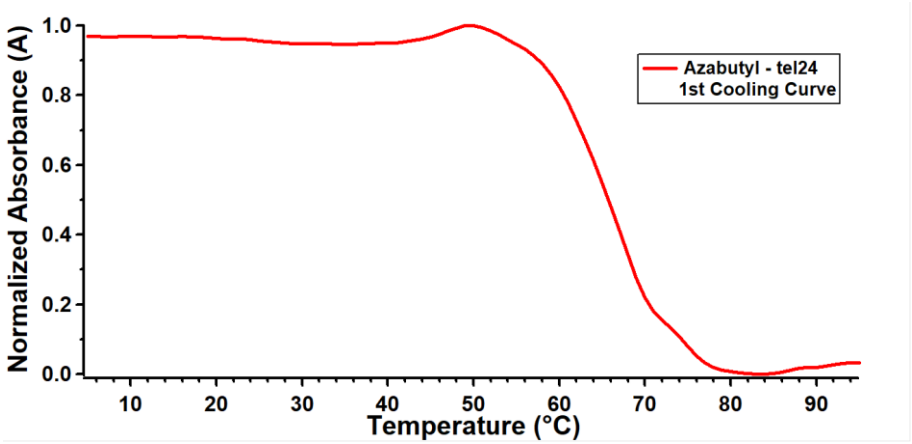

Figure 124: Thermal denaturation curve for tel24 (2.5 µM) in the presence of Azabutyl (2.5 µM) obtained by monitoring the UV-VIS absorbance at 290 nm.

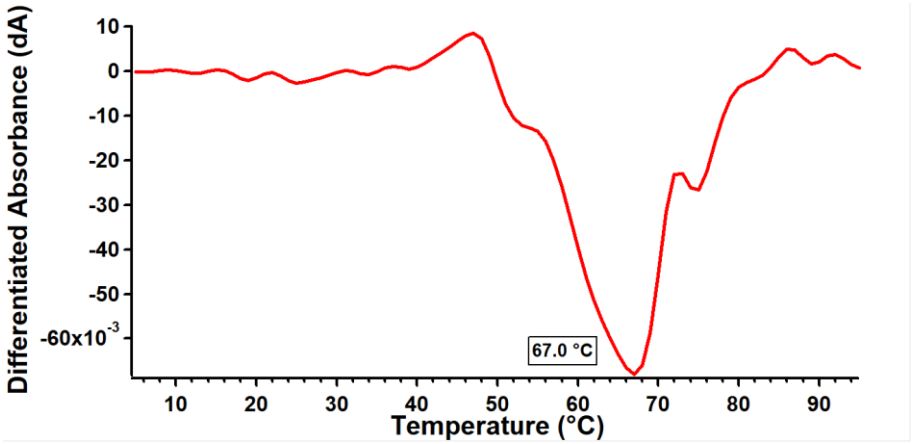

Figure 125: First derivative spectrum of the thermal denaturation curve in Figure 119.

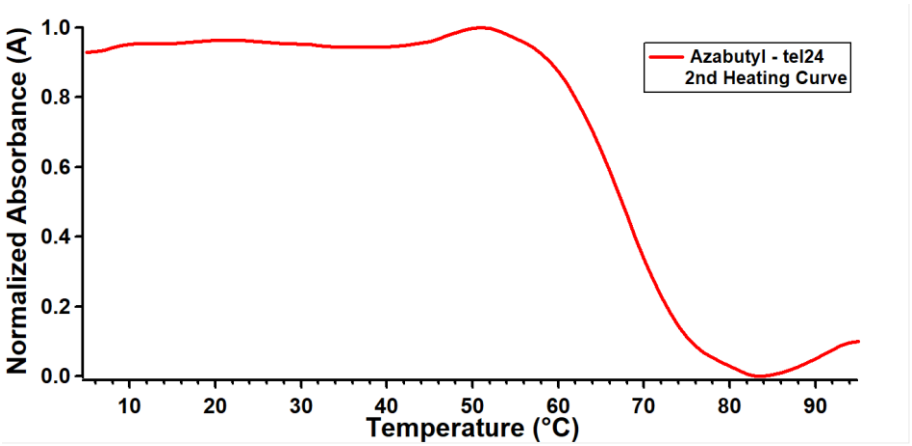

Figure 126: Thermal denaturation curve for tel24 (2.5 µM) in the presence of Azabutyl (2.5 µM) obtained by monitoring the UV-VIS absorbance at 290 nm.

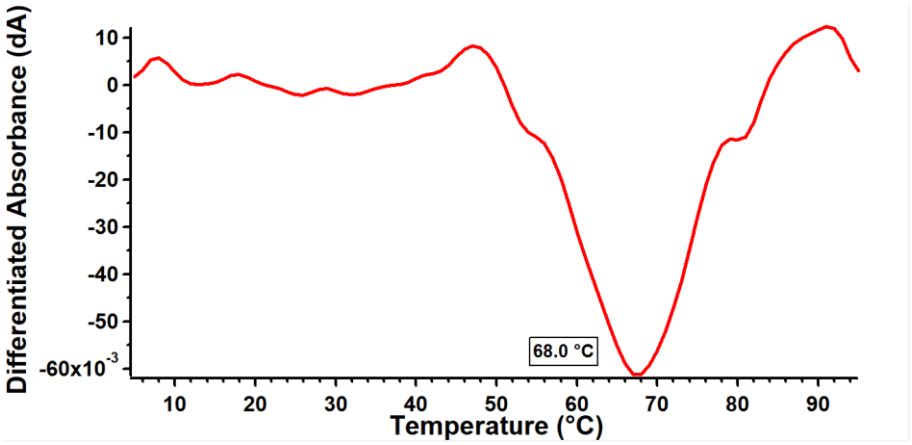

Figure 127: First derivative spectrum of the thermal denaturation curve in Figure 121.

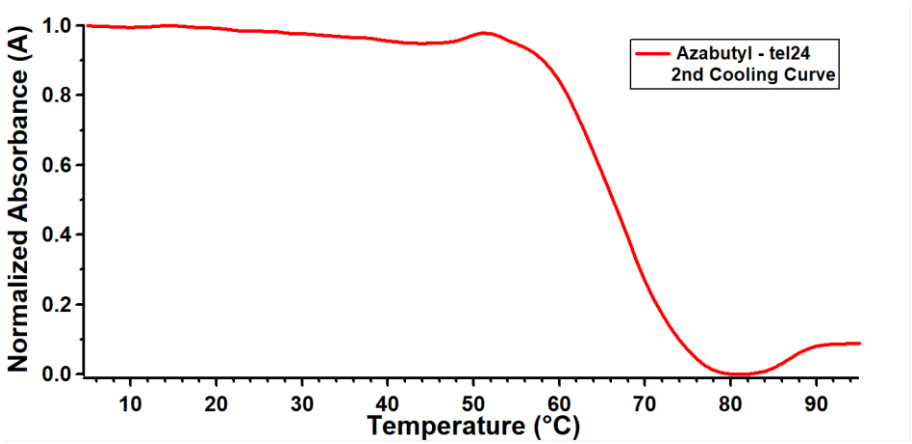

Figure 128: Thermal denaturation curve for tel24 (2.5 µM) in the presence of Azabutyl (2.5 µM) obtained by monitoring the UV-VIS absorbance at 290 nm.

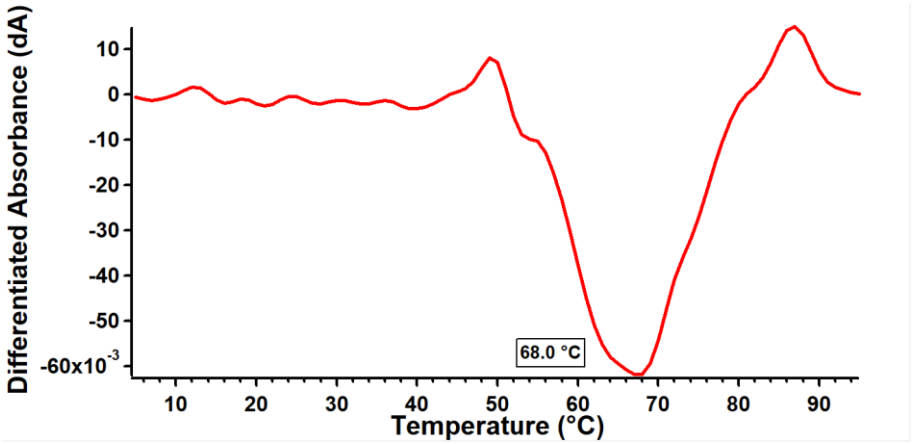

Figure 129: First derivative spectrum of the thermal denaturation curve in Figure 123.

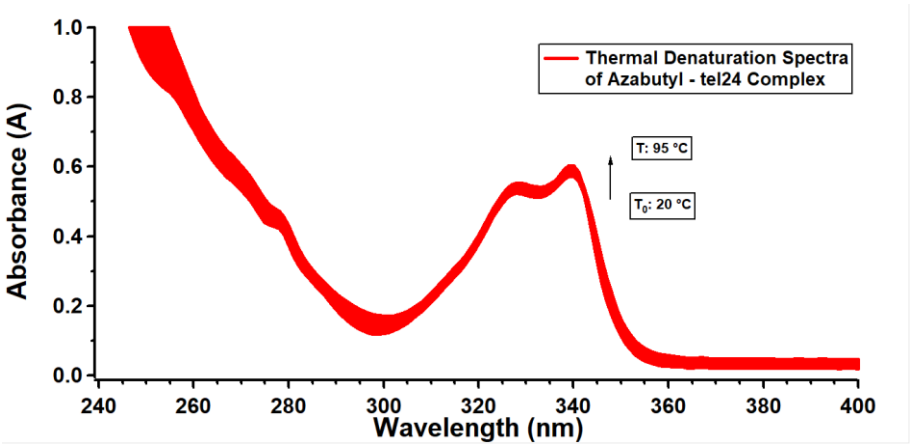

Figure 130: UV-VIS absorbance spectra of tel24 (2.5 µM) in the presence of Azabutyl (15.0 µM) obtained during thermal denaturation experiments.

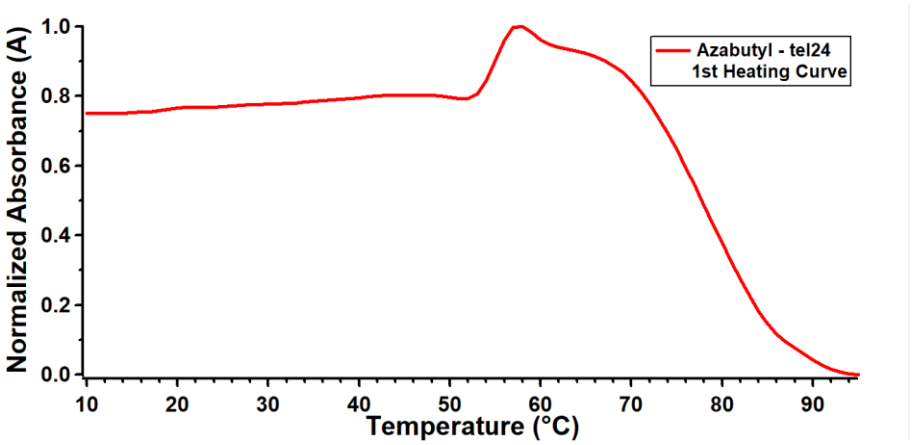

Figure 131: Thermal denaturation curve for tel24 (2.5 µM) in the presence of Azabutyl (15.0 µM) obtained by monitoring the UV-VIS absorbance at 290 nm.

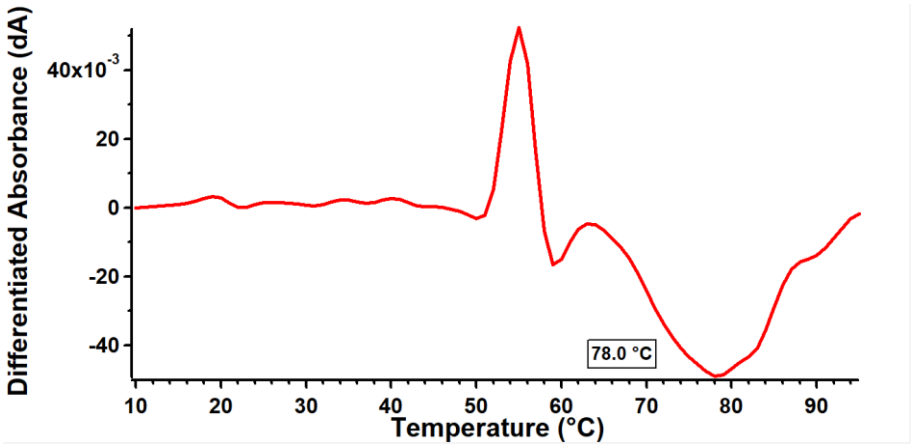

Figure 132: First derivative spectrum of the thermal denaturation curve in Figure 126.

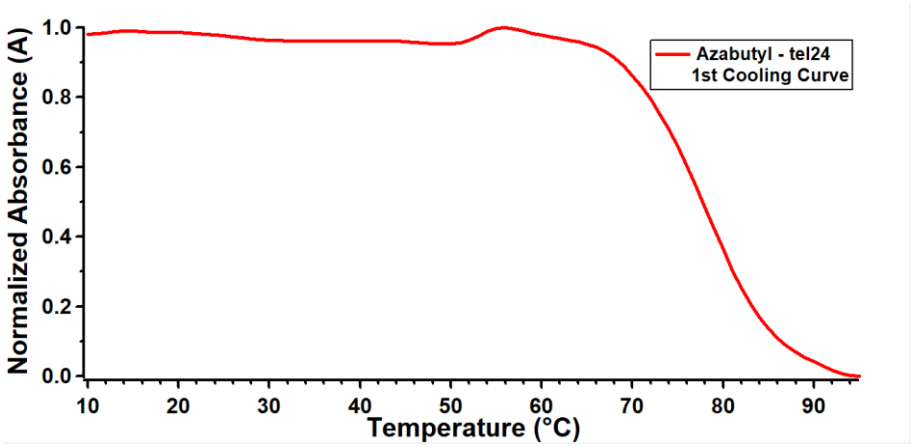

Figure 133: Thermal denaturation curve for tel24 (2.5 µM) in the presence of Azabutyl (15.0 µM) obtained by monitoring the UV-VIS absorbance at 290 nm.

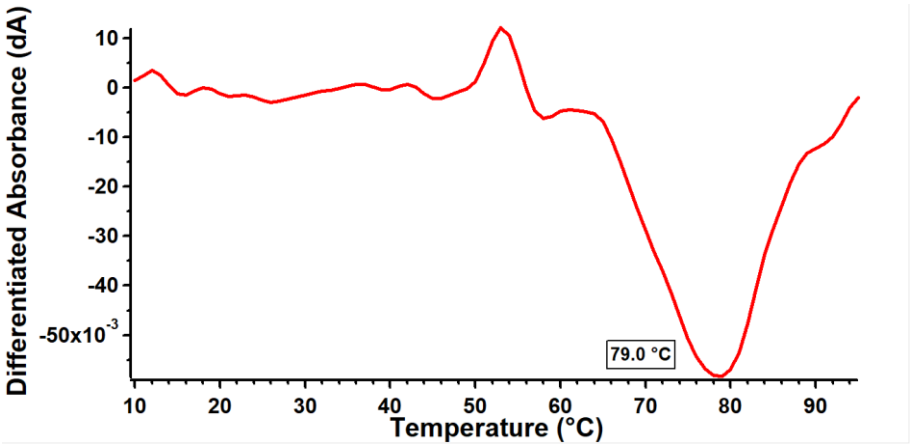

Figure 134: First derivative spectrum of the thermal denaturation curve in Figure 128.

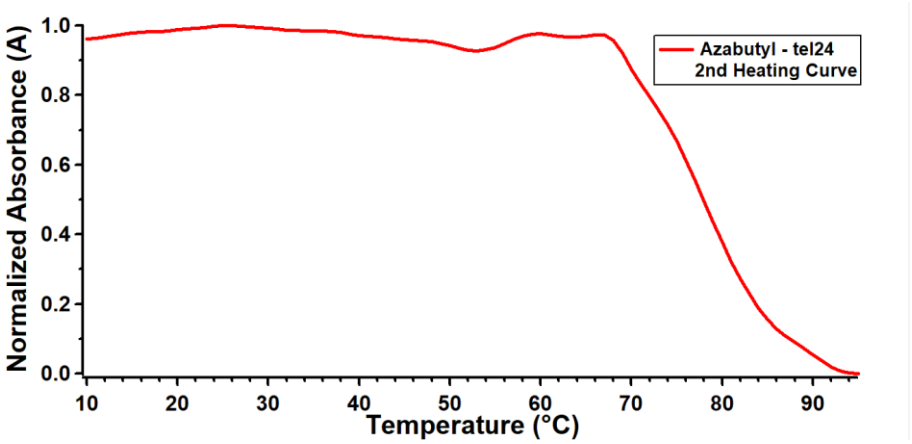

Figure 135: Thermal denaturation curve for tel24 (2.5 µM) in the presence of Azabutyl (15.0 µM) obtained by monitoring the UV-VIS absorbance at 290 nm.

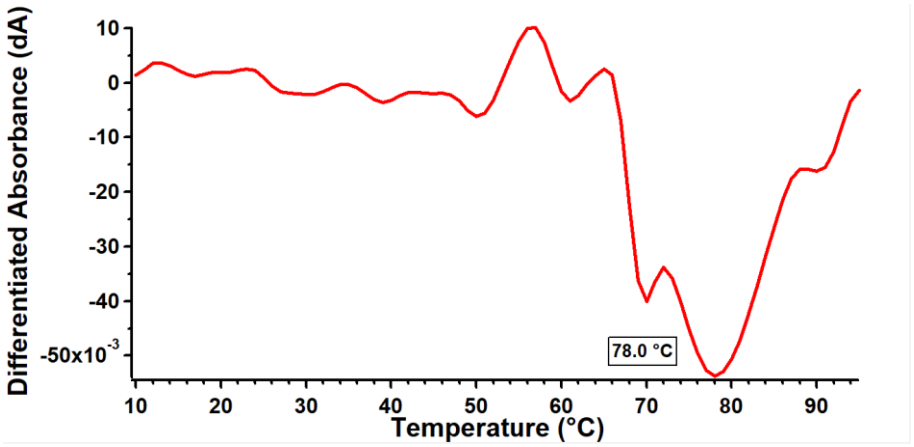

Figure 136: First derivative spectrum of the thermal denaturation curve in Figure 130.

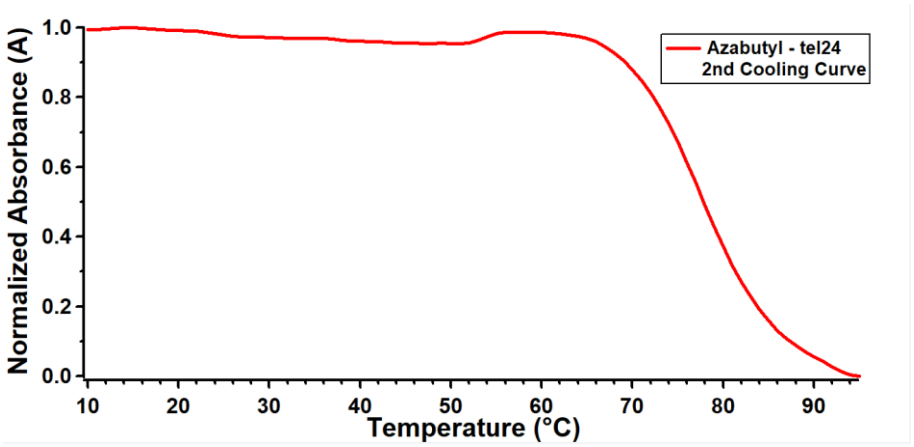

Figure 137: Thermal denaturation curve for tel24 (2.5 µM) in the presence of Azabutyl (15.0 µM) obtained by monitoring the UV-VIS absorbance at 290 nm.

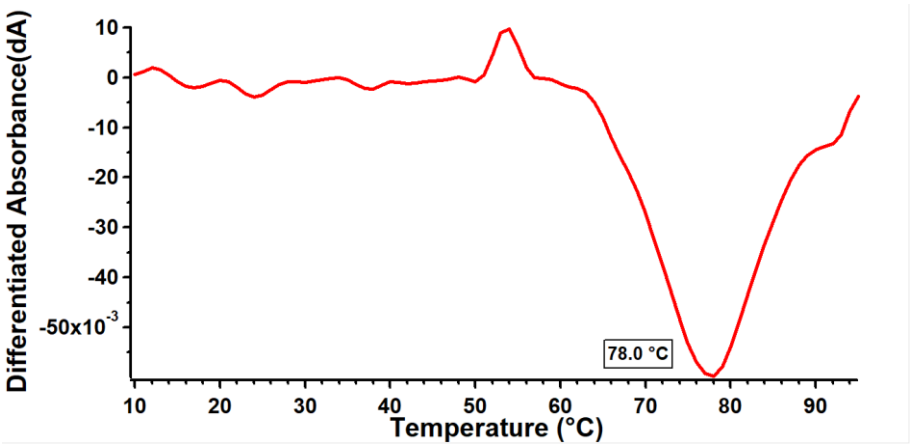

Figure 138: First derivative spectrum of the thermal denaturation curve in Figure 132.

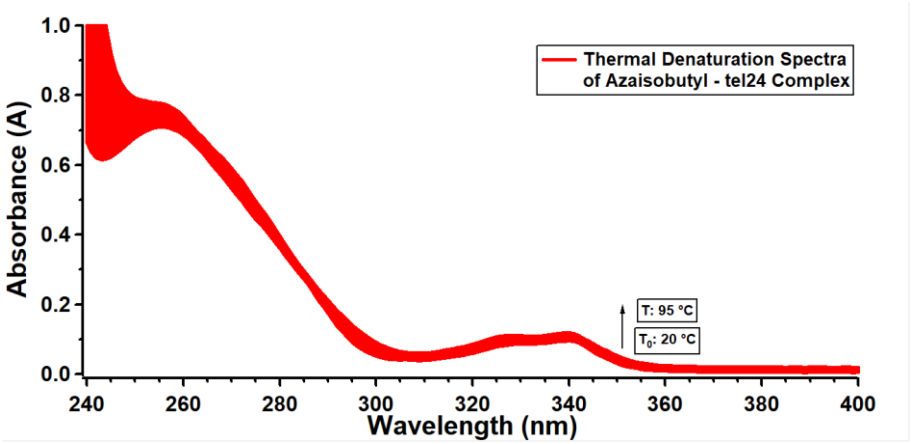

Figure 139: UV-VIS absorbance spectra of tel24 (2.5 µM) in the presence of Azaisobutyl (2.5 µM) obtained during thermal denaturation experiments.

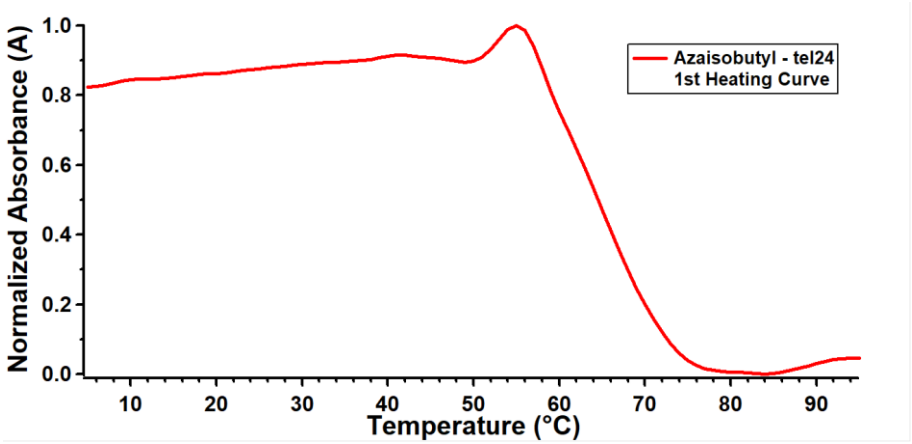

Figure 140: Thermal denaturation curve for tel24 (2.5 μM) in the presence of Azaisobutyl (2.5 μM) obtained by monitoring the UV-VIS absorbance at 290 nm.

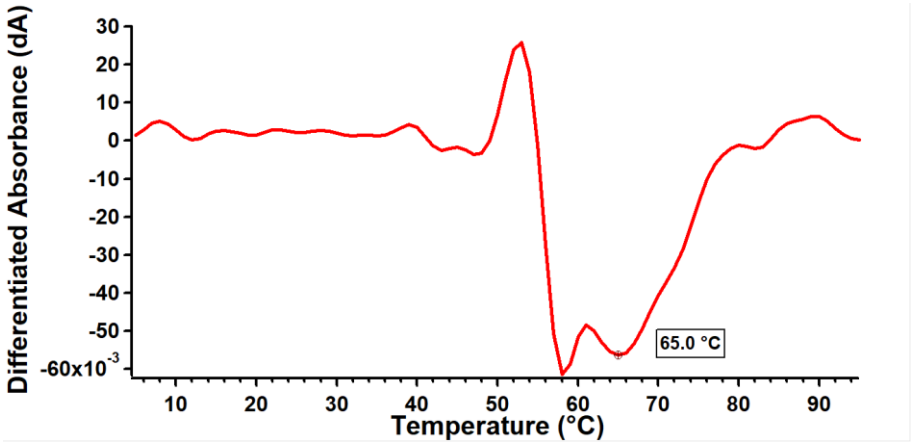

Figure 141: First derivative spectrum of the thermal denaturation curve in Figure 135.

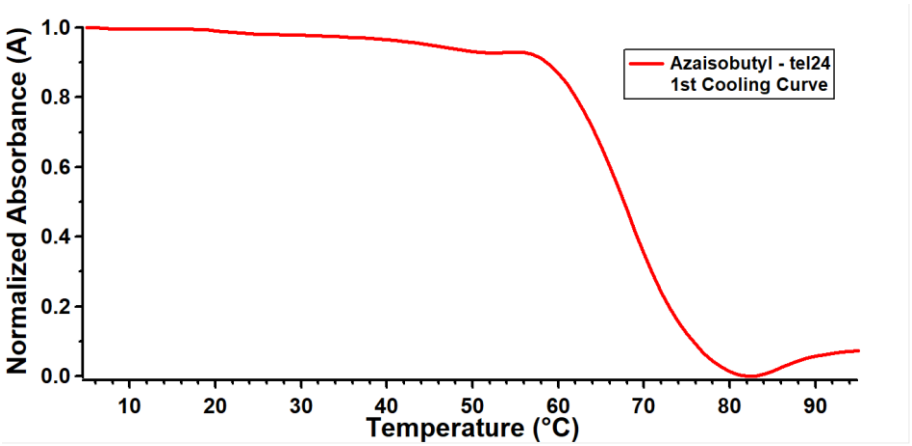

Figure 142: Thermal denaturation curve for tel24 (2.5 µM) in the presence of Azaisobutyl (2.5 µM) obtained by monitoring the UV-VIS absorbance at 290 nm.

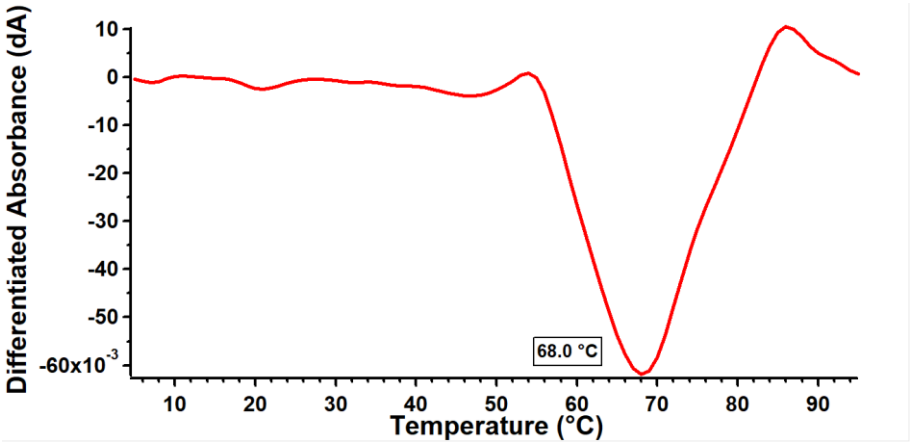

Figure 143: First derivative spectrum of the thermal denaturation curve in Figure 137.

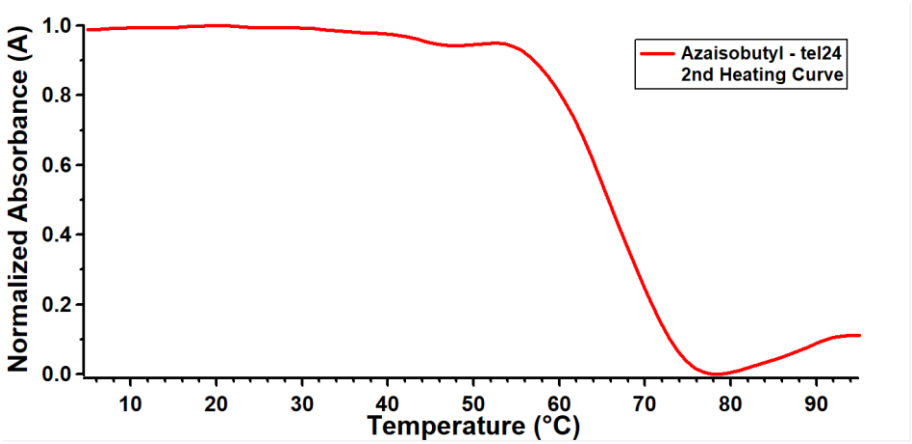

Figure 144: Thermal denaturation curve for tel24 (2.5 µM) in the presence of Azaisobutyl (2.5 µM) obtained by monitoring the UV-VIS absorbance at 290 nm.

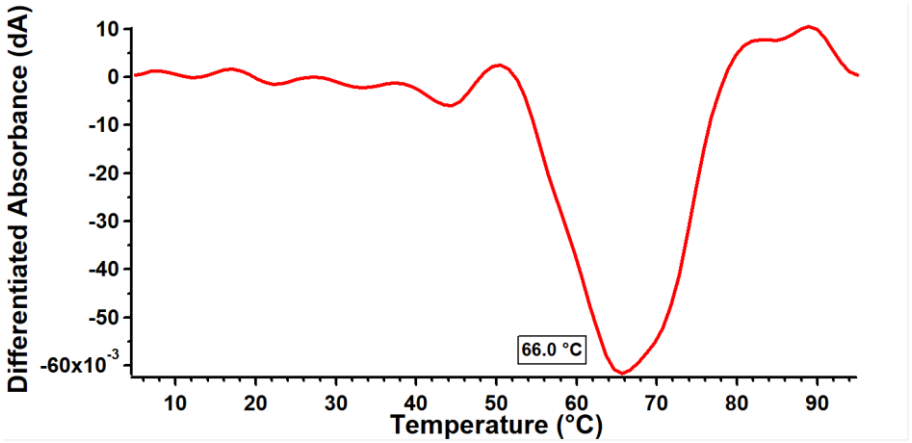

Figure 145: First derivative spectrum of the thermal denaturation curve in Figure 139.

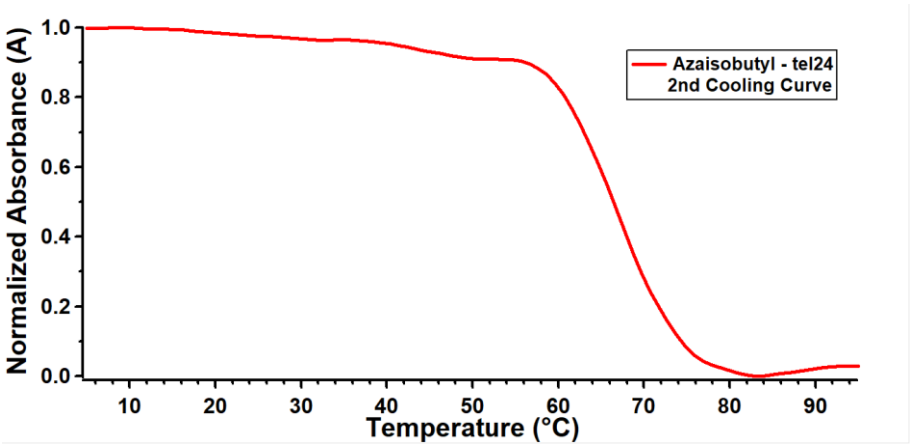

Figure 146: Thermal denaturation curve for tel24 (2.5 µM) in the presence of Azaisobutyl (2.5 µM) obtained by monitoring the UV-VIS absorbance at 290 nm.

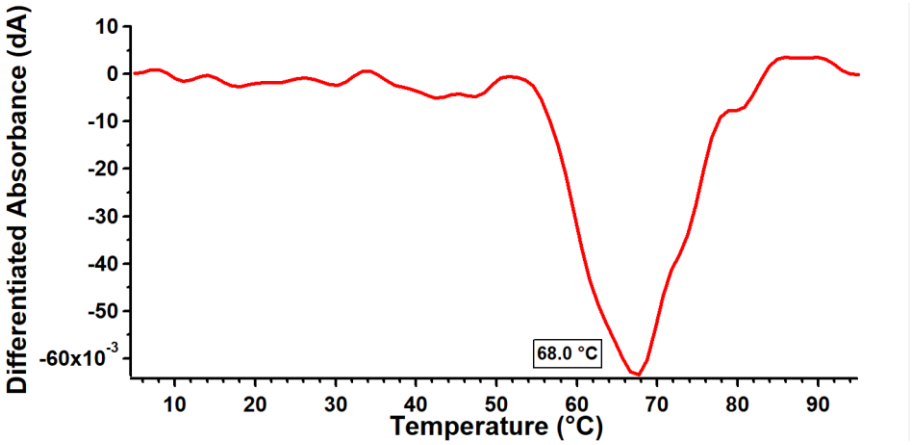

Figure 147: First derivative spectrum of the thermal denaturation curve in Figure 141.

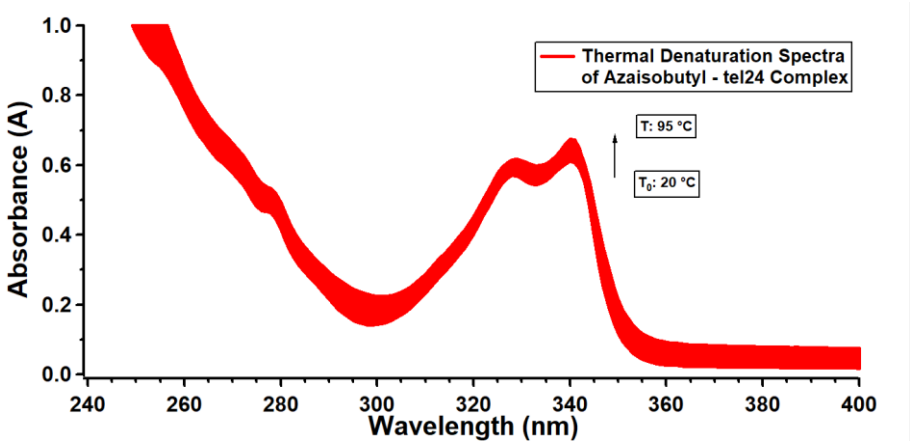

Figure 148: UV-VIS absorbance spectra of tel24 (2.5 µM) in the presence of Azaisobutyl (15.0 µM) obtained during thermal denaturation experiments.

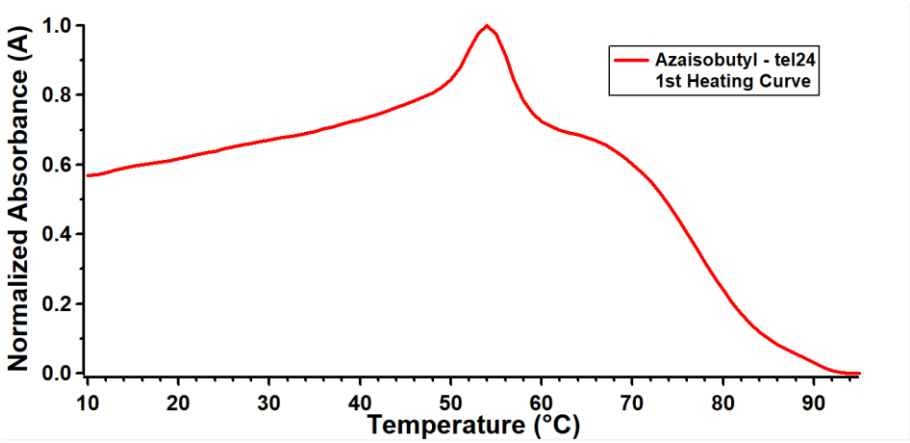

Figure 149: Thermal denaturation curve for tel24 (2.5 µM) in the presence of Azaisobutyl (15.0 µM) obtained by monitoring the UV-VIS absorbance at 290 nm.

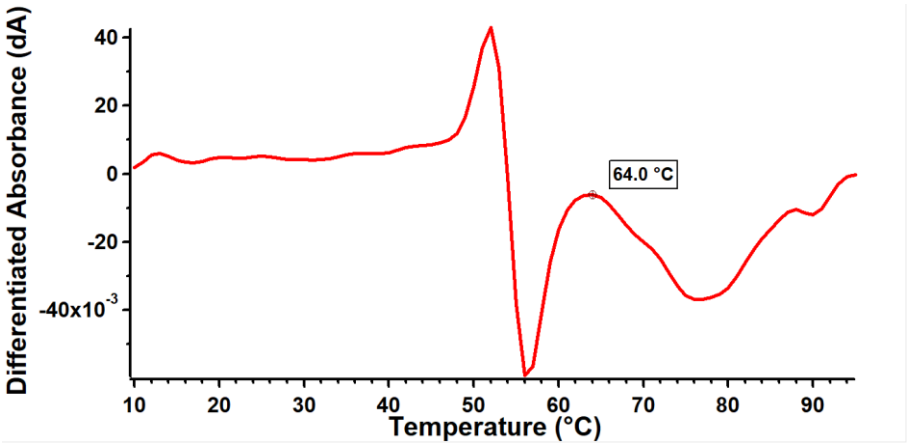

Figure 150: First derivative spectrum of the thermal denaturation curve in Figure 144.

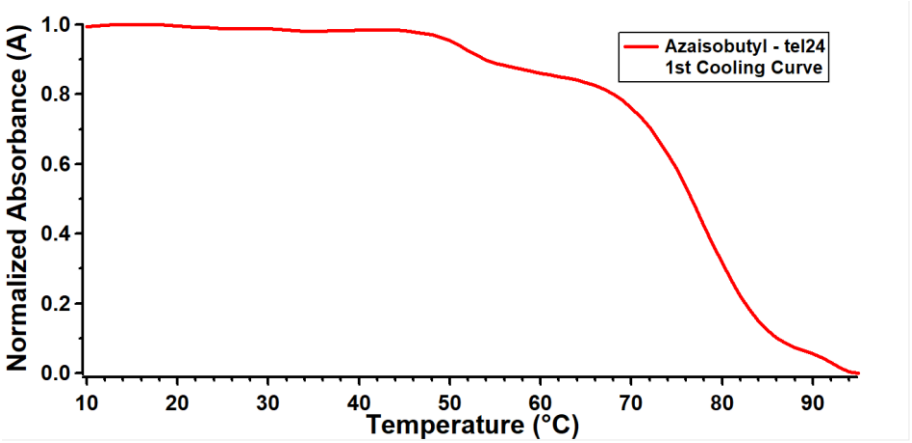

Figure 151: Thermal denaturation curve for tel24 (2.5 μM) in the presence of Azaisobutyl (15.0 μM) obtained by monitoring the UV-VIS absorbance at 290 nm.

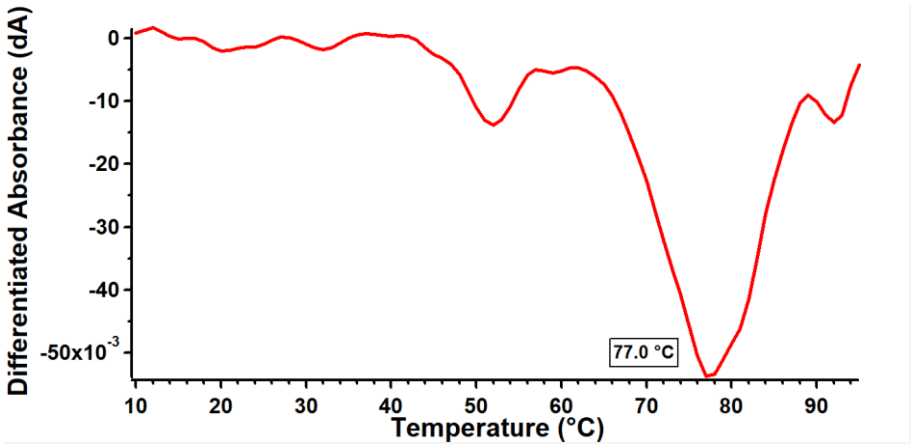

Figure 152: First derivative spectrum of the thermal denaturation curve in Figure 146.

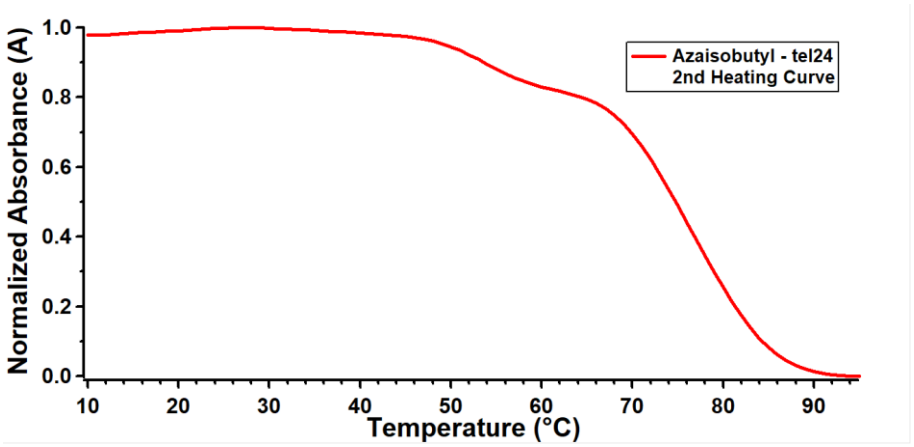

Figure 153: Thermal denaturation curve for tel24 (2.5 µM) in the presence of Azaisobutyl (15.0 µM) obtained by monitoring the UV-VIS absorbance at 290 nm.

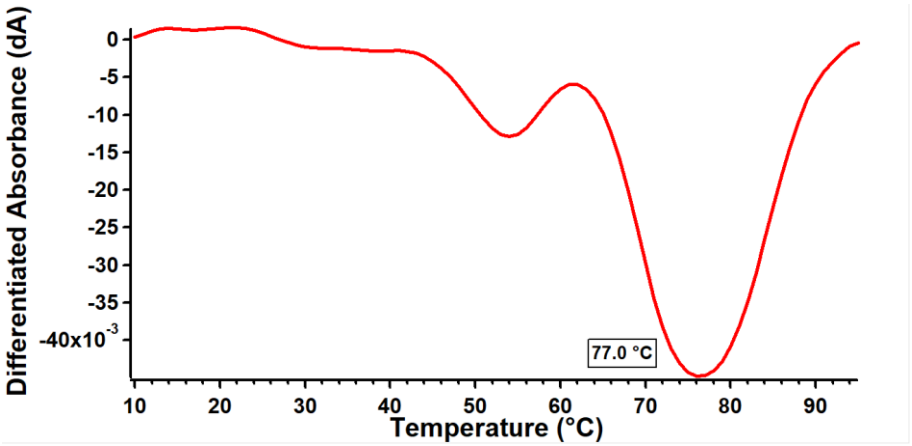

Figure 154: First derivative spectrum of the thermal denaturation curve in Figure 148.

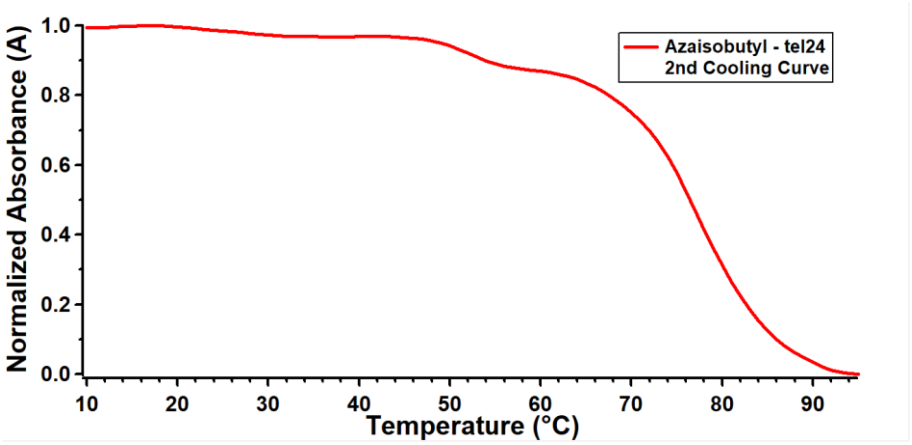

Figure 155: Thermal denaturation curve for tel24 (2.5 μM) in the presence of Azaisobutyl (15.0 μM) obtained by monitoring the UV-VIS absorbance at 290 nm.

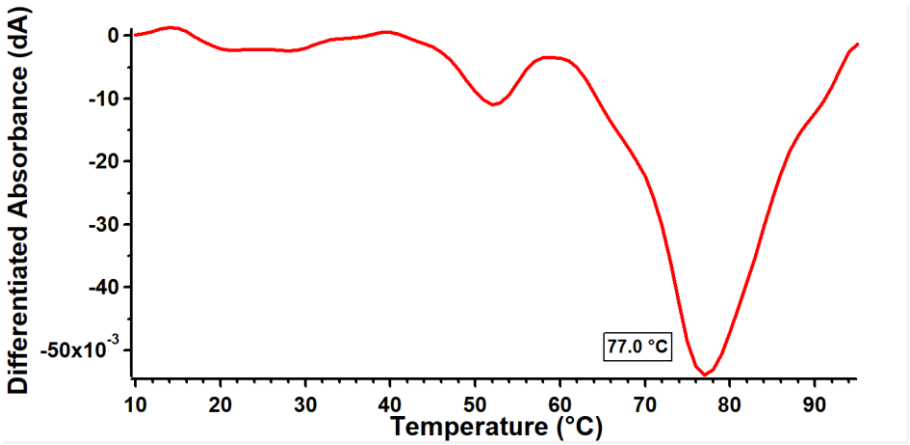

Figure 156: First derivative spectrum of the thermal denaturation curve in Figure 150.

C. FLUORESCENCE INTENSITY SPECTRA

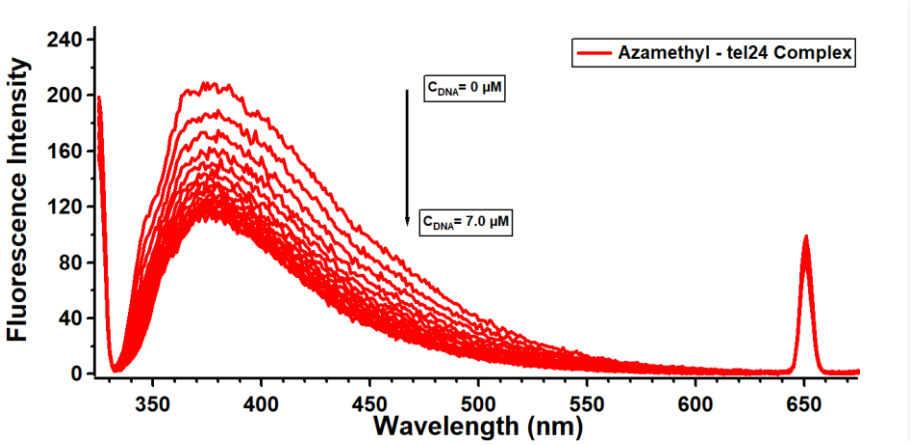

Figure 157: Fluorescence Intensity vs. Wavelength (nm) graph for 1µM Azamethyl solution titrated with increasing concentrations of tel24 solution (2nd replicate).

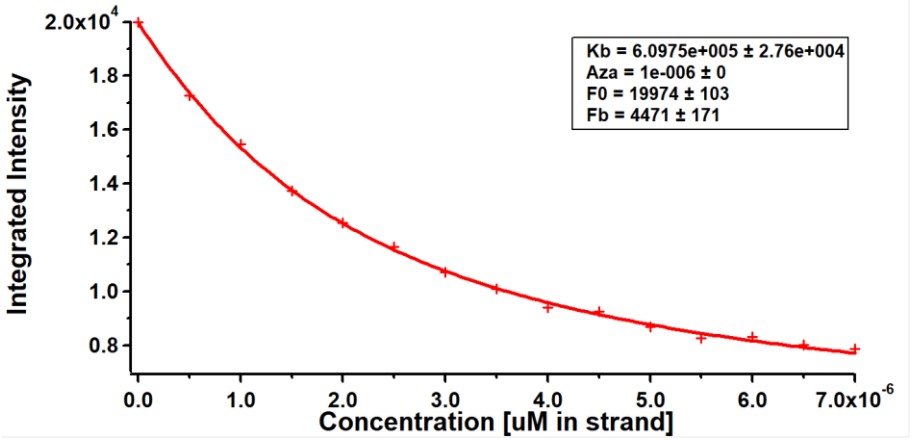

Figure 158: Integrated fluorescence intensity vs. DNA Concentration (µM, in strand) obtained from the Fluorescence Intensity vs. Wavelength (nm) graph 154.

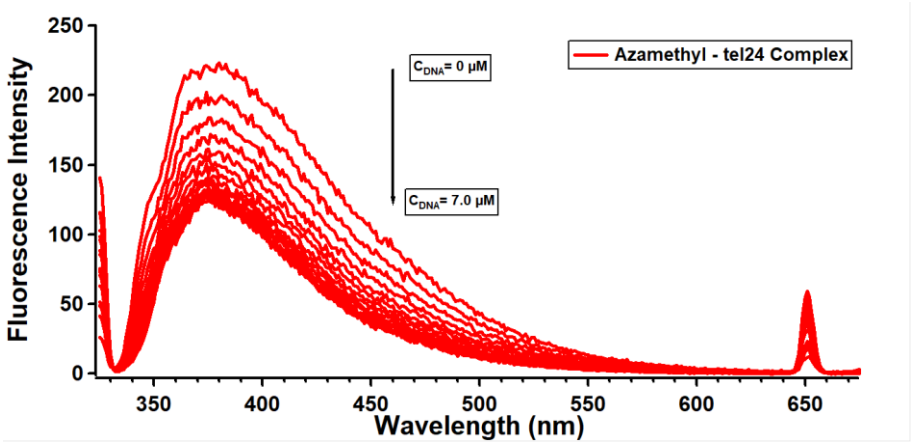

Figure 159: Fluorescence Intensity vs. Wavelength (nm) graph for 1µM Azamethyl solution titrated with increasing concentrations of tel24 solution (3rd replicate).

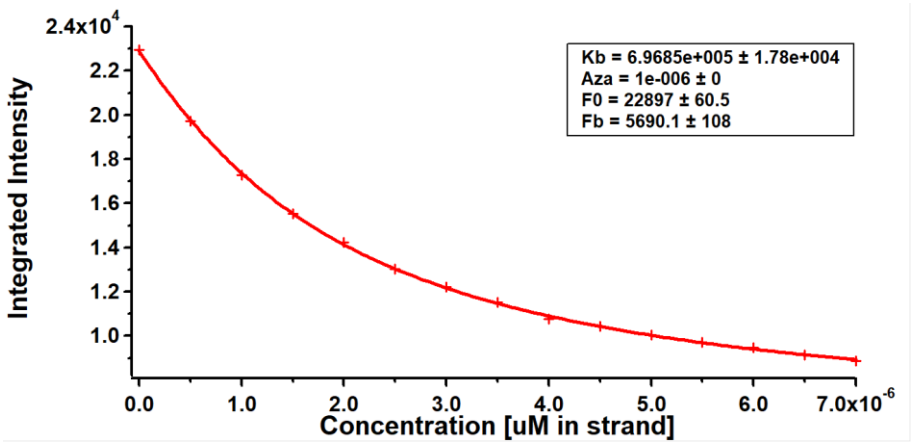

Figure 160: Integrated fluorescence intensity vs. DNA Concentration (µM, in strand) obtained from the Fluorescence Intensity vs. Wavelength (nm) graph 156.

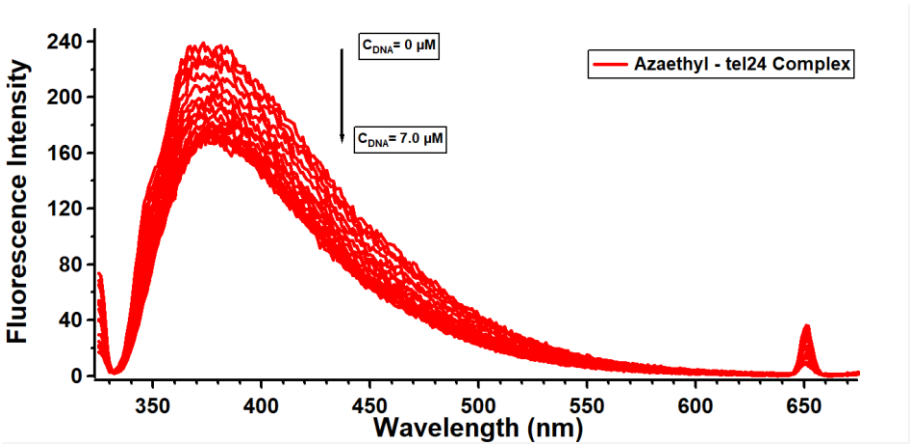

Figure 161: Fluorescence Intensity vs. Wavelength (nm) graph for 1µM Azaethyl solution titrated with increasing concentrations of tel24 solution (1st replicate).

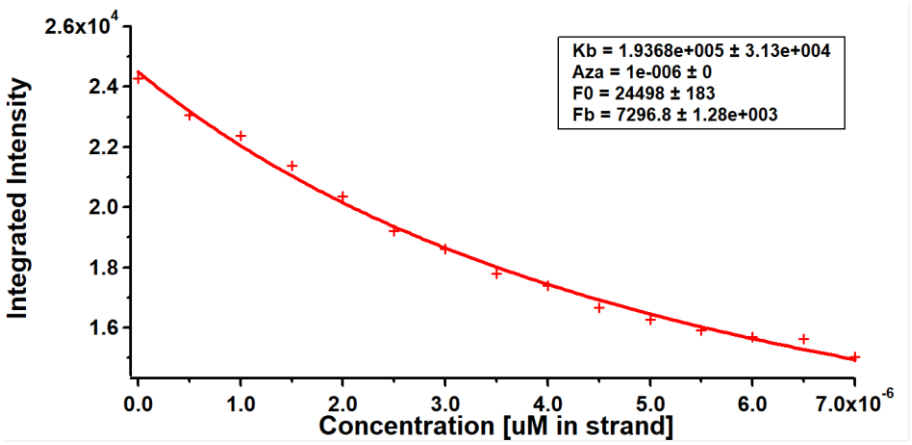

Figure 162: Integrated fluorescence intensity vs. DNA Concentration (µM, in strand) obtained from the Fluorescence Intensity vs. Wavelength (nm) graph 158.

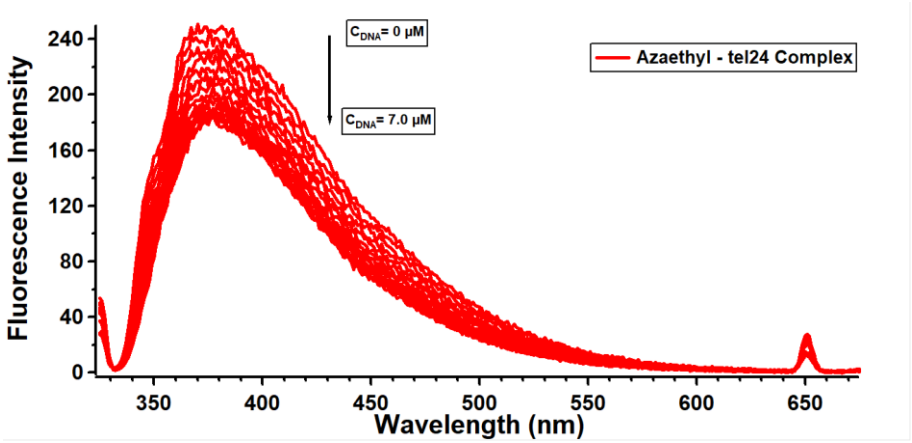

Figure 163: Fluorescence Intensity vs. Wavelength (nm) graph for 1µM Azaethyl solution titrated with increasing concentrations of tel24 solution (2nd replicate).

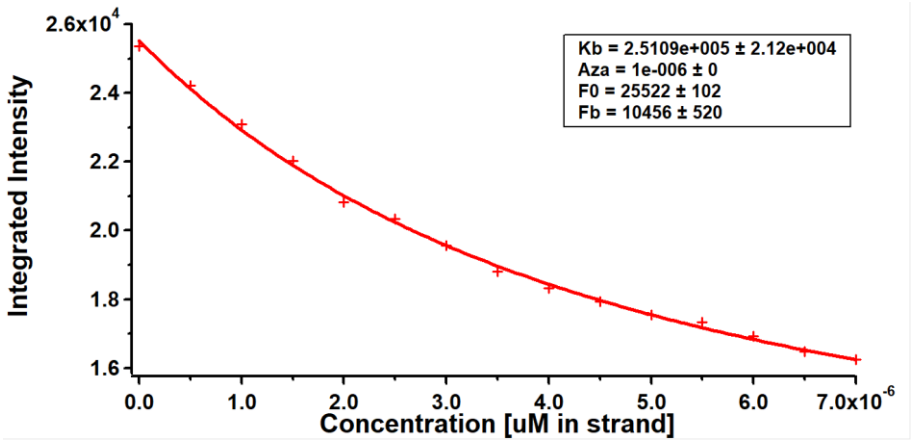

Figure 164: Integrated fluorescence intensity vs. DNA Concentration (µM, in strand) obtained from the Fluorescence Intensity vs. Wavelength (nm) graph 160.

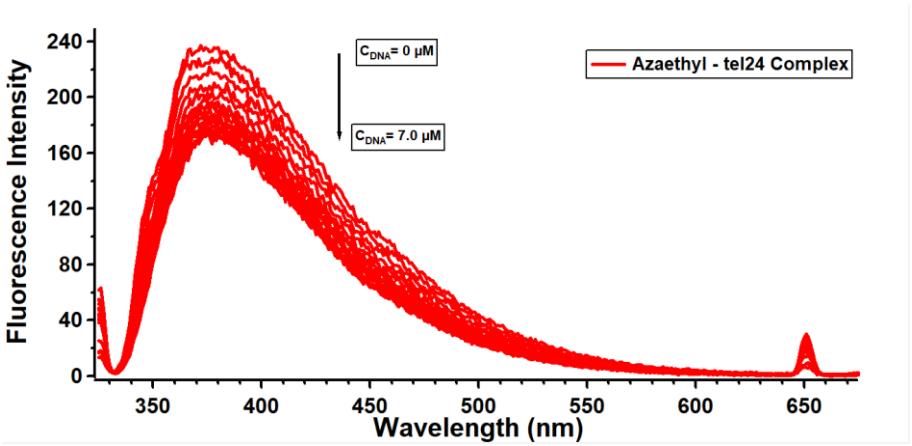

Figure 165: Fluorescence Intensity vs. Wavelength (nm) graph for 1µM Azaethyl solution titrated with increasing concentrations of tel24 solution (3rd replicate).

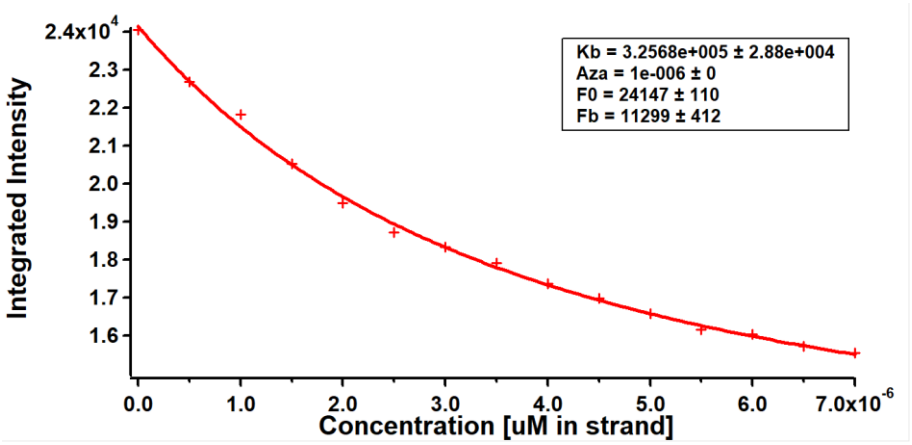

Figure 166: Integrated Fluorescence Intensity vs. DNA Concentration (µM, in strand) obtained from the Fluorescence Intensity vs. Wavelength (nm) graph 162.

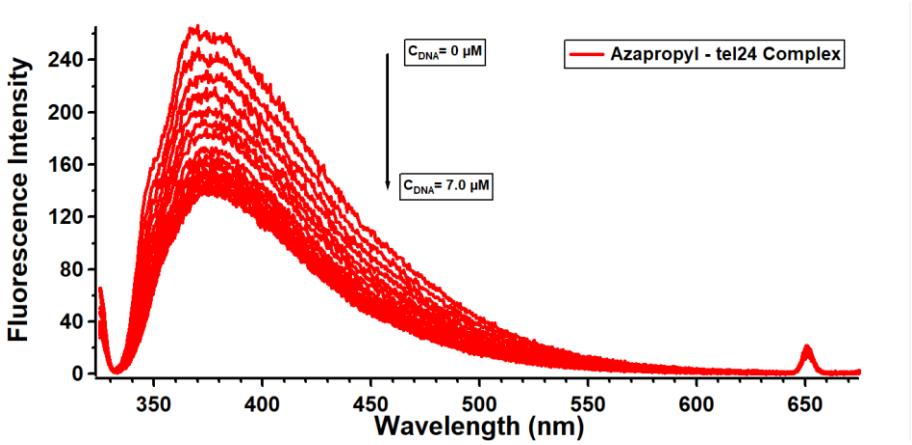

Figure 167: Fluorescence Intensity vs. Wavelength (nm) graph for 1µM Azapropyl solution titrated with increasing concentrations of tel24 solution (1st replicate).

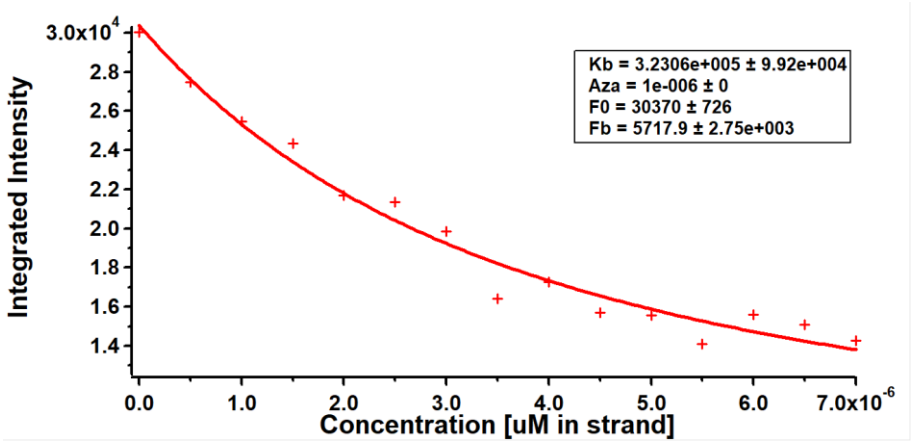

Figure 168: Integrated Fluorescence Intensity vs. DNA Concentration (µM, in strand) obtained from the Fluorescence Intensity vs. Wavelength (nm) graph 164.

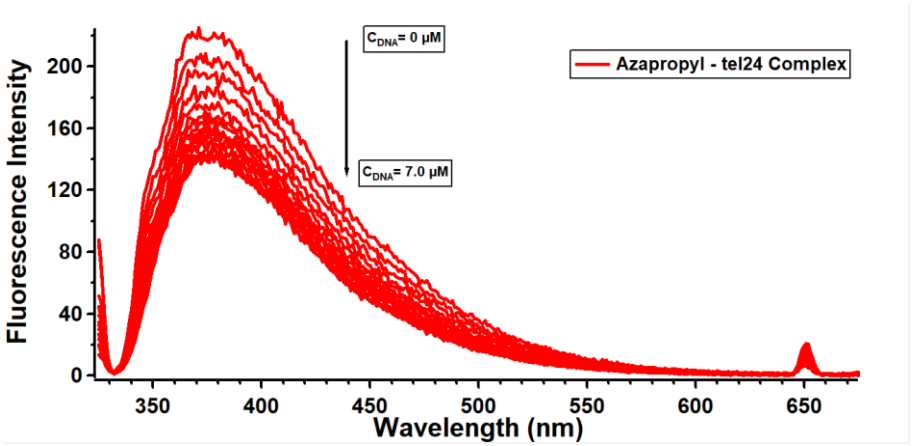

Figure 169: Fluorescence Intensity vs. Wavelength (nm) graph for 1µM Azapropyl solution titrated with increasing concentrations of tel24 solution (2nd replicate).

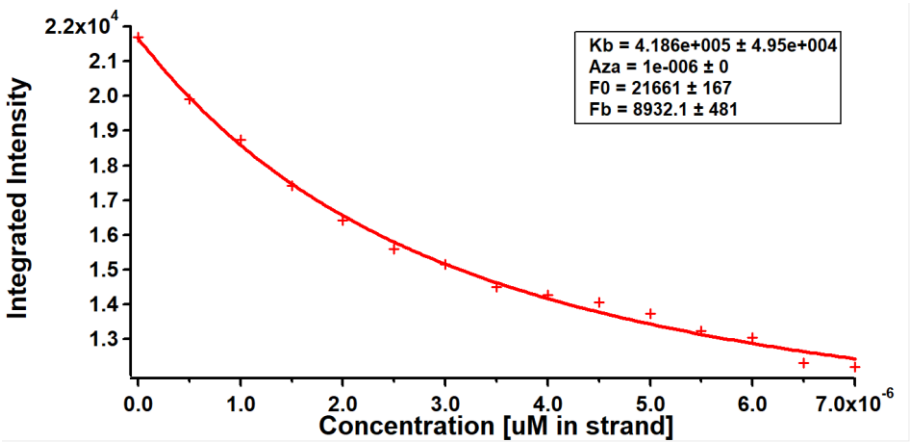

Figure 170: Integrated Fluorescence Intensity vs. DNA Concentration (µM, in strand) obtained from the Fluorescence Intensity vs. Wavelength (nm) graph 166.

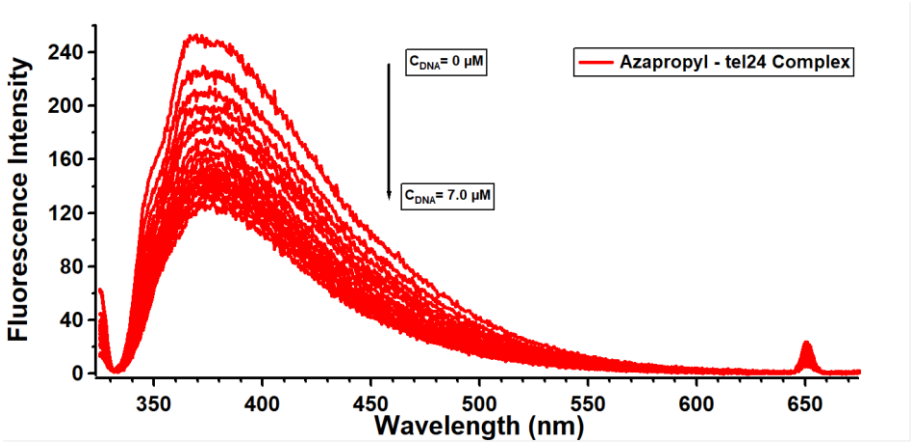

Figure 171: Fluorescence Intensity vs. Wavelength (nm) graph for 1µM Azapropyl solution titrated with increasing concentrations of tel24 solution (3rd replicate).

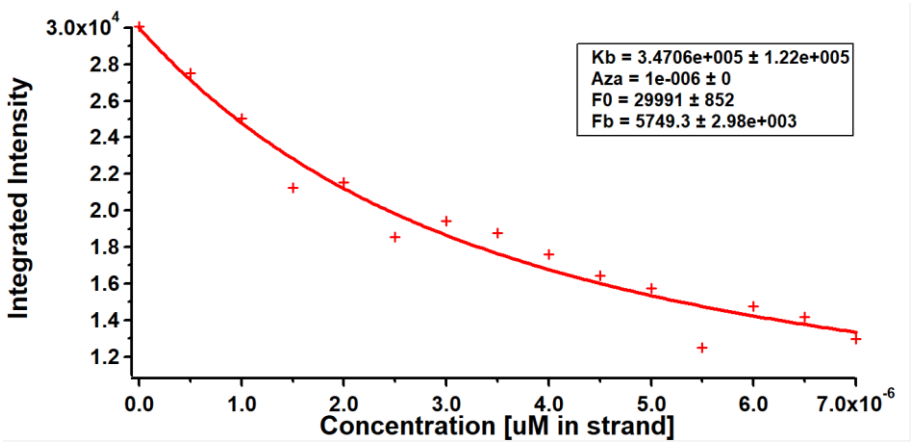

Figure 172: Integrated Fluorescence Intensity vs. DNA Concentration (µM, in strand) obtained from the Fluorescence Intensity vs. Wavelength (nm) graph 168.

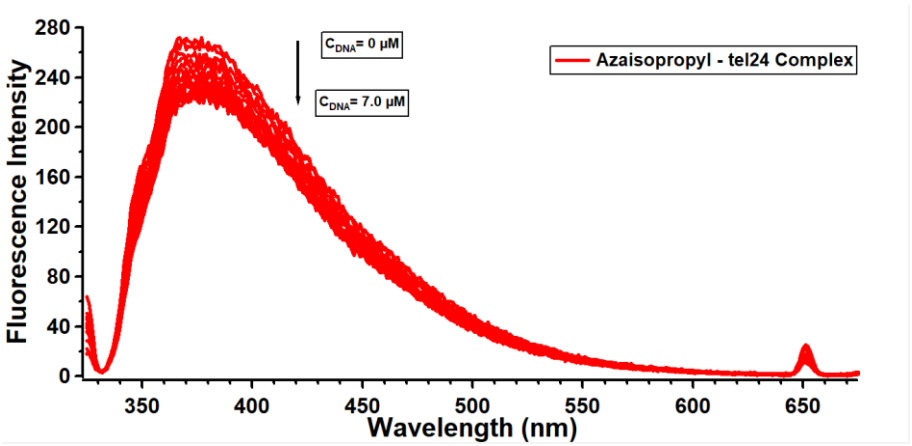

Figure 173: Fluorescence Intensity vs. Wavelength (nm) graph for 1µM Azaisopropyl solution titrated with increasing concentrations of tel24 solution (1st replicate).

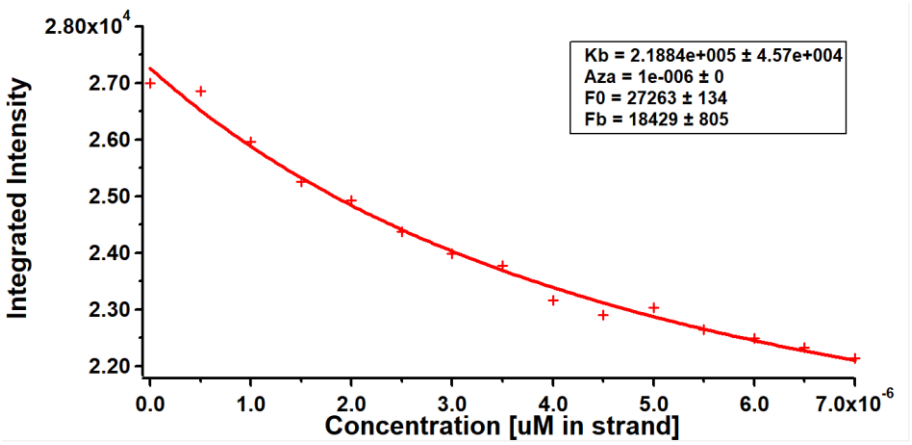

Figure 174: Integrated Fluorescence Intensity vs. DNA Concentration (µM, in strand) obtained from the Fluorescence Intensity vs. Wavelength (nm) graph 170.

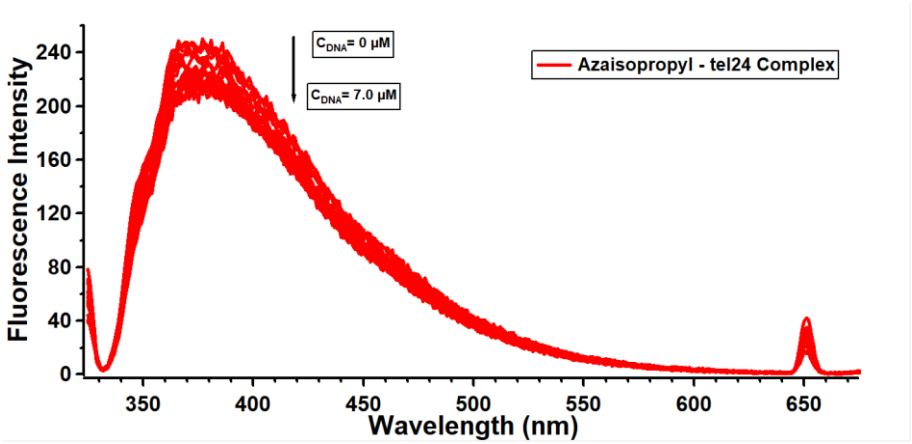

Figure 175: Fluorescence Intensity vs. Wavelength (nm) graph for 1µM Azaisopropyl solution titrated with increasing concentrations of tel24 solution (2nd replicate).

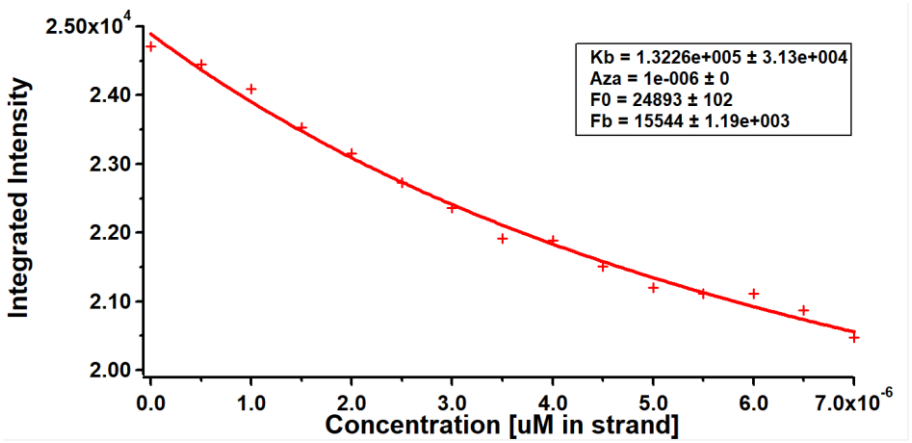

Figure 176: Integrated Fluorescence Intensity vs. DNA Concentration (µM, in strand) obtained from the Fluorescence Intensity vs. Wavelength (nm) graph 172.

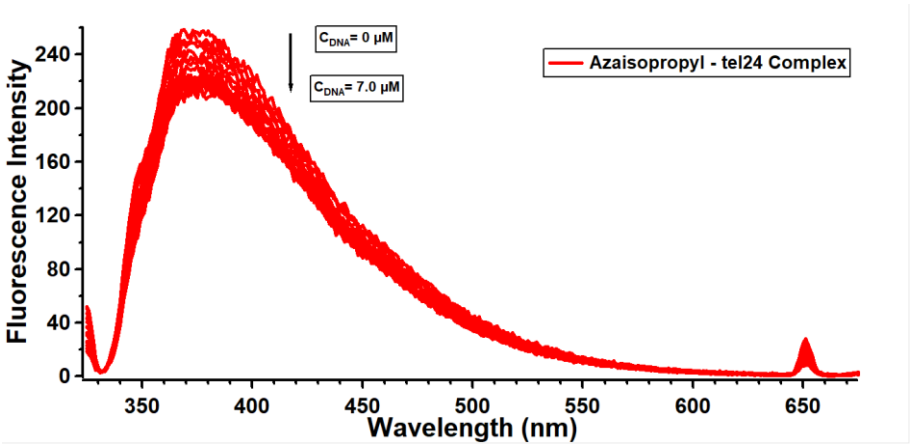

Figure 177: Fluorescence Intensity vs. Wavelength (nm) graph for 1µM Azaisopropyl solution titrated with increasing concentrations of tel24 solution (3rd replicate).

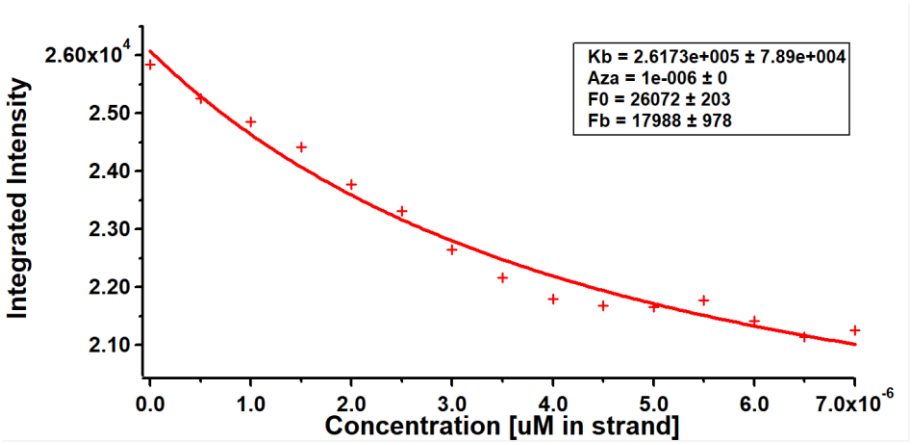

Figure 178: Integrated Fluorescence Intensity vs. DNA Concentration (µM, in strand) obtained from the Fluorescence Intensity vs. Wavelength (nm) graph 174.

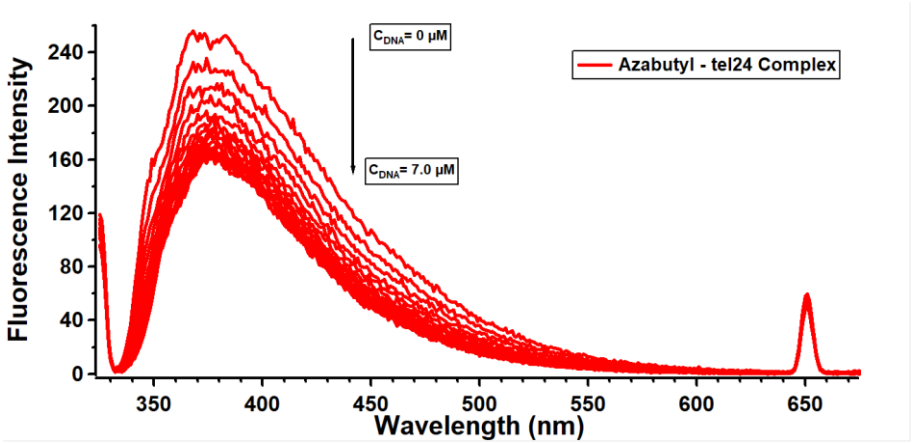

Figure 179: Fluorescence Intensity vs. Wavelength (nm) graph for 1µM Azabutyl solution titrated with increasing concentrations of tel24 solution (1st replicate).

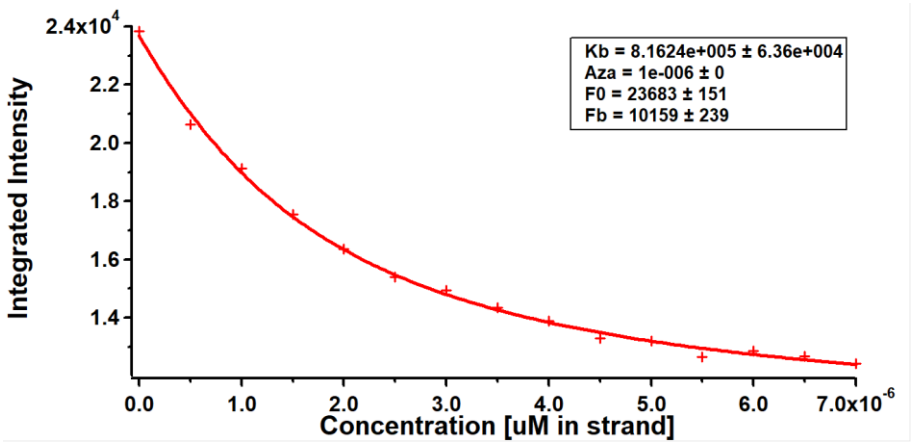

Figure 180: Integrated Fluorescence Intensity vs. DNA Concentration (µM, in strand) obtained from the Fluorescence Intensity vs. Wavelength (nm) graph 176.

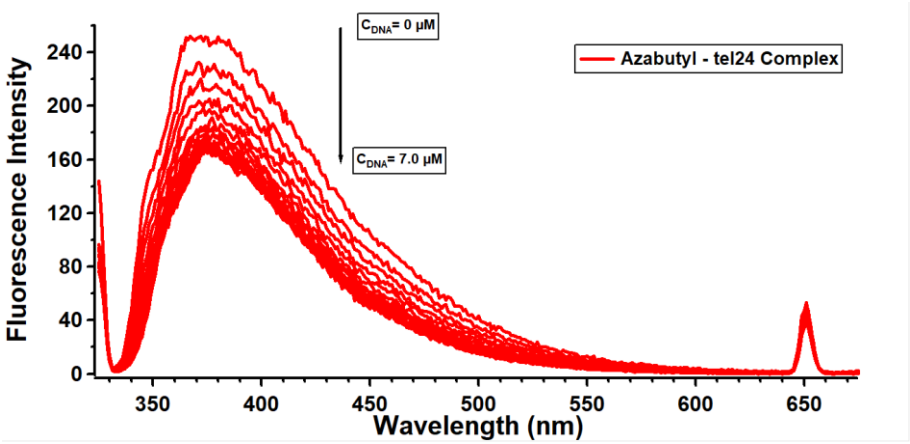

Figure 181: Fluorescence Intensity vs. Wavelength (nm) graph for 1µM Azabutyl solution titrated with increasing concentrations of tel24 solution (2nd replicate).

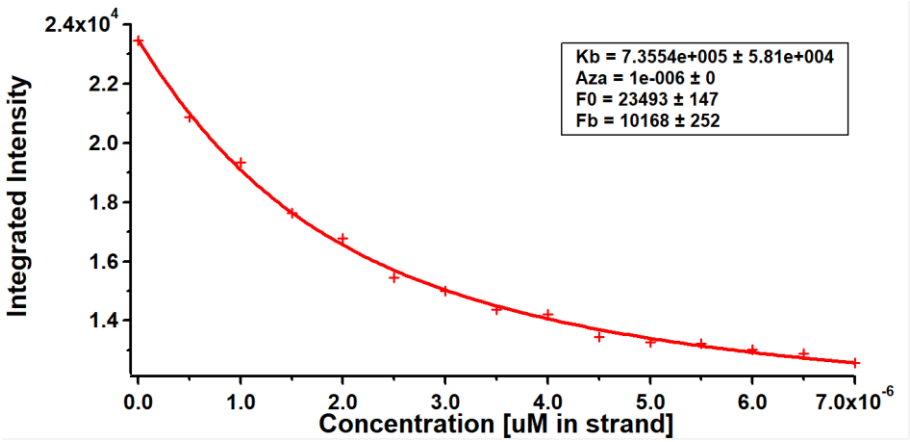

Figure 182: Integrated Fluorescence Intensity vs. DNA Concentration (µM, in strand) obtained from the Fluorescence Intensity vs. Wavelength (nm) graph 178.

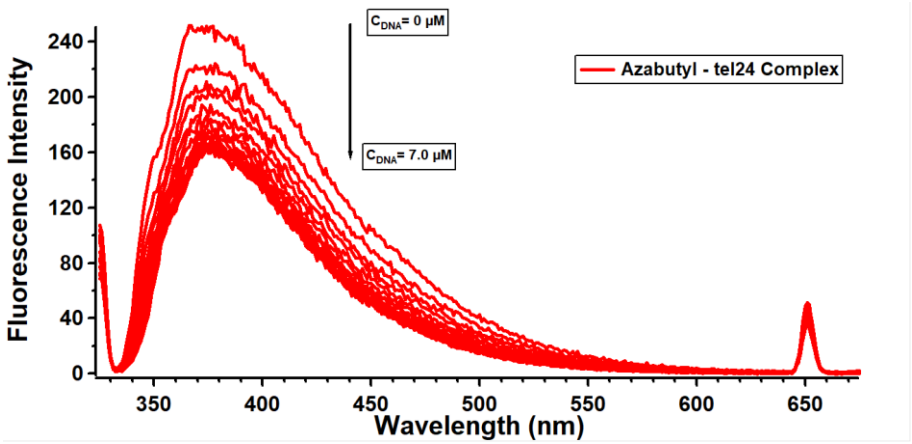

Figure 183: Fluorescence Intensity vs. Wavelength (nm) graph for 1µM Azabutyl solution titrated with increasing concentrations of tel24 solution (3rd replicate).

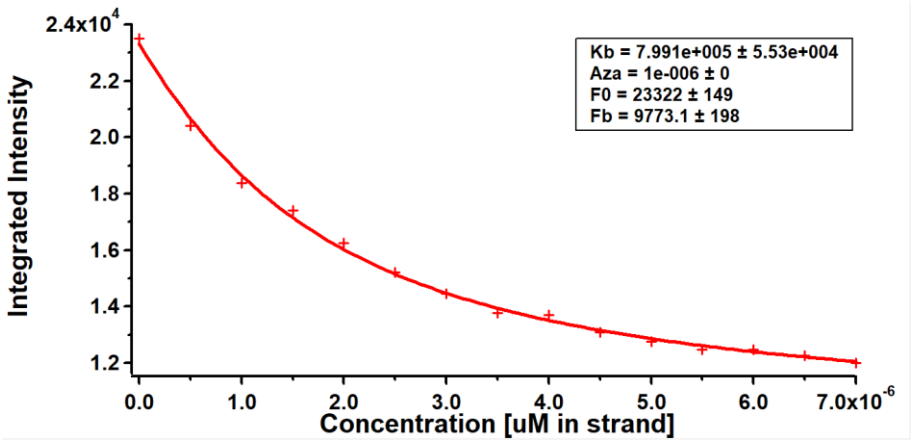

Figure 184: Integrated Fluorescence Intensity vs. DNA Concentration (µM, in strand) obtained from the Fluorescence Intensity vs. Wavelength (nm) graph 180.

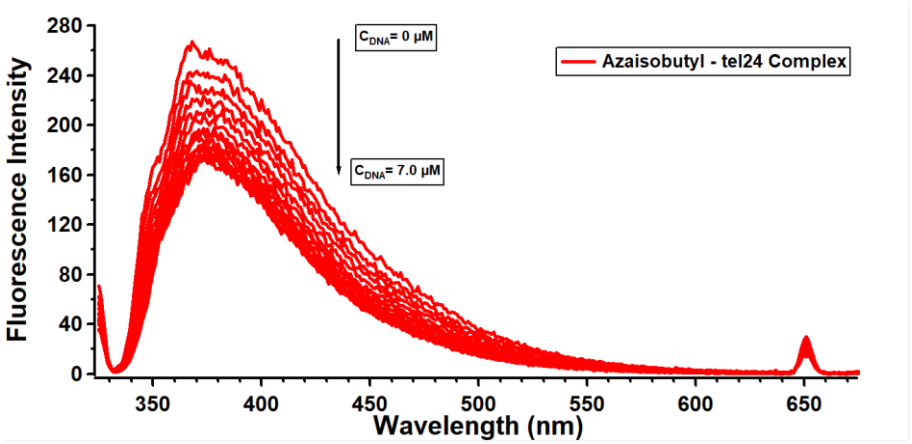

Figure 185: Fluorescence Intensity vs. Wavelength (nm) graph for 1µM Azaisobutyl solution titrated with increasing concentrations of tel24 solution (1st replicate).

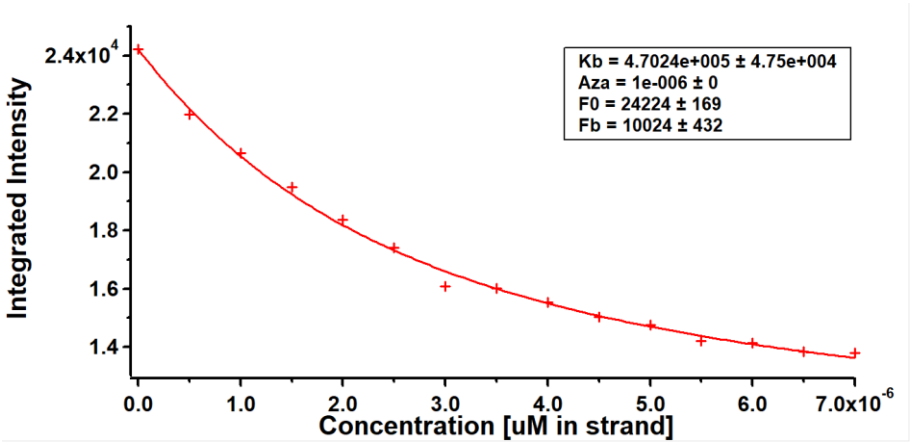

Figure 186: Integrated Fluorescence Intensity vs. DNA Concentration (µM, in strand) obtained from the Fluorescence Intensity vs. Wavelength (nm) graph 182.

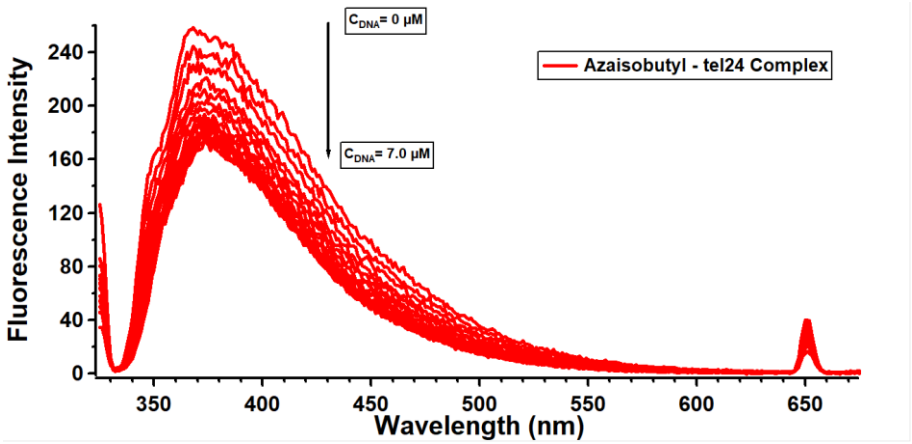

Figure 187: Fluorescence Intensity vs. Wavelength (nm) graph for 1µM Azaisobutyl solution titrated with increasing concentrations of tel24 solution (2nd replicate).

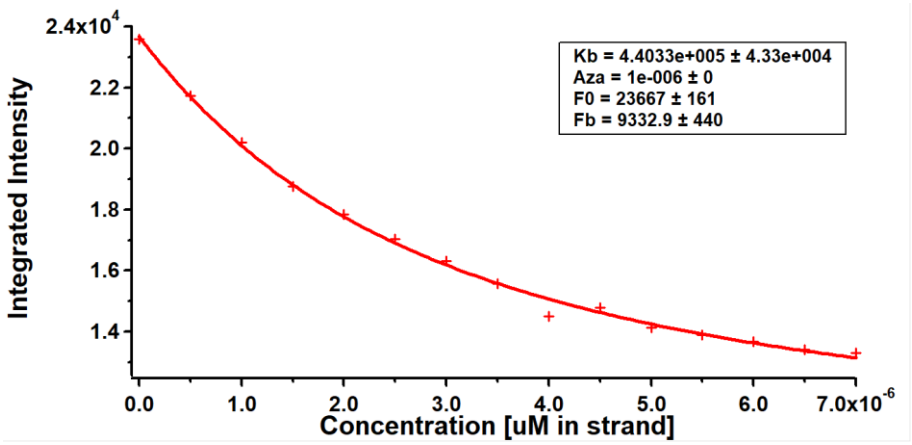

Figure 188: Integrated Fluorescence Intensity vs. DNA Concentration (µM, in strand) obtained from the Fluorescence Intensity vs. Wavelength (nm) graph 185.

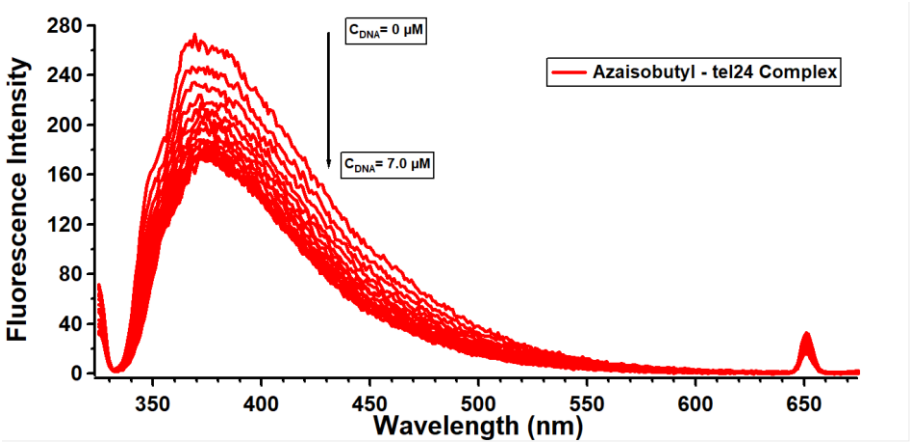

Figure 189: Fluorescence Intensity vs. Wavelength (nm) graph for 1µM Azaisobutyl solution titrated with increasing concentrations of tel24 solution (3rd replicate).

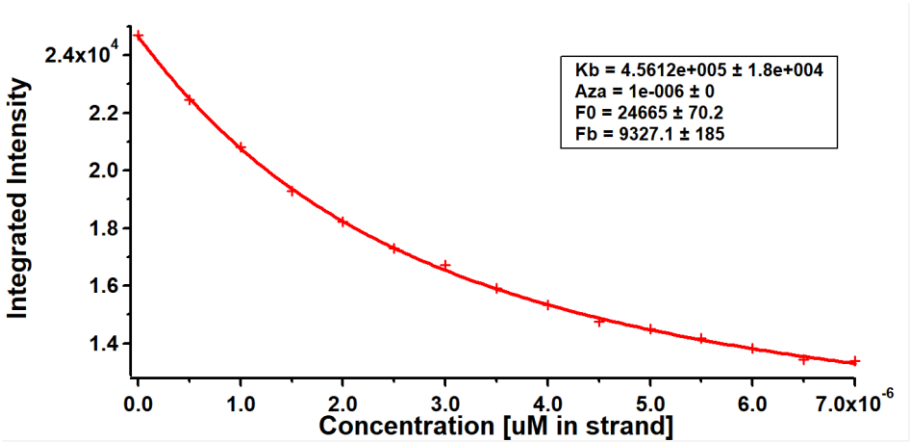

Figure 190: Integrated Fluorescence Intensity vs. DNA Concentration (µM, in strand) obtained from the Fluorescence Intensity vs. Wavelength (nm) graph 186.